Thèse
de doctorat
de l'UTT

Milagre Alfredo MANHIQUE

Multi-objective Optimization and Decision-making in the Context of Complex and Multi-physical Systems/Processes

Champ disciplinaire :
Sciences pour l'Ingénieur

2022TROY0037 **Année 2022**

utt
UNIVERSITÉ DE TECHNOLOGIE
TROYES

THESE

pour l'obtention du grade de

DOCTEUR
de l'UNIVERSITE DE TECHNOLOGIE DE TROYES

en SCIENCES POUR L'INGENIEUR

Spécialité : OPTIMISATION ET SURETE DES SYSTEMES

présentée et soutenue par

Milagre Alfredo MANHIQUE

le 13 décembre 2022

Multi-objective Optimization and Decision-making in the Context of Complex and Multi-physical Systems/Processes

JURY

M. Éric CHÂTELET	PROFESSEUR DES UNIVERSITES	Président
M. Abdelkhalak EL HAMI	PROFESSEUR DES UNIVERSITES	Rapporteur
Mme Nathalie LIDGI-GUIGUI	MAITRE DE CONFERENCES - HDR	Rapporteure
M. Dinis JUIZO	PROFESSOR ASSOCIADO	Examinateur
M. Dominique BARCHIESI	PROFESSEUR DES UNIVERSITES	Directeur de thèse
M. Raed KOUTA	MAITRE DE CONFERENCES - HDR	Directeur de thèse

Personnalité invitée

M. Marcelino RODRIGUES	PROFESSOR ASSOCIADO

To my family

My beloved wife
Almira NHABINDE-MANHIQUE

My children :
Lércia MANHIQUE, Nivaldo MANHIQUE and Milan MANHIQUE.

Acknowledgements

I **Milagre Alfredo MANHIQUE** express my gratitude for the institutional support given during the duration of my research program as a PhD student at the **Université de Technologie de Troyes** integrated in the **UR GAMMA3** research laboratory.
I deeply appreciate the collaboration of all the administrative, technical and pedagogical personnel of the GAMMA3 laboratory in general.

To my supervisors, **Prof. Dr. Dominique BARCHIESI** and **Prof. Dr. Raed KOUTA**, I am deeply grateful for your academic, scientific and pedagogical support. I take the opportunity to highlight your sense of mission.

I extend my eternal gratitude to all those who directly or indirectly contributed to the successful progress of this thesis that led to the acquisition of a doctoral degree in Systems Optimization and Security (Optimisation et Sûreté des Systèmes) at the the Université de Technologie de Troyes.

Résumé

The global energy sector is undergoing rapid changes from generation through fossil fuel sources (example : coal, oil and gas) to generation through Renewable Energy Sources (example : wind power and solar power). Hybrid Battery-Solar-Wind Power Generation Systems (HBSWPGS) are highly unstable due to the fluctuation of the output power generated by the system caused by instantaneous variations in the availability of solar and wind energy, making the output power an uncertain variable. This thesis intends to evaluate the influence of uncertainty and produce a risk analysis of each constituent subsystem, namely the Wind Turbine Generator (WTG), the Photovoltaic Generator (PVG) and Battery Energy Storage System (BESS) to provide quantified uncertainty information to aid in the decision-making process in designing an optimal configuration of an HBSWPGS. The electrical performance parameters of the subsystems are modeled as a function of environmental variables such as wind speed, solar radiation and ambient temperature. We model the uncertainty of the generated power and evaluate the sensitivity of the electrical parameters to describe their influence on the performance of hybrid system as a function of the variation of weather conditions throughout the hours of the day.

Le secteur mondial de l'énergie subit des changements rapides de la production par des sources de combustibles fossiles (exemple : charbon, pétrole et gaz) à la production par des sources d'énergie renouvelables (exemple : l'énergie éolienne et l'énergie solaire). Les systèmes de production d'énergie hybride batterie-solaire-éolienne sont très instables en raison de la fluctuation de la puissance de sortie générée par le système causée par les variations instantanées de la disponibilité de l'énergie solaire et éolienne, faisant de la puissance de sortie une variable incertaine. Cette thèse se propose d'évaluer l'influence de l'incertitude et de produire une analyse de risque de chaque sous-système constitutif, à savoir l'Éolienne, le Générateur Photovoltaïque et le système de stockage d'énergie par batterie, afin de fournir des informations quantifiées sur l'incertitude pour faciliter le processus de prise de décision dans la conception d'une configuration optimale d'un système de production d'énergie hybride batterie-solaire-éolienne. Les paramètres de performance électrique des sous-systèmes sont modélisés en fonction de variables environnementales telles que la vitesse du vent, le rayonnement solaire et la température ambiante. Nous modélisons l'incertitude de la puissance générée et évaluons la sensibilité des paramètres électriques pour décrire leur influence sur les performances du système hybride en fonction de la variation des conditions climatiques tout au long des heures de la journée.

Keywords
Renewable energy sources, Wind turbines, Photovoltaic cells, Energy storage, Uncertainty.
Mots clés
Énergies renouvelables, Éoliennes, Générateurs photovoltaïques, Énergie - Stockage, Incertitude.

Table des matières

Table des figures

Liste des tableaux

List of Abbreviations

WTG Wind Turbine Generator
PVG Photovoltaic Generator
P_{wtg} Wind turbine generator output power
P_{pvg} Photovoltaic generator output power
HDRES Hybrid Distributed Renewable Energe Sources
ESS Energy Storage System
RES Renewable Energy Source
IEA International Energy Agency
RE Renewable Energy/Energies
HSWPGS Hybrid Solar-Wind Power Generation System
v Wind speed
s Solar radiation
t_a Ambient temperature
MMC Multi-Model Combination
AIC Akaike Information Criteria
h_{ref} Reference height
h Hub wind speed
v_r Rated power (in W)
G Solar iradiance
v_{ci} Cut-in speed (in m/s)
i Index for data observation days

j Index for data observation hours
$v_{i,j}$ Wind speed with days and hours indexes
$P_{wtg(i,j)}$ WTG output power with days and hours indexes
$P_{pvg(i,j)}$ PVG output power with days and hours indexes
AIC Akaike Information Criteria
I_{ph} Photovoltaic current
T_a Ambient temperature
T_C Cell temperature
BESS Battery Energy Storage System
G Solar irradiance
HBSWPGS Hybrid Battery-Solar-Wind Power Generation System
GHG Green House Gas
v Wind speed
nPV Number of photovoltaic panels
nPVG Number of photovoltaic generators
nWT Number of wind turbines
nWTG Number of Wind Turbine Generators
nB Number of batteries

1

Introduction

1.1 | Summary description of the thesis

This thesis prepared under the title ***Multi-objective optimization and decision-making in the context of complex and multi-physical systems/process (Application in socioeconomic and industrial development in Mozambique)***, addresses modeling and optimization of a power generation system through renewable energy sources. The power generation system considered in this thesis is an isolated microgrid (off-grid microgrid) composed of two generation subsystems namely, Wind Turbine Generator (WTG) using wind power as input variable to generate output power P_{wtg} and Photovoltaic Generators (PVG) using solar power G and ambient temperature t_a to generate output power P_{pvg}. The input variables of the hybrid system, namely, wind speed, solar radiation and ambient temperature, are elements of connection between the environment and the microgrid. Weather conditions determine the availability and intensity of the input variables, there is a direct proportionality between the intensity of the input variables and the power generated, therefore, as the input variables as environmental variables have a fluctuating availability, the output power is fluctuating therefore uncertain. In power generation systems based on renewable energy sources, the impacts of the fluctuation of the output power are mitigated by the integration of energy storage systems, in this thesis we consider battery energy storage systems, thus, henceforth, the microgrid is called Hybrid Battery-Solar-Wind Power Generation System. The diagram and its description are presented in figure 3.1, page 38.

1.2 | Contextualization of the thesis

According to the International Energy Agency (IEA) access to electricity is a fundamental factor for sustainable industrial, socioeconomic and human development, however, about 20% of the world population (approximately 1.5 billion) does not have access to electricity. Furthermore, globally around 2.4 billion people meet their energy needs for cooking and heating by exploiting forest resources, thus contributing to deforestation [12, 13, 14]. Despite the fundamental importance of electricity in the development process, fossil fuels (coal, oil and gas) continue to be the main raw material in the generation of electricity, thus contributing to the emission of greenhouse gases leading to global warming as described in section 2.2. Deforestation and global warming are harmful to the ecological balance and the viability of life on earth, therefore, the use of clean and renewable energy sources is highly recommended.

1.3 | Problem statement

Power generation urgently needs to be fully sustainable, for that objective, the use of renewable energies (RE) is pointed out as an affordable, reliable and clean source of energy combined with the use of off-grid microgrids mainly in rural, remote and difficult to access regions. In this thesis, consider an isolated (or off-grid) Hybrid Battery-Solar-Wind Power Generation System (HBSWPGS) powered by the following renewable energy sources (RES), wind speed v that feeds the Wind Turbine Generator (WTG) subsystem, and the solar radiation G that feeds the Photovoltaic Generator (PVG) subsystem influenced by the ambient temperature t_a. Wind speed and solar radiation are environment variables with an instantaneous and stochastic variation pattern whose availability is only predictable through probabilistic models using historical data. The instantaneous variations and the intermittence of wind speed and solar radiation make the output power an uncertain variable, therefore, it is essential to design power microgrids with optimized configuration and parameters, including evaluation of the influence of uncertainty and risk analysis leading to the correct support in the decision-making process.

Uncertainty assessment, risk analysis and probabilistic modeling of output power in RES-based systems are important activities to ensure improved accuracy of estimation and prediction of output power, system reliability, power generation capacity that satisfies the power

demand, to avoid imbalance between generation and demand that leads to undersizing, oversizing, power fluctuations, supply interruptions and blackouts.

1.4 | Main modeling stages performed

(i) Modeling the output power of wind turbine generators (WTG)

(ii) Calculation of photovoltaic generator (PVG) parameters and comparison (validation) with existing parameter models in the literature

(iii) Calculation of battery parameters and comparison of models

(iv) Modeling the uncertainty of the output power and the sensitivity of the model parameters as a function of uncertainty using Monte Carlo method.

1.5 | Motivation

1.5.1 | Scientific motivation

Uncertainty remains a determining factor in the performance of RES-based power generation systems. Due to the persistent existence of uncertainty in complex systems, modeling, quantifying and understanding its propagation and impact on systems performance is crucial. Considering that hybrid power generation systems based on Wind Turbine Generators (WTG) and Photovoltaic Generators (PVG) with integrated Battery Energy Storage Systems (BESS) are affected by variations in weather conditions, namely, wind speed , solar radiation and ambient temperature, it is essential to evaluate the performance of the system under instantaneously variable weather conditions.
The WTG, PVG and BESS have a performance described by the respective characteristic curves and parameters, thus, it is important to evaluate the behavior of the parameters as a function of weather conditions, to understand the system response to environmental variations.

1.5.2 | Socioeconomic motivation

Mozambique is among the 20 countries with a lack of access to electricity, where 17.5 of the 30 million inhabitants live without access to electricity, mainly in rural areas where 66.6%

of the Mozambican population resides. In 2020, only 4.5% of the rural population had access to electricity, however, Mozambique has an identified and confirmed potential of renewable energy sources equivalent to 23,000 GW distributed almost evenly throughout the country [15]. To take advantage of available renewable potential, it is essential to invest in rural electrification infrastructure based on isolated Hybrid Battrery-Solar-Wind Power Generation Systems (HBSWPGS) as viable solution capable of ensuring accelerated access to clean and renewable energy sources for rural communities in Mozambique, including those of developing countries in general.

1.6 | Aims and Objectives

1.6.1 | General objectives

(i) To assess the impact of uncertainty on the output power of WTG and PVG as constituent parts of a hybrid power generation system.

(ii) To determine the sensitivity on the operating and performance parameters of the wind turbine generator, the photovoltaic solar panel and the battery.

1.6.2 | Specific objectives

(i) Model the operating and performance parameters of a photovoltaic cell and a battery as a function of changing weather conditions over the hours of the day.

(ii) Evaluate the uncertainty of the models of the parameters of the photovoltaic solar panel and the battery as a function of changing weather conditions over the hours of the day

(iii) Evaluate the sensitivity of the photovoltaic solar panel and battery operating parameters to provide quantified information on uncertainty as a function of changing weather conditions over the hours of the day

1.7 | Proposed Solution

This thesis uses historical data on wind speed v, solar radiation G and ambient temperature t_a observed and recorded hourly for two years (2019-2020). The data are organized in the form

of an hourly average during the day, i.e., Data is grouped into hourly averages for all 24 hours and all 731 days from 2019-2020. Therefore, we have a 731 X 24 matrix with hourly average values.

The proposed solution basically consists of mathematical modeling using equations of the characteristic parameters of the WTG, PVG and BESS operation.The equations are deduced and compared with those already existing in published studies. To these equations, we apply the input data (wind speed, solar radiation and ambient temperature) obtaining results that are later validated (or compared) with results of studies available in the literature.

1.8 | Document structure

After an introductory approach, the thesis is organized and structured as follows :

— **Chapter 2 : Background & and a literature Overview**
It addresses all theoretical foundations and scientific tools used in the development of the thesis. It was based on research of the scientific literature in the form of articles, books, online sites, including reports from governments, non-governmental organizations, and public and private institutions.

— **Chapter 3 : Material & Methods**
It describes the methodology used to search for the solution to the research problem, the simulation models, the computational tools for simulation and obtaining results, including the model validation process,

— **Chapter 4 : Conclusion**
It addresses the findings and achievements resulting from the critical observation of the results of computer simulations and validation of results.
The conclusion discusses the strengths and weaknesses of our approach, the achieved aims, a general criticism of the work, and final remarks.

2

Background & Literature Overview

2.1 | Fossil fuel energy versus Greenhouse gases

The International Energy Agency states that access to electricity is a fundamental condition for sustainable industrial, socioeconomic and human development [12, 16]. The global demand for electricity is still satisfied by the direct burning of fossil fuels (example : Coal, oil and gas) resulting in the emission of greenhouse gases (GHG) leading to environmental damage such as global warming, extreme heat waves, polar ice melting, rising sea levels, frequent floods, severe droughts, air, water and soil pollution, landslides, including deterioration in the health of plants, animals and human beings [17]. The seriousness of the consequences caused by anthropogenic actions on the environmental and climatic systems, due to the direct burning of fossil fuels and deforestation, require coordinated global action to drastically reduce greenhouse gas emissions. According to the World Bank and the International Energy Agency, if no coordinated action is taken globally, energy generation from fossil fuel sources will continue to be the main cause of greenhouse gas emissions [18, 19, 20].

It is our opinion that this situation is somewhat paradoxical, since, on the one hand, energy is a fundamental factor for industrial, socio-economic and human development, but on the other hand, the global energy demand is still mostly satisfied by fossil fuel sources (example : coal, oil and gas). In this regard, humanity may be in a conflict of interests..

According to [21] studies published in recent decades demonstrate that the increase in the amount of greenhouse gas emissions in the atmosphere, with emphasis on carbon dioxide,

is directly related to the growth and expansion of the global industrial sector, which in turn depends mostly on fossil fuel energy. The main greenhouse gases of anthropogenic origin are, among others, carbon dioxide (CO_2), methane (CH_4), nitrous oxide (N_2O), fluorinated gases such as hydrofluorocarbons (HFCs), perfluorocarbons (PFC_s), sulfur hexafluoride (SF_6) and nitrogen trifluoride (NF_3), approximately 41 billion tons of carbon dioxide are emitted annually into the atmosphere increasing the temperature of the planet, the total amount of greenhouse gases present in the atmosphere has the following proportions : 53% carbon dioxide, 17% methane, 12% chlorofluorocarbons (CFC), 6% Nitrous Oxide and 12% all others [22, 17].
In this critical context of climate change, the global community (governments, multinational companies, non-governmental organizations, academics, scholars and societies in their most varied forms of organization and representation) realizing the irreversible environmental cost due to the use of fossil fuel energies, mobilized for a global, coordinated, effective and progressive response aimed at reducing emissions of greenhouse gases to contain global warming, resulting in the Paris agreement on climate change aiming the following global objectives [23, 24] :

(i) Holding the increase in the global average temperature to well below 2^0 C above pre-industrial levels and pursuing efforts to limit the temperature increase to 1.5^0C above pre-industrial levels, recognizing that this would significantly reduce the risks and impacts of climate change (Article 2 of the Paris agreement on climate change) ;

(ii) The aim is to reach global peaking of greenhouse gas emissions as soon as possible (Point 1 of Article 4 of the Paris agreement on climate change).

The focus of the Paris Agreement on Global Warming is eradicating poverty through sustainable development, safeguarding the integrity of all ecosystems and protecting biodiversity on earth. The content of the Paris agreement suggests that global warming is a real problem, with irreversible environmental and economic consequences and potential to deteriorate the balance of the ecosystem and biodiversity, making life on earth unfeasible [25].
The essential aspect in global warming is the greenhouse effect which can be explained in two perspectives, the greenhouse effect due to ***natural causes*** which is beneficial and the greenhouse effect due to ***anthropogenic causes*** which is harmful. The greenhouse effect by natural causes is a phenomenon of the Earth's atmospheric system, which acts as a *"protective blanket"* that receives solar energy reflected by the Earth's surface, preventing that energy from being totally lost to space, aiming to maintain an optimal global average temperature

for the existence of life on earth, without this *"protective blanket"*, all energy would be lost in space, causing very low temperatures (global cooling) that would make life on earth completely impossible. Anthropogenic action related to the burning of fossil fuels (coal, oil and gas) leads to the massive presence of gases in the atmosphere, overloading the *"protective blanket"*, consequently retaining heat above the necessary resulting in global warming that underlies the agreement of Paris on Global Warming.

Global economic development is intrinsically dependent on the energy sector based on fossil energies, thus requiring a high sense of cost-benefit balance, since more than 60% of the energy produced globally is still assured by sources based on fossil fuels causing environmental damage, however, this energy is very necessary to ensure industrial, socioeconomic and human development. The intrinsic relationship between energy and economic development urgently needs to adopt a sustainability approach. Ultimately, the environmental crisis due to greenhouse gases underlies the problematization of energy generation through the use of fossil fuel sources.

2.2 | Fossil fuel energy versus renewable energy

The literature on power generation based on fossil fuels discusses environmental impacts and their consequences on living beings, highlighting, global warming, extreme heat waves, polar ice melt, rising ocean water levels, irregular rainfall, frequent flooding, severe droughts, deforestation, soil erosion and landslide, and pollutiom of soil, water and air, deterioration of the health of plants, animals and humans, including imbalance of ecosystem and biodiversity. These are direct and observable consequences on which the United Nations Organization's goal is based, which is to reduce greenhouse gas emissions by 45% by 2045 and achieve zero emissions by 2050 [22, 17]. Global agreements such as the United Nations Declaration on Climate Change, more specifically the Sustainable Development Goal 7 (SDG-7) and the Paris Agreement on Climate Change, converge on two fundamental pillars :

(i) The recognition that the generation of energy through the use of fossil fuel sources causes environmental problems of global impact demanding an urgent global solution ;

(ii) Acceptance of the use of clean and renewable energy sources as a globally sustainable solution requiring globally coordinated actions

Global agreements to reverse climate change include, among others the following actions [26] :

(i) Global migration from fossil fuel to renewable energies ;

(ii) Building sustainable and resilient cities and infrastructure ;

(iii) Sustainable management of forests and oceans ;

(iv) Ecological and environmentally friendly agriculture ;

(v) Zero greenhouse gas emissions leading to green and sustainable economies.

Some sectors of the international community believe that carrying out these actions requires a collective, coordinated and symbiotic commitment between governments, the private sector and financial institutions to avoid designing, financing and implementing coal-fired power plant projects. The global commitment to reduce greenhouse gas emissions, should be so incisive that no coal-fired power plant should be financed or installed. The commitment to reduce greenhouse gas emissions due to anthropogenic causes means, a gradual but effective abandonment of fossil fuels and the adoption of clean and renewable energy sources, addressed in the literature as ***Energy transition***.

Energy transition is a matter of ensuring sustainable industrial, socioeconomic and human development, therefore, it is urgent to decarbonize highly industrialized economies and support emerging and less industrialized economies towards green economies based on clean and renewable energies, thereby implementing an *Energy Transition* process based on the Paris Agreement on climate change.

2.3 | Energy transition and sustainability

The term transition is defined in online dictionaries as a movement, passage, or change of a position, state, or condition. According to [27] transition is a process (or period) of changing from one state (or condition), type (or form), place (or style) to another. Briefly, the term transition refers to a process (or period) of change from a well-defined starting point to a well-defined destination point.

Climate changes caused by greenhouse gas emissions have sparked the debate on the concept of energy transition defined as the emigration from current global systems based on fossil fuels (as a starting point) to new global systems based on clean and renewable energy sources (as

destination point).
In the context of the Paris Agreement on Climate Change (after signature) it can be said that the energy transition is the ongoing process of replacing power systems based on fossil fuel sources with power systems based on clean and renewable energy sources. Roughly speaking, energy transition means structural change in power systems [28, 29]. The energy transition process leading to a change in the global energy landscape has the challenge of overcoming multiple economic, social, technical, technological and political challenges, so the energy transition should be approached as a complex and dynamic process of change. When approaching the energy transition based on the Paris agreement on climate change, it is important to consider that there is a starting point (fossil fuel energy) and a desired destination point (clean and renewable energy), but also, there is a period (or energy transition). The success of a transition process depends on the understanding of the objectives and the meaning attributed to such a transition to a desired point, therefore, it might not be reasonable to approach the change from fossil fuels to clean and renewable energy sources minimizing the importance of the transition period (or process), the **Energy transition**. Every process of change impacts the life of the individual or the community, therefore, the energy transition as a process of change depends on the individual and collective understanding of the severity of the consequences of climate change caused by the use of fossil fuels, but it also depends on the global commitment to the transition to renewable energy sources, in this context, the energy transition should be a sustainable process, with meaning of common understanding, and with globally coordinated action [30].

In the context of the Paris Agreement on Climate Change, the effective change to low carbon power systems depends on the energy transition as a process of change which in turn depends on the collective understanding of the objectives and meaning given to such a desired change, there is an intrinsic interdependence between the energy transition and the effective implementation of low carbon power systems. Follow-up actions in the transition period determine the desired results, so the **Energy transition** is very important.

2.4 | Variability of Renewable Energy Sources

The ongoing energy transition based on the Paris Agreement on Climate and the SDG-7 decreed by the United Nations Organization, points clean and Renewable Energy Sources as a solution to achieving a low-carbon power system aiming at building green economies (low-

carbon economies) conducive to sustainable industrial, socioeconomic and human development. Despite the undeniable advantage of renewable energy sources such as wind power (for wind turbine generator) and solar power (for photovoltaic generator), there is a challenge related to its highly unstable availability pattern, the instantaneous variations (variability and intermittency) resulting from climate and environmental dynamics.
Power generation through the use of RES is environmentally sustainable, but power generated is fluctuating and uncertain due to the variable and intermittent availability of renewable power. The variable nature of RES is the main source of uncertainty causing fluctuation in output power, thus, availability of RES, estimation of output power and uncertainty quantification are best approached in probabilistic terms [31]. The instantaneous variations of the RES pose challenges to the continuous supply of power, the quality of power supplied, the reliability of the system, and the response to the needs of the demand of power, energy is generated at the exact moment it is consumed, the supply must respond to demand in real time [32].

The variable availability of RES is a natural phenomenon, artificially uncontrollable, impossible to predict precisely, making uncertainty persistently existent.

2.5 | Uncertainty : Definition and Concept

2.5.1 | Some theoretical definition

Uncertainty is a broad concept in its historical-evolutionary approach, it is a transversal concept without a globally accepted standard definition, its meaning depends on the scientific domain of application such as philosophy, physics, statistics, economics, finance, psychology and other areas of scientific domain. The absence of a theoretical definition of universal consensus makes uncertainty a concept that is not easy to define [33].
To illustrate the diversity in the approach and definition of the concept of uncertainty, some of the definitions available in the literature are presented below :

(i) **Definition 1**
Uncertainty is a multifaceted characterization of a data set of measurements and observations of certain phenomena including predictions made from such data [34].

(ii) **Definition 2**
In evaluating the dynamics of complex systems (or processes), including complex ma-

thematical models, uncertainty can be defined as the lack (or incompleteness) of data, or even the presence of uncomfortable, unforeseen and undesirable variables, making it difficult to obtain accurate results in a measurement process [35].

(iii) **Definition 3**
Uncertainty is relative to uncertain measure, some phenomena can be quantified by uncertain measure, therefore [36] defines uncertainty as anything (or phenomenon) quantified by an uncertain measure

(iv) **Definition 4**
Uncertainty is a term (or concept) that expresses (or describes) something (or phenomenon) definitely not known (or unknowable) only imprecisely and incompletely describable, based on vague information or vague knowledge [37].

(v) **Definition 5**
For [38] uncertainty and information are two closely linked concepts arguing that whenever we have an unsolved uncertainty problem, there is always information deficiency, in this approach, uncertainty is a property of information directly related to the limited perception of systems.

(vi) **Definition 6**
Uncertainty as an intrinsic property of information is so present and persistent (or omnipresent) [38] such that at any stage of a system (or process) a continuous decision-making process is required, in this context, the total (or partial) absence of data (or information) leading to a correct (or effective) decision-making process becomes a source of uncertainty [39].

(vii) **Definition 7**
Uncertainty is a state (or condition) of limited perception of phenomena, resulting from the total (or partial) absence of information (or data) leading to the description of such phenomena through degrees of belief [40, 39].

(viii) **Definition 8 (in Metrology)**
Acording to [41], Uncertainty (of measurement) is a non-negative parameter, associated with the result of a measurement, which characterizes the dispersion of the value that could reasonably be attributed to the quantity intended to be measured (or to the measurand). For [42] the uncertainty of a measurement result reflects a lack of accurate knowledge about the value of the measurand.

Despite the diversity of definitions available in the literature, it is perceived that uncertainty is addressed under the condition of ***not knowing for sure*** [33, 43]. According to [44], the choice of an adequate (or appropriate) definition in view of the multiplicity of meanings and attempts to define the concept of uncertainty available in the literature, demand a deep knowledge and correct characterization of the system (or process) under consideration (or of interest), the type of related information, including the nature of the intrinsic uncertainty of the system (or process).

In an attempt to formulate a generic definition applicable in various scientific domains, Baoding Liu formulated uncertainty theory in 2007 [45] and refined it in 2010 [46], using three cornerstones namely :

- **Uncertain measure** : To measure the belief degree of an uncertain event [46]
- **uncertain variable** : To represent imprecise quantities [46]
- **Uncertainty distribution** : To describe uncertain variables in an incomplete but friendly way (easy-to-use) [46].

Using axiomatic mathematics on the three foundations mentioned above, Baoding Liu formulated the theory of uncertainty based on four fundamental axioms namely Normality, Duality, Subadditivity and Product summarily described as [45, 46, 36] :

Let Γ be a nonempty set, and $\mathcal{L}$ a σ-algebra over Γ. Each element Λ in $\mathcal{L}$ is called an event. A set function $\mathcal{M}$ from $\mathcal{L}$ to $[0,1]$ is called un uncertain measure if it satisfies the following axioms :

- Axiom 1 : Normality Axiom
  For the universal set Γ [36] :
  $M\{\Gamma\} = 1$
- Axiom 2 : Duality Axiom
  For any event Λ [36] :
  $M\{\Lambda\} + M\{\Lambda^c\} = 1,$
- Axiom 3 : Subadditivity Axiom
  For every countable sequence $\Lambda_1, \Lambda_2, ...$ [36]
  $M\left\{\bigcup_{i=1}^{\infty} \Lambda_i\right\} \leq \sum_{i=1}^{\infty} M\{\Lambda_i\}$
  The triplet $(\Gamma, \mathcal{L}, \mathcal{M})$ are called uncertainty space.
- Axiom 4 : Product Axiom
  Let Γ_k, $\mathcal{L}_k$, $\mathcal{M}_k$ be uncertain spaces for $k = 1, 2, \ldots, n$. The product uncertain measure

$\mathcal{M}$ is an uncertain measure on the product σ-algebra $\mathcal{L}_1 \cdot \mathcal{L}_2 \cdot \mathcal{L}_3 \ldots \mathcal{L}_n$ satifying [36] :
$\mathcal{M}\left\{\prod_{i=1}^{n} \Lambda_i\right\} = \min_{1 \leq k \leq n} \mathcal{M}_k\{\Lambda_k\}$

In the mathematical (or scientific) context based on the uncertainty theory of [45], some phenomena can be quantified by uncertain measure, the so-called uncertain phenomenon, thus, without prejudice to the transversality (or multidisciplinarity) of the concept, ***uncertainty*** is formally defined as anything that can be quantified by uncertain measure, satisfying the axioms of uncertainty theory in [36].

2.5.2 | Comment on section 2.5

Carrying out a critical analysis, it can be seen that the various theoretical approaches to defining the concept of uncertainty still do not have consensus within the scientific community, there are different perceptions in different fields of science and engineering, however, the theory of uncertainty based on axiomatic foundations formulated by Baoding Liu, made uncertainty theory a branch of mathematics that addresses the mathematical modeling of uncertain phenomena based on mathematical foundations [45, 47, 36]. In this context, within the scope of this thesis and in subsequent works of continuous research, special attention will be given to the theory of uncertainty based on the foundations of axiomatic mathematics formulated by Baoding Liu discribed in [45, 36].

2.6 | Uncertainty Modeling : Definition and Concept

System dynamics deals with instantaneous changes in system behavior over time [48], i.e., deals with how things change over time, such changes often unforeseen and undesirable are a potential source of uncertainty. In complex systems, uncertainty is always present and persistent, it is omnipresent, therefore intrinsic to systems [38], negatively impacting the decision-making process [49]. In this context, one of the challenges that needs to be addressed is how to effectively model the uncertainties persistently present in systems [50], there are two types of uncertainty in complex systems, namely, *probabilistic uncertainty* describing the uncertainty of the sensor data (or measurement uncertainty), and *possibilistic uncertainty* describing the uncertainty of the data (or parameters) of the model, i.e., computation, however, the dynamics of complex systems is generally influenced by human behavior which, due to its qualitative (or

abstract) nature, is difficult to include as a controllable variable (or parameter) of the model, but human behavior impacts the quantitative (definitive) results of the modeling [48].
Although engineering systems are inevitably affected by uncertainties inherently generated by multiple sources directly or indirectly associated with the systems, it is desirable for engineering systems to operate effectively while maintaining reliability in service, therefore, it is essential to assess possible sources of uncertainty, forecast qualitative and quantitative uncertainties to better understand the impact of such uncertainties on engineering systems and help in the decision-making process, which means, assessing the impact of uncertainties in complex engineering systems involves aggregating and modeling them quantitatively (example : recorded data) and qualitatively (example : human factors and expert opinions) [51]. Uncertainty analysis investigates the uncertainty of variables that significantly impact the performance of a system giving a technical contribution to the decision-making process through the uncertainty quantification of the relevant variables.

2.6.1 | Uncertainty Quantification

Uncertainty quantification (UQ) is the science that studies the quantitative characterization, reduction and mitigation of the effects of uncertainties in computational and real-world applications [52]. UQ is essentially an activity of identifying and understanding "almost" all uncertainties generally classified into two categories, *epistemic uncertainties* (eliminable) and *aleatory uncertainties* (non-reducible). Epistemic uncertainties arise due to lack of knowledge, if knowledge about the system is sufficient, epistemic uncertainties can be reasonably reduced, while aleatory uncertainties are generally irreducible, however, the probable reducibility depends on the randomness (or stochastic variations) of the phenomenon under observation [53]. Briefly, uncertainty quantification is an activity exclusively dedicated to quantitative characterization and reduction of uncertainties present in computer model simulations aiming to identify the main sources of uncertainties in the model, characterize such uncertainties present in the model, improve the understanding of the model and facilitate the decision-making process. Every modeling process (or computer simulation) is essentially a process of abstraction, simplification and interpretation of reality, i.e., the incompleteness of a model and the mismatch between a model and reality are the main source of uncertainty even in carefully designed models [54]. The models are designed to express the fundamental principles of the systems, helping to understand the dynamics of the processes, despite this, all models have have errors

whose sources are grouped into three categories namely [55] :

(a) **Model error :**
Forecasting systems are based on probability density functions, however, it is difficult to find perfect single probabilistic models for a perfectly accurate forecast, being therefore a source of predictive uncertainty [54]. Currently, the multi-model combination (MMC) strategy is used to reduce the so-called **model error** [55].

(b) **Data error :**
All computer models require input data to run simulations. Observed data (recorded data) should be as small a difference approximation as possible to real-world phenomena, to reduce error as a source of uncertainty about the data. If the simulation data is an imperfect approximation of the real world, the error is called **data error** [55].

(c) **Parameter error :**
Computer simulated systems depend on simulation models characterized by specific parameters such as constants or coefficients that characterize each model individually. If model parameters are incorrectly specified it affects model performance and output results giving rise to **parameter error** [55].

2.6.2 | Comment on section 2.6

Computer models are a very useful and indispensable tool for simulating the dynamic behavior of complex systems, however, uncertainty is an ever-present phenomenon. Quantifying uncertainty improves knowledge about the system and facilitates the decision-making process.

Any decision taken without considering uncertainties has no condition to be considered as a decision

When studying a complex system, identifying potential sources of uncertainty, characterizing, quantifying and reducing its influence should be a priority activity to ensure reliable system output results.

2.7 | Uncertainties of renewable energy sources

Conventional power generation systems based on fossil fuels (coal, oil and gas) have over time been identified as the main cause of greenhouse (GHG) gas emissions that cause global warming and climate change, therefore, the global community is mobilizing for a migration to the use of power generation systems based on RES with emphasis on wind speed for Wind Turbine Generators (WTG) and solar radiation for Photovoltaic Generators (PVG). Wind speed v and solar radiation G are environmental variables, their stochastic availability (instantaneous variations) depends on the dynamics of the climate system, i.e., vary over time on scales from minutes to seasons. [31].

2.7.1 | Balance between generation and demand

The desirable scenario is a power generation system providing continuous stable power, satisfying demand (consumption needs), permanently ensuring the balance between generation $G(t)$ and demand $D(t)$ as :

$$G(t) = D(t) \tag{2.1}$$

Satisfying equation 2.1 is just a probable scenario, it is not certain, as there are instantaneous variations on both the generation side and the demand side, for the following reasons :

(i) Generation side $G(t)$:

  (a) **Dependence on weather and environmental variables :** Wind speed, solar radiation, air temperature, air density, season, and other environmental variables and parameters.

  (b) **Generation pattern :** Fluctuating and uncertain

(ii) Demand side $D(t)$:

  (a) **Dependence on human factors :** Industrial development, production of goods and services, modernization of the residential sector, calendar of events of public interest, need for heating or cooling according to the season, and other.

  (b) **Demand behavior :** Varies according to social dynamics and immediate needs.

Despite the usefulness of forecasting models based on probability density functions, accurately predicting the generation or demand is a difficult challenge, because the uncertainty based on error (data error, parameter error, model error and including error by human factors) is a persistently present phenomenon. In this sense, to mitigate the effects of variability on the gereration side (mainly at times of low (or no) availability of Renewable Energies (RE)), and to reduce the effects of variation of power consumption on the demand side (mainly in periods of system overload and peak consumption), the Energy Storage Systems (ESS) play the role of compensating the generation deficit (when demand is greater than generation), dampening in case of system overload and demand peaks, including compensation for instantaneous system output power fluctuations in real time.

2.7.2 | Comment on section 2.7

Integrating Energy Storage Systems (ESS) into purely RES-based hybrid power systems is not a guarantee of total elimination of the challenges of fluctuations and interruptions in the power supply, since, on the one hand, ESS mainly based on batteries have parameters of operation and performance that can be affected by several factors, and on the other hand, the PVG subsystems do not generate power in the long night period in which only the WTG can generate power, which challenges the autonomy and the state of charge of the batteries

2.8 | Mathematical modeling of RES

The power generation systems based on RES, as considered in this thesis, have as input variables the wind power and solar power, and as output variables the power of the WTG Wind Turbine Generator and the PVG Photovoltaic Generator, thus, knowing If both the input variables and the output variables are uncertain in nature, they are best approached in terms of probabilistic models.

2.8.1 | Mathematical modeling of wind speed

According to [56, 57, 58] the best expression often recommended for modeling wind speed is the Weibull probability density function $f_w(v_j)$ expressed as :

$$f_w(v_j) = \frac{K}{C} \cdot \left(\frac{v_j}{C}\right)^{K-1} \cdot \exp\left[-\left(\frac{v_j}{C}\right)^{K}\right], \qquad v_j \geq 0. \tag{2.2}$$

Where :
$f_w(v_j)$ is the probability density function, v_j is the observed wind speed data set. K and C are parameters of the Weibull probability density function described as K is the shape index and C is the scale index.
If the shape index parameter K takes the value 2 (K = 2), the Weibull probability density function becomes a special case (particular case) called the Rayleigh probability density function expressed as :

$$f_r(v_j) = \left(\frac{2 \cdot v_j}{C^2}\right) \cdot \exp\left[-\left(\frac{v_j}{C}\right)^{2}\right], \qquad v_j \geq 0. \tag{2.3}$$

By processing historical wind speed data v_j, the scale index C can be obtained using an acceptable approximation expressed as :

$$C = 1.128 \cdot v_{mean} \tag{2.4}$$

where :
v_{mean} is the hourly average forecasted wind speed obtained from a time series.
The probability of the wind speed state v at any specific forecast time h_j can be expressed as :

$$\rho(v_j) = \int_{v_1}^{v_2} f_w(v) \cdot dv \tag{2.5}$$

In this thesis, the period of interest varies in the time series from 06 :00 a.m. to 19 :00 p.m., $h_j = h_6, h_7, \cdots h_{18}, h_{19}$.

2.8.2 | Mathematical modeling of solar radiation

The variation in solar radiation s_j is best modeled using the Beta probability density function $f_b(s_j)$ expressed as [56, 57, 58] :

$$f_b(s) = \begin{cases} \frac{\Gamma(\alpha+\beta)}{\Gamma(\alpha)\cdot\Gamma(\beta)} \cdot s^{(\alpha-1)} \cdot (1-s)^{(\beta-1)} & for \quad 0 \leq s \leq 1, \quad \alpha \geq 0, \quad \beta \geq 0. \\ 0, & otherwise \end{cases} \tag{2.6}$$

Where α and β are Beta pdf parameters expressed as :

$$\alpha = \frac{\mu \cdot \beta}{1-\mu} \quad and \quad \beta = (1-\mu) \cdot \left[\frac{\mu(1+\mu)}{\sigma^2} - 1\right] \tag{2.7}$$

Where μ represents the means (statistical mean), and σ represents the standard deviation of the random variable, the solar radiation G.
The probability of the solar radiation state s at any specific forecast time h_j within the range of interest $h_j = h_1, h_2, \cdots h_{23}, h_{24}$ can be expressed as :

$$\rho(s) = \int_{s_1}^{s_2} f_b(s) \cdot ds \tag{2.8}$$

2.8.3 | Comment on section 2.8

Equations 2.2 and 2.6 allow modeling the intensity of wind speed and solar radiation as input variables for the production of quantified information on the estimate, uncertainty and risk assessment in the process of power generation and decision making.

2.9 | Mathematical modeling of output power

2.9.1 | Modeling the output power of the wind turbine generator

The output power of a wind turbine generator P_{wtg} depends on wind speed v and the parameters of the wind turbine power curve, namely cut-in speed v_{ci}, rated speed v_{rated}, cut-out speed v_{co}, rated power P_{rated} and power coefficient C_p below represented by the parameter $param$ as :

$$param = \{v_{ci}, v_{rated}, v_{co}, P_{rated}, C_p\} \tag{2.9}$$

The output power is a wind turbine generator P_{wtg} it is a function of the wind speed v and the characteristic parameters $param$ of the power performance curve expressed as :

$$P_{wtg} = f(v, param) \tag{2.10}$$

The wind-to-power conversion used the test data provided in the manufacturer's data sheet. From such manufacturer's test data, namely, wind speed and output power, the interpolation was performed using the piecewise cubic spline interpolation technique.
Cubic spline interpolation is a non-parametric fitting technique used to estimate values that fall between two known data points by drawing a simple smooth curve through the data, i.e., it fits different polynomial cubic functions between two known data points [59]. The typical fitting equation that characterizes the output power of the wind turbine generator P_{wtg} using the cubic spline interpolation functions technique can be expressed as :

$$P_{wtg}(v) = \begin{cases} 0 & for \quad v \leq v_{ci} \\ a_1 v^3 + b_1 v^2 + c_1 v + d_1 & for \quad v_{ci} \leq v \leq v_1 \\ a_2 v^3 + b_2 v^2 + c_2 v + d_2 & for \quad v_1 \leq v \leq v_2 \\ \cdots \quad \cdots & \quad \cdots \\ a_n v^3 + b_n v^2 + c_n v + d_n & for \quad v_{n-1} \leq v \leq v_r \\ P_r & for \quad v_r \leq v \leq v_{co} \\ 0 & for \quad v \geq v_{co} \end{cases} \tag{2.11}$$

Where :
a, b and c are the polynomial coefficients of cubic spline interpolation functions, n is the number of cubic spline interpolation functions corresponding to $n+1$ data pairs (wind speed, power)=(v, P_{wtg}) provided by the manufacturer datasheet, $P_{wtg}(v)$ is the output power generated by the wind turbine at wind speed v, v_{ci} is the cut-in wind speed, v_{co} is the cut-out wind speed, v_r is the rated wind speed and P_r is the rated output power P_{wtg}.

Normally, data is recorded at a certain height (reference height) but is applied at another height, i.e., the wind speed data used in this thesis were recorded by a device located at a height of 10 meters, but the wind turbine generator selected in this thesis is 50 meters high, therefore, the vertical profile of the wind speed must be adjusted. The vertical profile of wind speed at a given geographical point can be adjusted through the power law expressed as [8, 60, 61, 62] :

$$\frac{v}{v_{ref}} = \left(\frac{h}{h_{ref}}\right)^{\alpha} \tag{2.12}$$

Where :
v (in $\mathrm{m\,s^{-1}}$) is the wind speed at the height of the wind turbine generator, also called hub height h (in m), v_{ref} (in $\mathrm{m\,s^{-1}}$) is the wind speed measured at the reference height (height of observation and recording point) h_{ref} (in m), α (dimensionless) is the surface roughness coefficient.

2.9.2 | Modeling the output power of the photovoltaic generator

The irradiance-to-power conversion is done through photovoltaic modules that basically consist of photovoltaic cells that convert solar radiation into phtovoltaic power P_{pvg} mathematically expressed as :

$$P_{pvg} = N_i \cdot FF_i \cdot V_{yi} \cdot I_{yi} \tag{2.13}$$

Where :
N_i is the total number of solar cells in the i-th solar generator.
FF_i is the fill factor (dimensionless).
V_{yi} is the voltage across the PV cell terminals in open circuit mode (in V).
I_{yi} is the light generated current (photocurrent) neglecting parasitic resistance (in A)

$$FF_i = \frac{V_{MPP_i} \cdot I_{MPP_i}}{V_{OC_i} \cdot I_{SC_i}} \tag{2.14}$$

Where :
V_{MPP_i} is the voltage at maximum power point measured in V.
I_{MPP_i} is the current at maximum power point measured in A.
V_{OC_i} is the Open-Circuit voltage measured in V.
I_{SC_i} is the Short-Circuit current measured in A.

$$V_{y_i} = V_{OC_i} - K_{v_i} \cdot T_{C_i} \tag{2.15}$$

Where :
V_{OC_i} is the Open-Circuit voltage measured in V.
K_{v_i} is the voltage temperature coefficient measured in $V/^0C$.
T_{C_i} is the cell temperature measured in ^0C.

$$I_{y_i} = s_i \cdot \left[I_{SC_i} + K_{C_i} \cdot (T_{C_i} - 25) \right] \tag{2.16}$$

Where :

I_{SC_i} is the short circuit current measures in Ampere (A).

K_{C_i} is the current temperature coefficient measured in $A/^0C$.

T_{C_i} is the PV cell temperature during a certain weather state measured in ^0C.

$$T_{C_i} = T_a + \frac{S_i}{800} \cdot (T_{NOCT} - 20) \tag{2.17}$$

Where :

T_{a_i} is the ambient temperature measured in ^0C.

S_i is the solar radiation measured in W/m^2

T_{NOCT} is the nominal operating temperature measured in ^0C.

2.10 | Modeling battery energy storage systems (BESS)

Battery is defined as a set of electrochemical cells capable of storing energy in chemical form and converting it back to electrical form when necessary. Power fluctuation in RES-based systems requires the integration of efficient Energy Storage Systems (ESS) [4]. Figure 2.1 illustrates the electrical equivalent circuit of a battery.

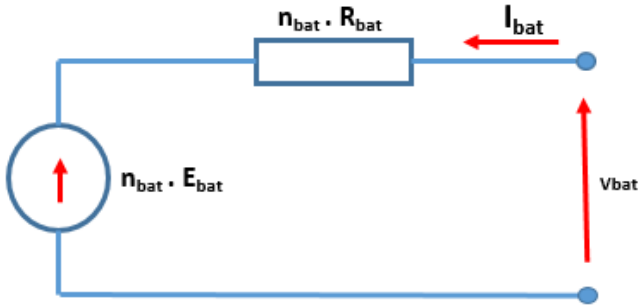

FIGURE 2.1 – Equivalent circuit of a battery energy storage system [4, 5]

.

Where :

n_b is the number of batteries, V_{bat} is the voltage of the battery, I_{bat} is the current of the battery,

E_{bat} is the electromotive force, and R_{bat} is the internal resistance of the battery.

The voltage across the battery terminals represented by the electrical equivalent circuit in figure 2.1 can be expressed as :

$$V_{bat} = n_{bat} * E_{bat} + n_{bat} * R_{bat} * I_{bat} \tag{2.18}$$

2.10.1 | Modeling the capacity of a BESS

To describe the physical phenomena that govern the operation of a battery energy storage system (BESS), it is important to consider the influence of temperature T, therefore, the mathematical model that expresses the capacity of a battery C_{bat} (in Ah) can be written as [4, 5] :

$$C_{bat} = \frac{1.76 \cdot C_{10}}{1 + 0.67 \cdot \left(\frac{\bar{I}}{I_{10}}\right)^{0.9}} \cdot (1 + 0.005 \cdot \Delta T) \tag{2.19}$$

Where : ΔT is the battery heating compared to ambient temperature 25^{o}C (assumed to be identical for all battery elements), I_{10} is the Nominal battery current (in A) given by the manufacturer, $\bar{I}$ is the average battery discharge current, and C_{10} is the Nominal capacity of the battery (in Ah) at constant current discharge for 10 hours (given by the manufacturer) expressed as [4, 5, 63] :

$$C_{10} = 10 \cdot I_{10} \tag{2.20}$$

Battery capacity C_{bat} and state-of-charge SOC are two closely related variables. The state of charge of a battery is defined as a function of the capacity and amount of charge missing Q_m, expressed as [4, 5, 63] :

$$SOC = 1 - \frac{Q_m}{C_{bat}} \tag{2.21}$$

being

$$Q_m = I_{bat} \cdot t \tag{2.22}$$

Where t is the operating time of the battery.
Perfect knowledge of the real state-of-charge $SOC(t)$ at the time of interest t depends on

knowledge of the initial state-of-charge $SOC_0(t_0)$ at the starting point t_0. Therefore, the mathematical model for calculating the state of charge for an ideal battery neglecting the losses during charging, discharging and self-discharge during storage time can be expressed as [64] :

$$SOC(t) = SOC(t_0) + \int_{t_o}^{t} \left(\frac{I_{bat}}{C_{bat}} \right) d\tau \tag{2.23}$$

Considering the charge, discharge and self-discharge losses during the storage time, we will have [64] :

$$SOC = SOC_0 \cdot \left[1 - \frac{\sigma}{24} \cdot (t - t_0) \right] + \int_{t_0}^{t} \left(\frac{I_{bat} \cdot \eta_{bat}}{C_{bat}} \right) d\tau \tag{2.24}$$

Where, σ is the self-discharge rate, it is usually recommended to assume $0.2\%/day$, η_{bat} is the battery charging and discharging efficiency, normally assumed 90% during charging and 100% during discharge.

A lead-acid battery is an electromechanical device based on chemical processes influenced by temperature, the temperature variation proportionally affects the battery capacity (in Ah) which decreases with the decrease in temperature, i.e. the battery capacity is a function of temperature and can be expressed as [63, 4, 5] :

$$C_{bat} = C_{bat}^{'} \cdot [1 + \delta_C \cdot (T_{bat} - 298.15)] \tag{2.25}$$

Where C_{bat} is the battery capacity (in Ah) when the battery temperature is T_{bat}, $C_{bat}^{'}$ is the rated (or Nominal) capacity of the battery provided by the manufacturer, and δ_C is the normal operating condition, generally assumed to be 0.006 ($\delta_C = 0.6\%/^0C$).

A realistic modeling of a battery energy storage system should consider the losses at all stages of the system, however, if we neglect the cable losses, the battery current I_{bat} can be expressed as :

$$I_{bat} = \frac{P_{Solar} + P_{Wind} \cdot \eta_{rectifier} - P_{Load}/\eta_{inverter}}{V_{bat}} \tag{2.26}$$

Where P_{Solar} is the power the power of the PVG (in Watt), P_{Solar} is the power of the WTG (in W), P_{Load} is the power demanded (or consumed) by the load (in W), V_{bat} is the battery voltage, $\eta_{rectifier}$ is the rectifier efficiency, and $\eta_{rectifier}$ is the inverter efficiency.

2.10.2 | Battery floating charge voltage modeling

The floating charge voltage $V_{bat}^{'}$ (voltage across the battery terminals) can be expressed as a function of state-of-charge (SOC) as follows [4, 5] :

$$V_{bat}^{'} = a \cdot (SOC)^3 + b \cdot (SOC)^2 + c \cdot (SOC) + d \tag{2.27}$$

Considering the effects of temperature on electrochemical processes, the temperature coefficient δ_V is applied, therefore, the voltage V_{bat} at the battery terminals can be expressed as :

$$V_{bat} = V_{bat}^{'} + \delta_V \, (T_{bat} - 298.15) \tag{2.28}$$

The temperature coefficient is normally assumed to be $-4mV/^0C/2V$ compared to ambient temperature 25^0C

2.10.3 | Modeling the charging and discharging voltage

(i) **Battery discharging voltage model**
The mathematical model of the discharge voltage of a battery is deduced from the equations for voltage across the battery terminals (equation 2.18) and battery capacity (equation 2.19), so the equation for the discharging voltage V_d of a battery can be expressed as [64] :

$$V_d = [2.085 - 0.12 \cdot (1 - SOC)] - \frac{I}{C_{10}} \cdot \left(\frac{4}{1 + I^{1.3}} + \frac{0.27}{(SOC)^{1.5}} + 0.02 \right) \cdot (1 - 0.007 \cdot \Delta T) \tag{2.29}$$

(ii) **Battery charge voltage model**
The battery charging model follows the same structure as the discharge model, differing in terms of parameter values, so the charging model V_c can be expressed as [64] :

$$V_c = [2 + 0.16SOC] + \frac{I}{C_{10}} \cdot \left(\frac{6}{1 + I^{0.86}} + \frac{0.48}{(1 - SOC)^{1.2}} + 0.036 \right) \cdot (1 - 0.025 \cdot \Delta T) \tag{2.30}$$

(iii) **Battery voltage model in overcharge regime**
The battery voltage in the overcharge regime considers two physical phenomena namely,

gassing voltage V_g and saturation voltage (or end of charge voltage) V_{ec}.
The mathematical model that represents the battery voltage in the over-charge regime can be expressed as :

$$V_{overch} = n_b V_g + n_b \left(V_{ec} - V_g\right) \cdot \left[1 - \exp\left(\frac{t - t_g}{\tau_g}\right)\right] \tag{2.31}$$

Where t_g is the instant after which $V_{bat-chrg} = V_g$ and τ_g is a time constant.

The parameters of equation 2.31 can be expressed as :

a) Gassing voltage V_g :

$$V_g = \left[2.24 + 1.97 \ln\left(1 + \frac{I_{bat}}{C_{10}}\right)\right] (1 - 0.002\Delta T) \tag{2.32}$$

b) End of charge voltage V_{ec} :

$$V_{ec} = \left[2.45 + 2.01 \ln\left(1 + \frac{I_{bat}}{C_{10}}\right)\right] (1 - 0.002\Delta T) \tag{2.33}$$

c) Time constant τ_g :

$$\tau_g = \frac{1.73}{1 + 852\left(\frac{I_{bat}}{C_{10}}\right)^{1.67}} \tag{2.34}$$

2.10.4 | Modeling faradic performance

A battery's ability to store energy is directly related to faradic performance, characterized by charging performance and discharging performance.

(i) **Battery charging efficiency**
The mathematical model that represents the variation of the battery charging efficiency η_c as a function of the state-of-charge SOC and current I can be expressed as :

$$\eta_c = 1 - \exp\left[\frac{a}{\frac{I}{I_{10}} + b} \cdot (SOC - 1)\right] \tag{2.35}$$

Where $a = 20.73$ and $b = 0.55$ are battery recharge constants determined by fitting the equation to the data

(ii) **Battery discharging efficiency**
The battery efficiency in discharge regime is assumed to be 1.

$$\eta_{disc} = 1 \tag{2.36}$$

2.11 | Uncertainties in distributed generation systems

2.11.1 | Uncertainties in wind turbine generators

Power generation through wind-to-power conversion is normally done through wind turbine clusters that make up the production field, in this sense, the wind power function P_i^W of i-th wind power can be expressed as [65] :

$$P_i^W = g_W(v_i, \theta_i^W) \tag{2.37}$$

Where :
θ_i^W represents the operating parameters of the i-th wind turbine model provided by the manufacturer as coefficients such as v_{ci_i}, v_{r_i}, v_{co_i} and P_{r_i}.

— **Source of uncertainty in wind turbine generators**
As mentioned above, the power generation by wind turbines depends on the parameters of wind speed modeled through probabilistic distributions, and the wind turbine operating parameters modeled through possibilistic distributions. The set of these parameters constitutes an inevitable source of uncertainty that propagates throughout the entire power system, making the generation of power an uncertain event.

2.11.2 | Uncertainties in photovoltaic generators

The power generation through the irradiance-to-power conversion is normally done through modular groupings of photovoltaic cells that make up the production field, thus, the solar power function of the i-th photovoltaic generator can be expressed as [65] :

$$P_i^s = g_s(v_i, \theta_i^s) \tag{2.38}$$

Where :
θ_i^s represents the operating parameters of the i-th photovoltaic generator provided by the manufacturer as coefficients such as K_v, K_i, I_{sc}, V_{oc} I_{MPP}, V_{MPP} and T_{NOCT}, including variable parameters such as ambient temperature T_a.

— **Source of uncertainty in photovoltaic generators**
Environmental variables such as solar radiation s_i and ambient temperature t_a are based on historical data sets (measured and recorded) are typically modeled using probability density functions (pdf), the operating parameters (or operating coefficients) of photovoltaic generators K_v, K_i, I_{sc}, V_{oc} I_{MPP}, V_{MPP} and T_{NOCT} are provided by the manufacturer on a limited basis, without detailed information to preserve *trade secrets*. In addition, opinions, views, and judgments of experts and specialists must be incorporated which are obviously inherently inaccurate information. Therefore, it is reasonable to represent the solar irradiance as a probabilistic variable and the operating parameters (operating coefficients) as possibilistic variables. The set of factors described above constitute inevitable sources of uncertainty that propagates through the photovoltaic generation system, making the generation of output power P_i^S an uncertain event.

2.12 | Probabilistic Multi-Model Combination model

A phenomenon or event can be predicted through deterministic models or probabilistic models. In forecasting, uncertainty is always present caused by incompleteness of the models and mismatch between the model and reality. According to [54] it is not possible to design a model that incorporates all the variables describing a physical phenomena (example : environment, climate, natural processes), modeling is a process of abstraction, simplification and interpretation of reality, therefore, model inaccuracy, estimation errors, and measurement errors of the input variables, will propagate through the system resulting in prediction errors in the generated output power. Due to the persistent presence of uncertainty even in carefully designed models, designing a perfect forecasting model is an *"almost impossible"* task. In the

literature, uncertainty is described as persistent and omnipotent presence in complex systems, thus probabilistic modeling has become increasingly significant to quantify such uncertainties and forecast the output power of the system.

Probability density functions (pdf) as forecasting models are rarely perfect, they have imperfections (forecasting inaccuracies) but they also have qualities and advantages, eliminating forecasting inaccuracies is an impossible task, so instead of looking for perfection in individual probabilistic models, a statistically valid strategy is to combine models to exploit individual advantages for the sophistication and improvement of probabilistic forecasting of combined models. Based on the multi-model combination principle, the combination of k individual models can be expressed as [54] :

$$P(y|F_1, F_2, \cdots, F_K) = \sum_{i=1}^{K} \omega_i \cdot P_i(y|F_i) \tag{2.39}$$

Where :
K is the number of individual models (or member models) participating in the combination, y is the input dataset to the model, $P(y|F_1, F_2, \cdots, F_K)$ is the predictive pdf of y obtained by the combined model, F_K is the K-th member model, ω_K in the weight of the k-th member model, $P_i(y|F_i)$ is the forecast pdf generated by F_i.

2.12.0.1 | Description of Multi-Model Combination (MMC)

— A multi-model combination (MMC) is a grouping of individual models also called a member model or a single model each containing its respective fit to the dataset of interest. The set M of K member models $f_i(x)$, $i = 1, \cdots, K$ can be expressed as :

$$M = \{f_1(x), f_2(x), \cdots, f_k(x)\} \tag{2.40}$$

For a dataset of interest, each member model has its particular fit to the data. When the member models are combined it results in a more skillful model called the multi-model combination model. If the member models to be combined are probabilistic we have a probabilistic multi-model combination model also called predictive PDF as $P(dataset|f_1(x), f_2(x), \cdots, f_K(x))$.

— Each member model $f_i(x)$ belonging to the set M participates in the combination with its particular weight ω_i and must satisfy the following conditions :

(i) The weight of each member model $f_i(x)$ must be greater than or equal to 0 and less than or equal to 1.

$$0 \leq \omega_i \leq 1 \tag{2.41}$$

(ii) The sum of the weights of all member models participating in the combination must equal 1.

$$\sum_{i=1}^{K} \omega_i = 1 \tag{2.42}$$

— The main objective of combining single models $f_i(x)$ is to explore the advantages of each single model to build an even more skillful model expressed as $P(dataset|f_1(x), f_2(x), \cdots, f_K(x))$, so, it is expected that each member model contributes with its predictive capacity expressed by its predictive pdf $P(dataset|f_i(x))$.

For clarity, we can rewrite the MMC model formula of equation 2.39 as :

$$P\left(dataset|f_1(x), f_2(x), \cdots, f_K(x)\right) = \sum_{i}^{K} \omega_i \cdot P_i\left(dataset|f_i(x)\right) \tag{2.43}$$

All member models $f_i(x)$ participating in the MMC model must be able to provide a probability density or have predictive abilities.

2.12.0.2 | Example of an MMC model

Let's consider an example where we combine three single probabilistic models capable of providing predictive pdf results having x as input dataset, the multi-model combination model (MMC) would be expressed as :

$$P(x|f_1(x), f_1(x), f_1(x)) = \omega_1 \cdot P(x|f_1(x)) + \omega_2 \cdot P(x|f_2(x)) + \omega_3 \cdot P(x|f_3(x)) \tag{2.44}$$

Where :

— $P(x|f_1(x))$, $P(x|f_2(x))$ and $P(x|f_3(x))$ represent the forecasted probability density functions (pdf's) obtained by the single probabilistic models $f_1(x)$, $f_2(x)$ and $f_3(x)$ respectively.

— $P(x|f_1(x), f_1(x), f_1(x))$ represents the forecasted probability density function (pdf) obtained by combining single probabilistic models $f_1(x)$, $f_2(x)$ and $f_3(x)$.

— ω_1, ω_2 and ω_3 represent the weight with which each single model $f_1(x)$, $f_2(x)$ and $f_3(x)$ participates in the combination, respectively.

2.12.0.3 | Akaike Information Criteria (AIC)

On a dataset x, we can test several probabilistic models $f_i(x)$ to test the goodness of fit of each model on such dataset. Each tested probabilistic model has an Akaike Information Criteria (AIC) value, providing information on how the model is fitted to the dataset. AIC value of only one model does not provide enough information to formulate an opinion or conclusion, for the AIC value to be meaningful should be compared with AIC values of other models tested on the same dataset. Thus, the AIC values of each tested model are compared and placed in descending order.

The best model is the one with the lowest AIC value [66].

The lower the AIC value, the better the goodness-of-fit. The traditional formulation of the Akaike information criterion (AIC) is based on maximized likelihood value $L(\theta)$ as [67, 66] :

$$AIC = -2 \cdot \ln L(\theta) + 2 \cdot K \tag{2.45}$$

Where :
K is the number of estimable parameters in the model, $L(\theta)$ is the maximized likelihood value.

2.12.0.4 | Computation of Model likelihood and Akaike weights

Consider a set of AIC values from all individual probabilistic models tested on a data set, the difference between each value in the set and the minimum value of the same set is expressed as [67] :

$$\Delta_i = AIC_i - min(AIC) \tag{2.46}$$

Where the $min(AIC)$ is the smallest value of AIC in the model set.
The likelihood of each probabilistic model over the data set can be expressed as [67] :

$$L\left(f_i(x)|dataset\right) = \exp\left(\frac{-\Delta_i}{2}\right) \tag{2.47}$$

Akaike weights can now be calculated from the following equation [67] :

$$\omega_i = \frac{\exp\left(\frac{-\Delta_i}{2}\right)}{\sum_{r=1}^{M} \exp\left(\frac{-\Delta_i}{2}\right)} \tag{2.48}$$

Where M is the number of models.

2.13 | Related Work

For the elaboration of this thesis, a wide range of publications on Renewable Energies was consulted in the form of articles, books, online content, official reports from governmental authorities and non-governmental organizations, as the list of references attests. However, four (4) studies were taken as related studies (reference studies) namely :
[4, 5, 54, 63, 68].

(i) **Overview of [4]**
The authors present simplified mathematical models that govern the operation of a battery based on Lead Acid technology, simulating battery charging and discharging behavior by varying electrical parameters.

(ii) **Overview of [5]**
This study simulates the physical operation of an Energy Storage System (ESS) integrated in a hybrid system, using mathematical modeling and graphical representation of the performance curves of each modeled parameter, and evaluates the influence of each parameter on the performance of the Energy Storage System.

(iii) **Overview of [54]**
In this study, a complex probabilistic model is presented, built by the Multi-Model combination principle, where several probabilistic models are combined to explore individual predictive qualities of each model, aiming to improve the wind power forecast. This study demonstrates the superiority of probabilistic models over deterministic models in predictive applications

(iv) **Overview of [63]**
The authors proposed a battery model as a tool to simulate and optimize photovoltaic systems, present normalized equations to determine the battery capacity that allows generalizing its use for any type and size of batteries, and evaluated the battery voltage

during the charging processes, overload and discharge and predict the performance of solar systems under different operating conditions.

(v) **Overview of [68]**
This paper proposes a probabilistic power curve model, to represent the probability density function of power output at various wind speed, using Monte Carlo simulation to generate random predicting power output, and found performs better than other deterministic models and probabilistic models.

In studies [4, 5, 63] we took advantage of the principles, models and results regarding the parameters of operation and performance of the battery in charging and discharging regimes. In the [54, 68] we took advantage of the probabilistic modeling approach (use of predictive models) to predict the power generation capacity in a generation system based on renewable energy sources.
In general, all articles were useful in conceiving the idea of the proposed solution, however the five articles briefly described above were taken as reference in the formulation of the research problem, and in the use of probabilistic and mathematical models.

2.13.0.1 | Similarities with related work

In this thesis we use an approach of equations (or models) similar to those available in the literature, such that the models were compared and validated based on the articles taken as reference. We use the simulation and optimization models available in these reference articles to build a hybrid generation approach

2.13.0.2 | Differences with related work

The equations (models) used in this thesis are essentially similar, however, differentiation approaches can be noted regarding the assumptions during the deduction of the equations. A notable difference lies in the fact that this thesis essentially focuses on the analysis of all the parameters of the models as a function of the hourly variation of the weather.

2.14 | Articles published during the PhD program

(i) First article : [16]

(a) Title : Rural Electrification in Mozambique : Challenges and Opportunitie

(b) Published in : ICSREE 2021 : 6th International Conference on Sustainable and Renewable Energy Engineering

(c) Date of Conference : 5th May 2021 to 7th May 2021

(d) Publication date : July 2021

(e) Conference Location : France, Strasbourg

(ii) Second article : [69]

(a) Title : Energy Transition X Energy Inclusion : A Community Energy Concept for Developing Countries

(b) Published in : 2021 IEEE International Humanitarian Technology Conference (IHTC)

(c) DOI : 10.1109/IHTC53077.2021.9698969

(d) Date of Conference : 2-4 Dec. 2021

(e) Date Added to IEEE Xplore : 11 February 2022

(f) Conference Location : United Kingdom

(iii) Third article : [70]

(a) Title : Social innovation for community energy in developing countries – new models and a Mozambican case study

(b) Published in : MIT-2022 (Energy Proceedings)

(c) Date of symposium : July 5-8, 2022

(d) Publication date : July 2021

(e) Conference Location : Cambridge, USA

NOTE : The published articles are attached in the indexing section of this thesis in PDF format

3

Materials & Methods

3.1 | Introductory note to the chapter

In this chapter is presented the modeling of a hybrid power generation microgrid composed of two generation subsystems namely, the Wind Turbine Generator (WTG) with wind speed v as the input variable, the Photovoltaic Generator (PVG) with solar radiation G as an input variable. A Battery Energy Storage System (BESS) is integrated into the microgrid. The generation side consisting of WTG, PVG and BESS is designed to satisfy the demand load with variable power consumption. Each element that constitutes the microgrid considered in this thesis is modeled considering particular characteristics and parameters. The influence of uncertainty on operating and performance parameters is evaluated to describe the behavior of the microgrid in the generation of output power as a function of the hours of day. The detailed description is presented in section section 3.2 below.

3.2 | Description of the power microgrid

This thesis is fundamentally based on the modeling of a Hybrid Solar-Wind Power Generation System (HSWPGS), composed of wind turbine generators (WTG),Photo-Voltaic generators (PVG) with an Energy Storage System (ESS) coupled to the power microgrid. It is an isolated microgrid, without connection to the conventional power grid based on fossil energy sources (coal, oil and gas), i.e., it depends solely and exclusively on renewable energy sources (RES) namely, wind speed v and solar radiation s without any external source of energy supplement.

It is a completely isolated microgrid, which despite the stochastic variations (variability and intermittency) of the renewable energy sources (RES) on which it depends, must fully respond to consumer demand, which in turn presents a pattern of stochastic variation that is difficult to predict precisely. The diagram in Figure 3.1 represents a microgrid configured as HDRES composed of 5 main parts described below :

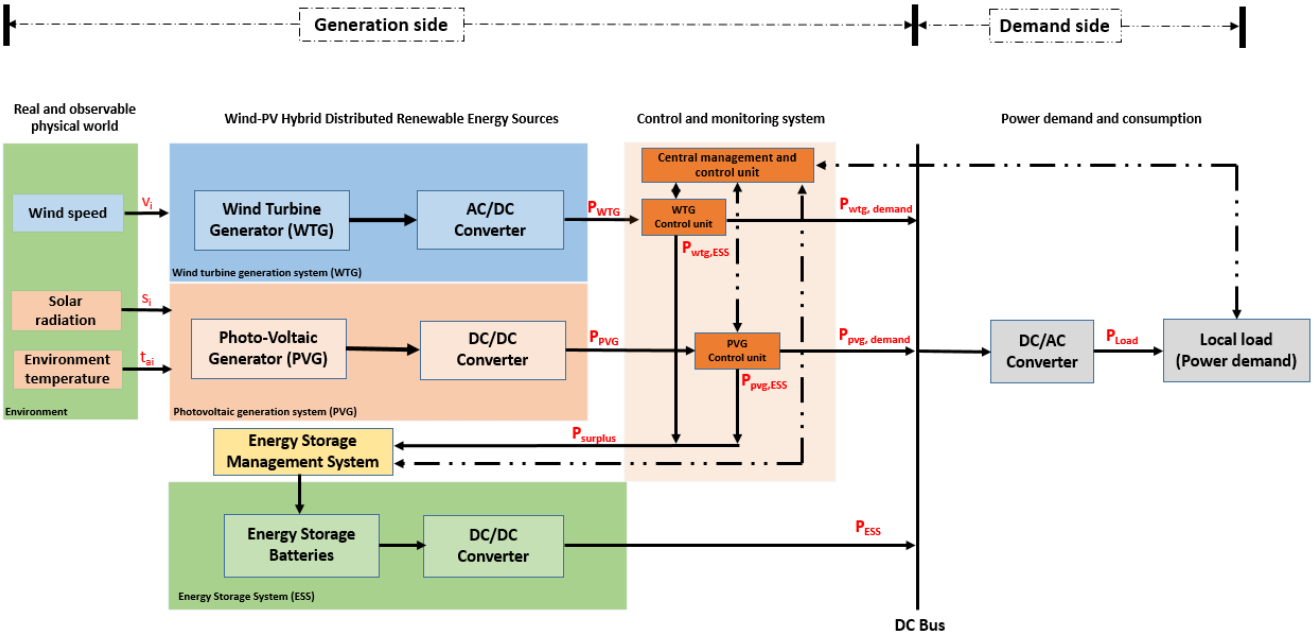

FIGURE 3.1 – Generic diagram of a hybrid Battery-Solar-Wind power generation system

(i) **Environment (real world)**

The environment is a complex system with an enormous amount of variables that determine the state of the weather at a given instant. Based on the principle that modeling is a process of abstraction, simplification, and interpretation of reality [54], for this thesis, the environmental variables of interest are wind speed v, solar radiation G and ambient temperature t_a.

(ii) **Generation systems**

Is the part of the system where the RES-to-Power conversion takes place as :

— **Wind-to-Power Conversion** : Wind speed v_i (in m/s) is converted into Wind Turbine Generator (WTG) output power P_{wtg} (in kW).

— **Irradiation-to-power conversion** : Solar radiation G is converted into output power of the Photovoltaic generator (PVG) P_{pvg}, influenced by the ambient temperature t_a.

(iii) **Energy Storage System (ESS)**
The HSWPGS microgrid, considered in this thesis, has an Energy Storage System based on a battery bank (also called Battery Energy Storage System-BESS) that performs the task of compensating the generation deficit due to generation fluctuations, and damping the consumption overload and demand peaks. The task of compensating and dampening is more significant at times of unfavorable weather conditions for power generation, example : windless and cloudy days (days with reduced or no availability of wind speed and solar radiation).

(iv) **Control and monitoring system**
In an isolated microgrid, the power balance between generation $G(t)$ and demand $D(t)$ as

$$G(t) = D(t) \tag{3.1}$$

is a difficult and highly unstable condition as both sides (generation and demand) have variations that are difficult to predict accurately, i. e., the prediction is persistently imprecise. The equilibrium condition described by equation 3.1 varies instantly over time. The Energy Storage System (ESS) should compensate for the generation deficit, buffer consumption overload and demand spikes in real time to avoid power supply fluctuations, interruptions and blackouts, including system collapse. The compensatory dynamics for power balance depends on the coupling of a control and monitoring system capable of making decisions locally in real time.

(v) **Demand and consumption side**
While the variation of power generation is caused by the variation of environmental variables, the variation of power demand is caused by human factors such as standard of living, habits, way of life, holding of social events, schedules of school and work activities, weather forecast, thus, the power demand can be relatively predictable despite the uncertainty

In the following sections, the modeling of the parts that make up the HSWPGS illustrated in Figure 3.1 is presented in the following order :

(i) Description and characterization of input data

(ii) Modeling the power generated by a Wind Turbine Generator (WTG)

(iii) Modeling the power generated by a photovoltaic cell (PVG)

(iv) Modeling the Energy Storage System (ESS)

(v) Probabilistic modeling of the power generated in the HSWPGS

3.3 | Description and characterization of input data

3.3.1 | Input data source

The input data used in this thesis were provided by the *Instituto Nacional de Meteorologia de Moçambique* (National Institute of Meteorology of Mozambique), collected at the meteorological observation, measurement and recording station of Maputo province in southern Mozambique.
The data are hourly average values, recorded hourly over the 24 hours of the day, i.e., for each hour of the day we have a set of data corresponding to the average of that hour observed daily for two years, between January 1, 2019 and December 31, 2020.

3.3.2 | Input data structure

The data (wind speed v, solar radiation G and ambient temperature t_a) are structured in column-oriented matrix form with the following interpretation :

— Each row i of the matrix represents the i-th day over the two years of observation 01/01/2019 to 12/31/2020 corresponding to 731 days. Each row of the matrix is a vector containing hourly averages over the 24 hours of the day

— Each column j of the matrix represents the j-th hour of the 24 hours of the day, the average value of each hour is observed and recorded during the two years (2019-2020)

The main objective of this thesis is to evaluate the uncertainty and its influence on the parameters of the subsystems and on the output power, to evaluate the sensitivity of the parameters of the subsystems as a function of uncertainty, and produce a risk analysis of the power generation system as a function of environmental conditions throughout the 24 hours of the day.
The following generic matrices illustrate the data structure of wind speed v, solar radiation G and ambient temperature t_a :

$$v_{i,j} = \begin{pmatrix} v_{1,1} & v_{1,2} & \cdots & v_{1,n} \\ v_{2,1} & v_{1,2} & \cdots & v_{2,n} \\ \vdots & \vdots & \ddots & \vdots \\ v_{m,1} & v_{m,2} & \cdots & v_{m,n} \end{pmatrix} \qquad G_{i,j} = \begin{pmatrix} G_{1,1} & G_{1,2} & \cdots & G_{1,n} \\ G_{2,1} & G_{2,2} & \cdots & G_{2,n} \\ \vdots & \vdots & \ddots & \vdots \\ G_{m,1} & G_{m,2} & \cdots & G_{m,n} \end{pmatrix}$$
$$ta_{i,j} = \begin{pmatrix} ta_{1,1} & ta_{1,2} & \cdots & ta_{1,n} \\ ta_{2,1} & ta_{2,2} & \cdots & ta_{2,n} \\ \vdots & \vdots & \ddots & \vdots \\ ta_{m,1} & ta_{m,2} & \cdots & ta_{m,n} \end{pmatrix} \tag{3.2}$$

Where, G is the solar irradiance, v is the wind speed, t_a is the ambient temperature, i is the indexing for days (i-th day), j is the hour index (j-th hour), m is the total number of days (in this case m = 731 days), n is the number of hours in the day (n = 24 hours).

3.3.3 | Definition of data vectors

— **Vector for hours** h

$$h\{:, j\} = \{h_1, h_2, \cdots h_{23}, h_{24}\} \tag{3.3}$$

— **Vector for days** d

$$d\{i, :\} = \{d_1, d_2, \cdots, d_{23}, d_{24}\}^T \tag{3.4}$$

For the purposes of this thesis, the input data are organized and structured as column-oriented matrices and each column represents a variable containing the model's input data (24 sets of input data equivalent to 24 hours a day).

3.3.4 | Data pre-processing

The pre-processing of the input data basically consisted of verifying the possible existence of negative values due to a registration error in the collection source, verification of values that are manifestly suspicious or excessively outside the admissible ranges as environmental variables, however, despite the notorious existence of extreme weather events, outliers were not removed as a way to maintain the originality of the data and avoid introducing a "fictitious" normality of the input data, leading to poor decision making.

3.3.4.1 | Wind speed input data

The Wind speed data v was recorded using an anemometer installed at a reference height h_{ref} of 10 meters, however, the height of the selected wind turbine generator (also called hub height) h is 50 meters, therefore, it is necessary to adjust the vertical wind speed profile to estimate the wind speed at the desired height (hub height) using the power law described in Equation 2.12.Therefore, the hourly distribution of wind speed v at the height of the wind turbine generator (hub wind speed) throughout the 24 hours of the day is shown in the figure 3.2 :

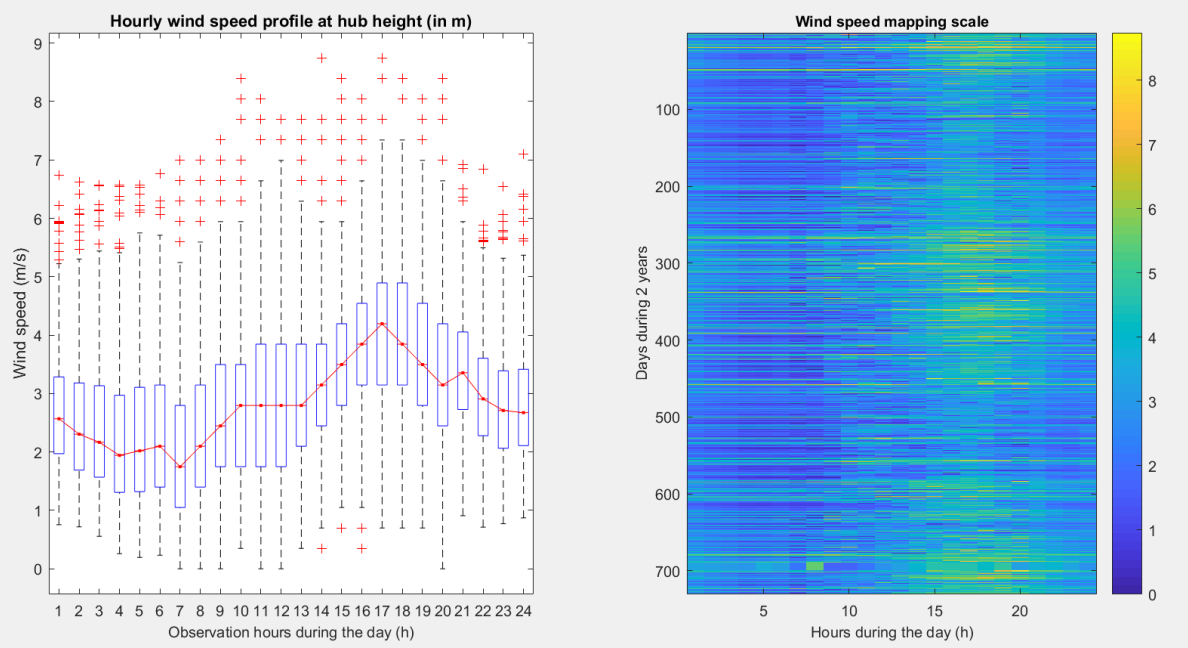

FIGURE 3.2 – Wind speed profile

According to the Global Wind Atlas (*https ://globalwindatlas.info/*), Mozambique does not have a significant global wind energy potential when compared to countries such as Ireland, Denmark, and those of the regions of North Africa and the south of Latin America.
The behavior of the average wind speed intensity curve shows that Mozambique is a country with moderate wind potential, according to [15] Mozambique has a medium-low intensity wind regime with a speed predominantly between 4 and 6 meters per second at a height of 80 meters above ground level, which, despite not being an expressive potential, gives Mozambique a confirmed equivalent wind power potential of 5 GW.

The hourly distribution of the average wind speed illustrated in figure 3.2 illustrates the existence of outliers (indicated by red crosses at each hour) that indicate the occurrence of extreme or unusual weather events. Mozambique's wind potential, which is not very expressive, demands a careful choice of Wind Turbine Generator (WTG) to maximize power generation.

3.3.4.2 | Solar radiation input data

Mozambique has a very high solar potential, a consistent solar radiation regime is available throughout the entire territory, placing Mozambique as one of the countries with the highest solar potential in the world [69]. Figure 3.3 illustrates the distribution of hourly solar radiation data with a significant variation over the hours of the day, the maximum average of solar radiation G is observed around 13 :00 in the afternoon.

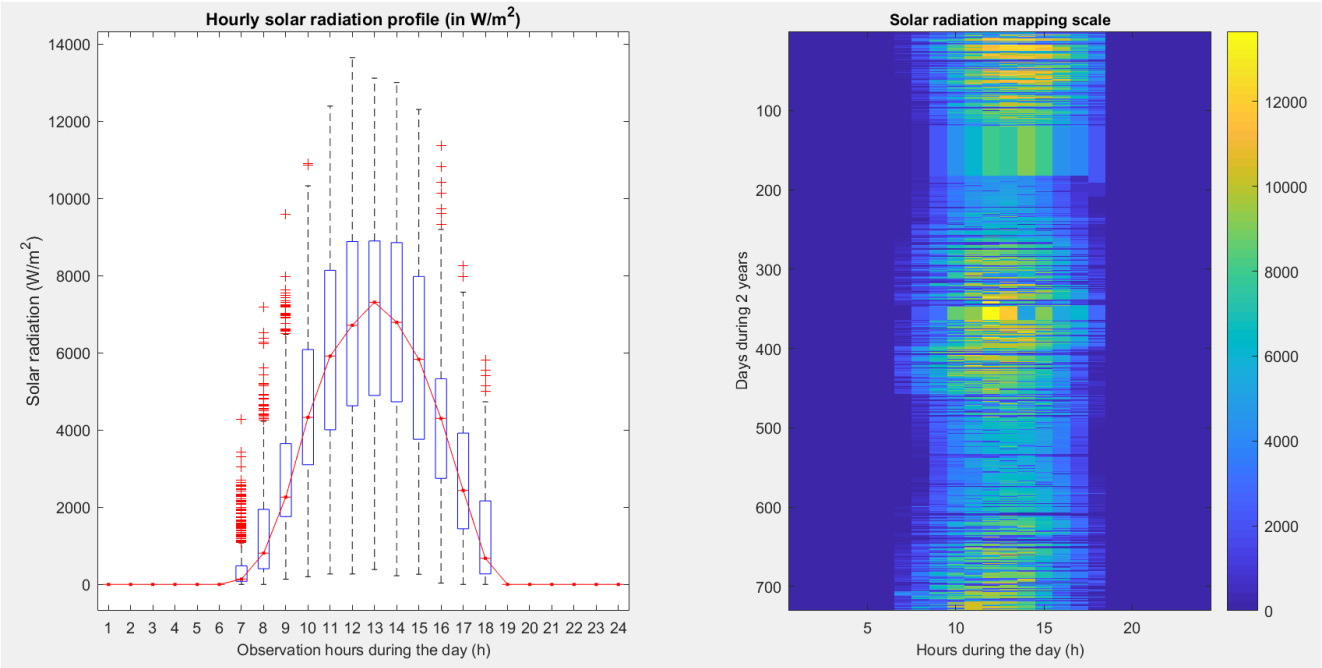

FIGURE 3.3 – Solar radiation profile

According to [15] solar radiation is the main renewable resource available in Mozambique, the global radiation in the horizontal plane varies between 1785 and 2206 kWh.m^{-2}.year^{-1}, is one of the highest in the world, giving Mozambique a global solar power equivalent to 23 TWp. The behavior of the average curve of the hourly distributions of solar radiation, show that the maximum output power of the PVG is most likely at 13h00 including surrounding hours.

3.3.4.3 | Ambient temperature input data

Mozambique is generally a country with a predominantly humid tropical climate throughout the year with average annual temperatures above 20°C ranging between 24°C and 26°C [71]. In this context, the distribution of the average hourly temperature in Maputo is illustrated in the following figure 3.4 :

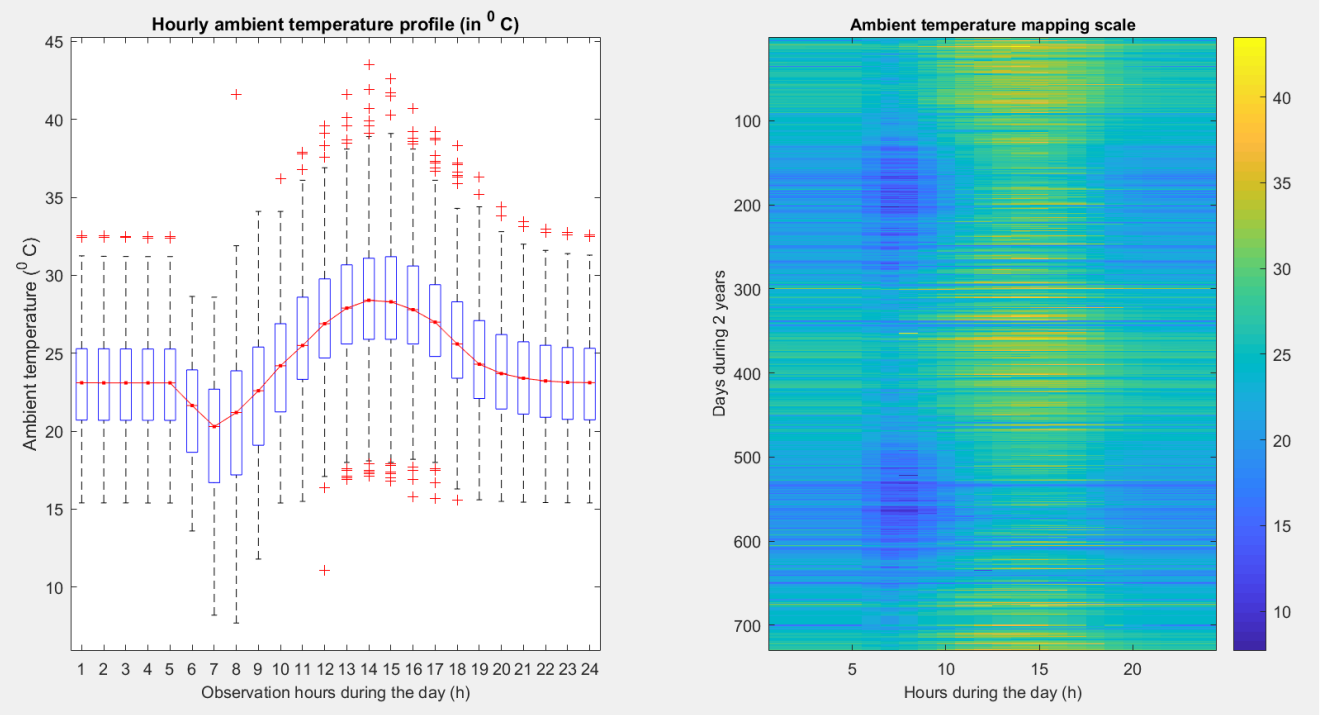

FIGURE 3.4 – Ambient temperature profile

According to [71] the average maximum temperature in Maputo is around 24^0C, rarely dropping below 20^0C or rising above 29^0C, and daily minimum temperatures hover around 17^0C, rarely dropping to 14^0C or rising above 20^0C. In this sense, the hourly temperature data used in this thesis (curve of figure 3.4) are reasonably adjusted to the intervals described in [71], thus, by evaluating the data from the solar panel manufacturers' catalogs, it can be said that the Maputo province in Mozambique (where the data were collected) has considerable solar potential for the installation of a PVG farm to generate power mainly in the afternoon as illustrated by the behaviour of the curve of average distributions shown in figure 3.4.

3.3.5 | Input data versus output data

In HSWPGS microgrid, wind speed v, solar radiation G and ambient temperature t_a are the variables connecting the microgrid to the environment to generate power, wind speed feeds the WTG to generate output power P_{wtg}, and solar radiation and ambient temperature feed the PVG to generate output power P_{pvg}. The following section 3.4 describes the models and the results obtained in the modeling of the output power P_{wtg} and P_{pvg}.

3.4 | RES-to-Power Conversion

3.4.1 | Wind-to-Power Conversion

This subchapter addresses the conversion of available wind power into electrical power, maximizing the wind potential available at the WTG farm site depends on the correct selection (or choice) of the WTG with parameters that best fit the wind profile of the site, since the output power performance curve should be compatible with the wind speed profile of the location. The output power of a WTG depends not only on the wind speed v at the installation site, but also depends on the parameters of the output power performance curve, especially in the non-linear part of the curve between the cut-in speed v_{ci} and the rated speed v_r.
After evaluating the wind profile illustrated in figure 3.2, which consisted essentially in verifying the prevailing minimum, average and maximum values, for this thesis the **ENERCOM E-53, 800 kW** is selected with the following technical specifications and test data provided by the manufacturer :

Wind (m/s)	Power P (kW)	Power Coef. C_p (dimensionless)
1	0.0	0.00
2	2.0	0.19
3	14.0	0.39
4	38.0	0.44
5	77.0	0.46
6	141.0	0.48
7	228.0	0.49
8	336.0	0.49
9	480.0	0.49
10	645.0	0.48
11	744.0	0.42
12	780.0	0.34
13	810.0	0.27
14	810.0	0.22
15	810.0	0.18
16	810.0	0.15
17	810.0	0.12
18	810.0	0.10
19	810.0	0.09
20	810.0	0.08
21	810.0	0.06
22	810.0	0.06
23	810.0	0.05
24	810.0	0.04
25	810.0	0.04

(a) Manufacturer's Test Data.

Parameter	Abbreviation	Value-Unit
Rated Power	P_r	800 kW
Rotor diameter	d_r	52.9 m
Tower/Hub height	h	50 m
Cut-in speed	v_{ci}	2 m/s
Rated speed	v_r	13 m/s
Cut-out speed	v_{co}	25 m/s
Max Power Coeff.	C_p	0.49

(b) Technical specifications.

TABLE 3.1 – Technical information of ENERCON E-53, 800 kW [8, 9].

The test data provided by the manufacturer (table 3.1a) using the E-53 wind turbine generator (table 3.1b) can be graphically illustrated by the following figure 3.5 :

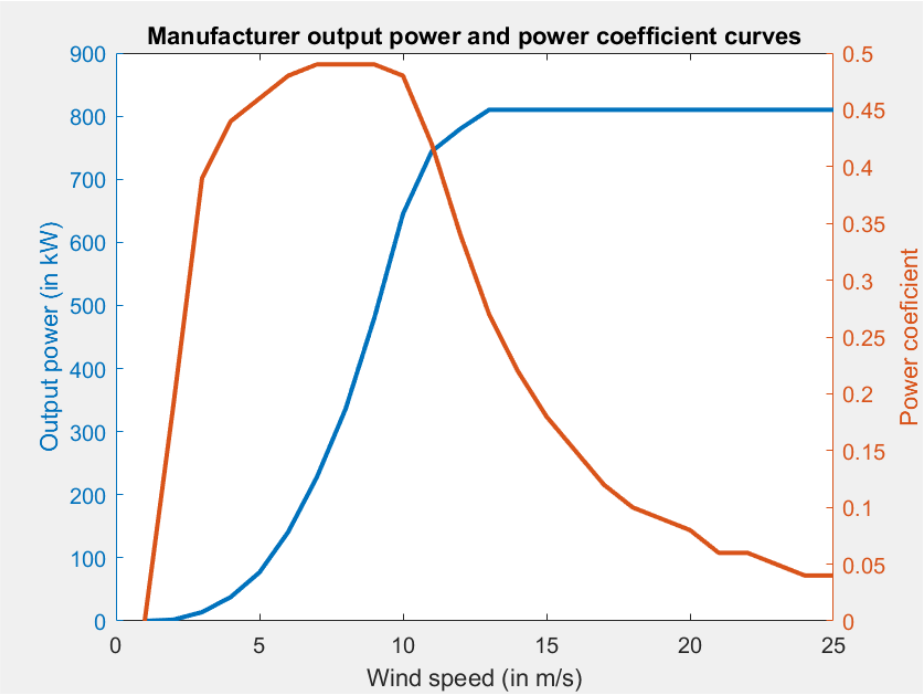

FIGURE 3.5 – Power curve and power coefficient curve of E-53, 800 kW

Applying the cubic spline interpolation method (described in section 2.9, Equation 2.11) on the test data provided by the manufacturer (table 3.1a) four piecewise functions were obtained that compose the conversion model from wind speed v to estimated output power of the wind turbine generator P_{wtg} graphically represented by figure 3.6 as :

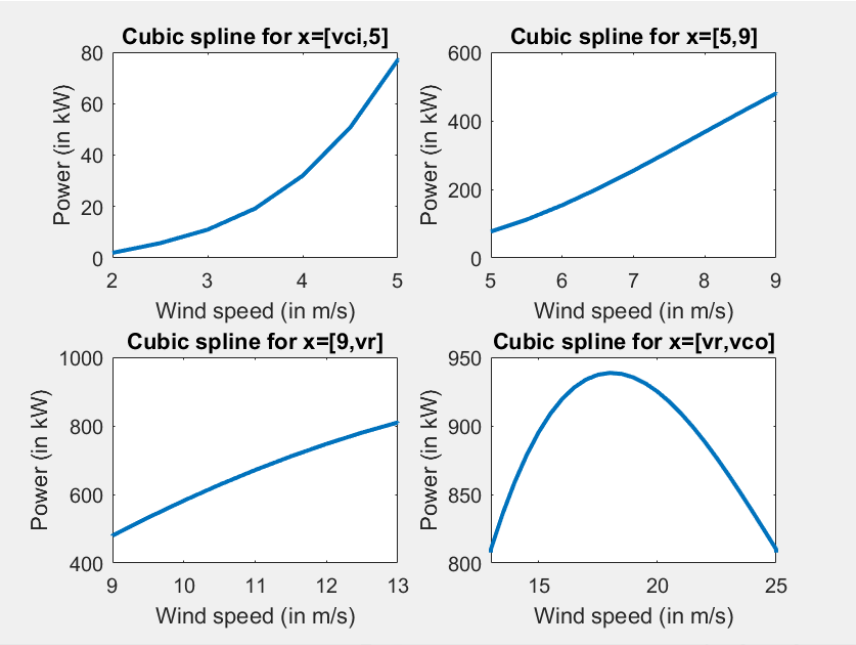

FIGURE 3.6 – Piecewise functions from manufacturer's test data

Combining (doing partial sums) of all four piecewise functions illustrated in Figure 3.6 we will obtain a complete model for converting wind speed v into estimated output power P_{wtg} of the E-53 Wind Turbine Generator (WTG) as shown in the curve of figure 3.7.

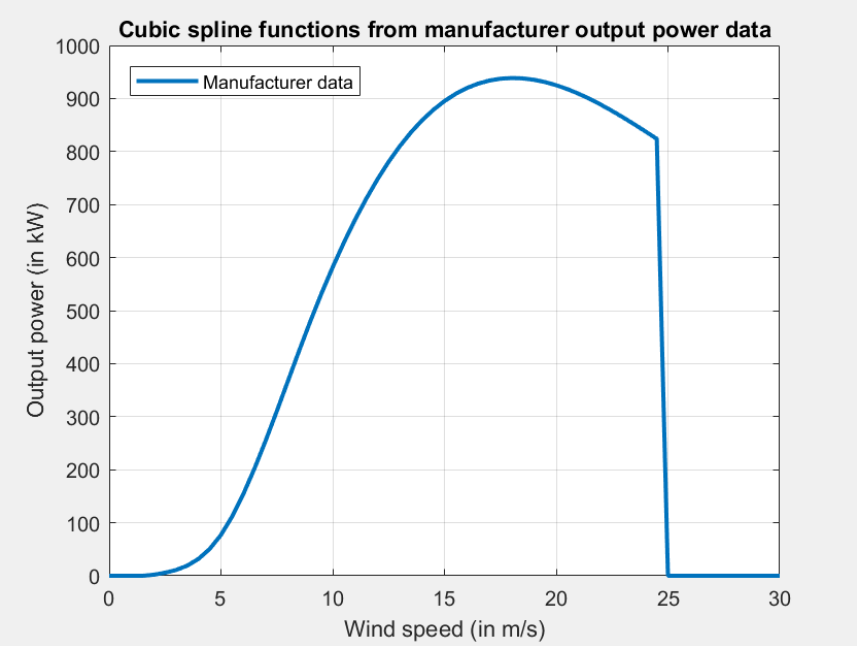

FIGURE 3.7 – Cubic spline function from manufacturer output power data

The mathematical model represented by the curve in figure 3.7 is the power performance curve of the E-53 WTG with technical specifications illustrated in table 3.1b. Is the model from which the wind speed v is converted to the estimated hourly output power in the 24 hours of a day over the two years (from January 1, 2019 to December 31, 2020). similarly to the wind speed data, the estimated power output of the WTG is structured in a column-oriented matrix form, generically represented as :

$$v_{(i,j)} = \begin{pmatrix} v_{1,1} & v_{1,2} & \cdots & v_{1,n} \\ v_{2,1} & v_{2,2} & \cdots & v_{2,n} \\ \vdots & \vdots & \ddots & \vdots \\ v_{m,1} & v_{m,2} & \cdots & v_{m,n} \end{pmatrix} \xrightarrow[\text{Conversion Model}]{\text{Wind-to-Power}} P_{wtg(i,j)} = \begin{pmatrix} P_{1,1} & P_{1,2} & \cdots & P_{1,n} \\ P_{2,1} & P_{2,2} & \cdots & P_{2,n} \\ \vdots & \vdots & \ddots & \vdots \\ P_{m,1} & P_{m,2} & \cdots & P_{m,n} \end{pmatrix} \tag{3.5}$$

Where, $v_{i,j}$ represents the matrix of hourly wind speed data with days and hours indexes (in m/s), $P_{wtg(i,j)}$ represents the estimated hourly power output of the WTG in kW, i represents observation days and j represents the observation hours.
Applying the wind-to-power conversion model represented by the curve in figure 3.7, the

WTG output power matrix was obtained, the hourly distributions are illustrated in figure 3.8 below :

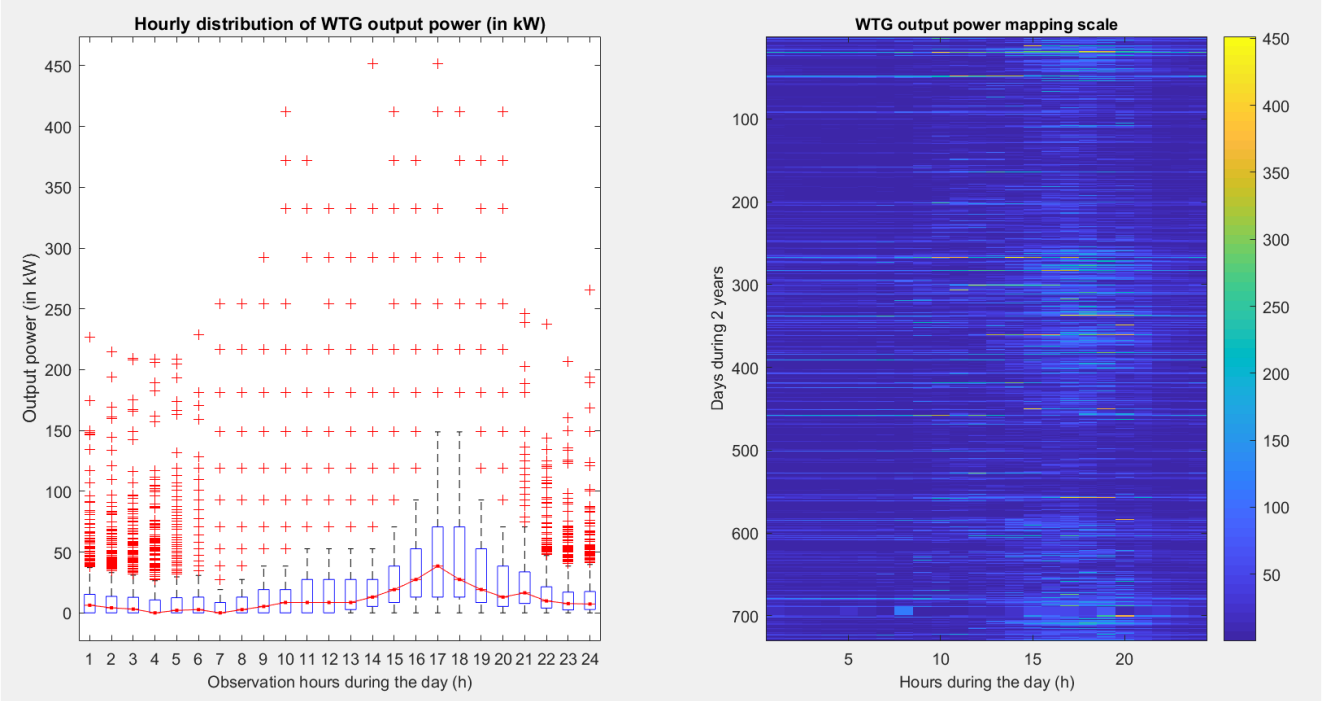

FIGURE 3.8 – Hourly distribution of WTG output power

3.4.2 | Solar-to-Power Conversion

Maximizing the solar potential available at the WTG farm site depends on the correct selection (or choice) of the photovoltaic cells with electrical parameters that best fit the solar radiation profile of the site, since the output power performance curve (P-V and I-V characteristics) should be compatible with the solar radiation profile of the location, however, the decision to select the type of photovoltaic panels is dependent on available information, often insufficient for an absolutely correct decision. In many cases, the decision on the selection of photovoltaic modules is made by the method of direct comparison of data from the manufacturers' catalogs, which obviously does not guarantee that the selected PV module is the best for a specific application, as this method ignores fundamentals aspects such as, deep knowledge about the resistance to losses, difference between the manufacturing and operating environments, in addition, comparison in absolute terms is always impossible [72].

In this thesis, the selection of the photovoltaic module was made through the direct comparison of catalogs from several manufacturers, evaluating electrical and temperature characteristics compatible with the solar radiation and ambient temperature input data available for this thesis. On this basis, the solar panel with the following characteristics is selected :

— **PV module name** :
RECOM 380 Wp, Mono crystalline module, Autarco MC-EU series solar pane : S1.MC305(B)-EU
— **Characteristics of the selected PV module**

Description	Abbrev	Value
Nominal power output (Wp)	P_{max}	305
Power output tolerance (W)	ΔP_{max}	$0/+3\%$
Open circuit voltage (V)	v_{oc}	39.76
Short circuit current (A)	I_{sc}	9.76
Max. power voltage (V)	V_{mp}	31.62
Max. power current (A)	I_{mp}	9.72
Module efficiency (%)	η	18.65

(a) electrical characteristics

Description	Abbrev	Value
I_{sc}	α	$+0.037\%/^0C$
V_{oc}	β	$-0.299\%/^0C$
P_{max}	Υ	$-0.416\%/^0C$
T_{NOCT}		$48^0(+/-2^\circ C)$
Temp range		-40^0C to 80^0C

(b) temperature characteristics

TABLE 3.2 – Technical information of Autarco MC-EU, S1.MC305(B)-EU

Based on solar radiation G and ambient temperature t_a data as input variables of the selected PVG whose electrical and temperature characteristics are illustrated in table 3.1, the estimated hourly output power of the $P_{pvg(i,j)}$ was obtained by the modeling procedure described in section 2.9.2. Similarly to the solar radiation data, the estimated power output of the PVG is structured in a column-oriented matrix form, generically represented as :

$$\left\{\begin{array}{l} G_{(i,j)} = \begin{pmatrix} G_{1,1} & G_{1,2} & \cdots & G_{1,n} \\ G_{2,1} & G_{2,2} & \cdots & G_{2,n} \\ \vdots & \vdots & \ddots & \vdots \\ G_{m,1} & G_{m,2} & \cdots & G_{m,n} \end{pmatrix} \\ ta_{(i,j)} = \begin{pmatrix} t_{1,1} & t_{1,2} & \cdots & t_{1,n} \\ t_{2,1} & t_{2,2} & \cdots & t_{2,n} \\ \vdots & \vdots & \ddots & \vdots \\ t_{m,1} & t_{m,2} & \cdots & t_{m,n} \end{pmatrix} \end{array}\right\} \xrightarrow[\text{Conversion Model}]{\text{Solar-to-Power}} P_{pvg(i,j)} = \begin{pmatrix} P_{1,1} & P_{1,2} & \cdots & P_{1,n} \\ P_{2,1} & P_{2,2} & \cdots & P_{2,n} \\ \vdots & \vdots & \ddots & \vdots \\ P_{m,1} & P_{m,2} & \cdots & P_{m,n} \end{pmatrix} \tag{3.6}$$

Applying the sequence of irradiance-to-power conversion models described in section 2.9.2, the PVG output power matrix was obtained, the hourly distributions are illustrated in figure 3.9 below :

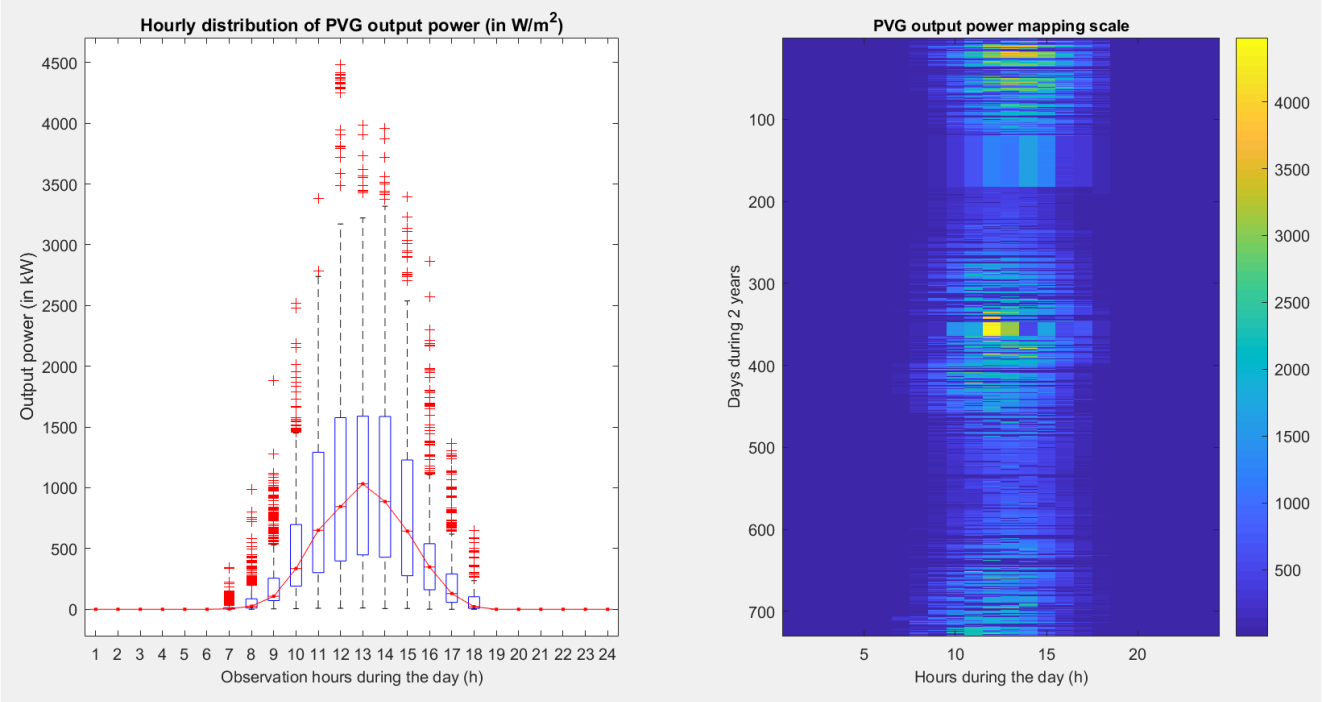

FIGURE 3.9 – Hourly distribution of PVG output power

3.4.3 | Comment on P_{wtg} and P_{pvg}

Making a comparative analysis between the input data curves and the output power curves, comparing wind speed and wind turbine output power curves, similarly, comparing the curves of solar radiation and the output power of the photovoltaic panel, a direct proportionality between the input variables and the output variables can be observed. The fluctuations observed in the input variables of wind speed and solar radiation are propagated by the system and can be proportionally observed in the output power of the wind turbine P_{wtg} and the photovoltaic generator P_{pvg}.

The power generated in each subsystem is an uncertain variable, as it varies instantaneously (in this case, hourly), depending on the variability of renewable resources, as a consequence of the instantaneous variation of the weather.

An important aspect to take into account is the fact that the output power of the wind turbine generator P_{wtg} and the output power of the photovoltaic generator P_{pvg} illustrated in figures 3.8 and 3.9 respectively, are both obtained through deterministic models. According to [54] deterministic models can hardly be perfect for the forecasting task, as they ignore the existence of sources of uncertainty, i.e., do not provide quantified uncertainty information. Therefore, to account for the persistently existing uncertainty caused mainly by the instantaneous variations of the RES (wind speed v and solar radiation G) It is essential to introduce an approach to modeling the propagation of uncertainty about the power produced and about the operating parameters of each subsystem, including risk analysis and probabilistic modeling.

3.5 | Modeling the demand load

The power consumption data used in this thesis are real consumption in the year 2018, in the isolated microgrid in the district of Mecula in the province of Niassa in northern Mozambique. In the process of modeling the demand load variation profile, we considered two scenarios, namely :

(i) Consumption of an essentially agrarian village without industrial units

(ii) Consumption of an agrarian village including industrial units

3.5.1 | Consumption of an agrarian village

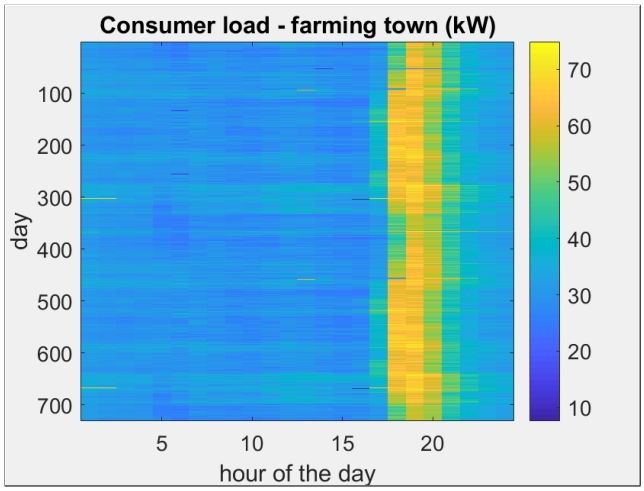

FIGURE 3.10 – Day-Hour consumption plot

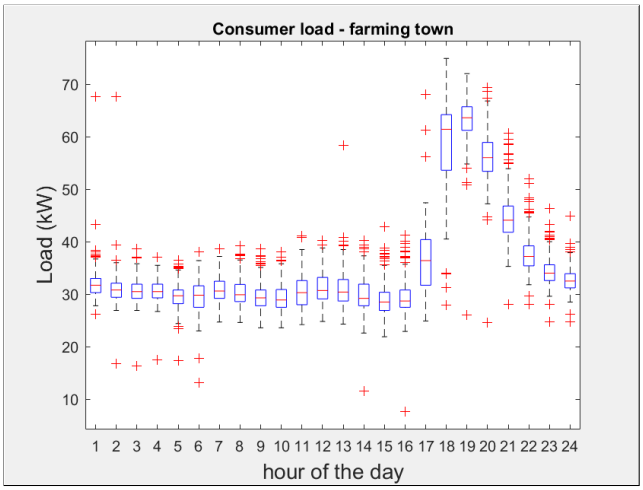

FIGURE 3.11 – Load as function of hour of the day

Figures 3.10 and 3.11 illustrate Consumer demand as a function of the hour of the day, in an agrarian village (kW)

The pattern of power consumption in Mozambique is intrinsically related to the way of life (habits and practices) and the socioeconomic conditions of local communities. In this case, the power consumption throughout the day has a very slight pattern of variation. The drastic increase in consumption (with some peaks in demand) is registered around 17 :00 (end of the day and beginning of the night), when communities return to their homes after their work activities throughout the day.

The mean value and the standard deviation of the consumer load over the two years are 35.3kW and 10.3kW respectively. The consumer lad shows high variations over the hours.

3.5.2 | Consumption of an industrial village

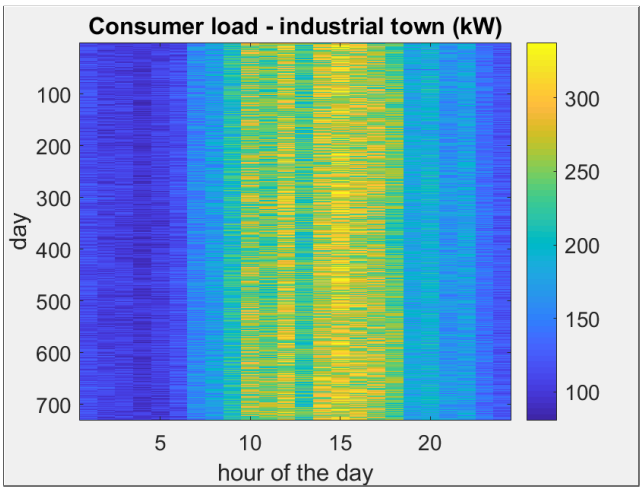

FIGURE 3.12 – Day-Hour consumption plot

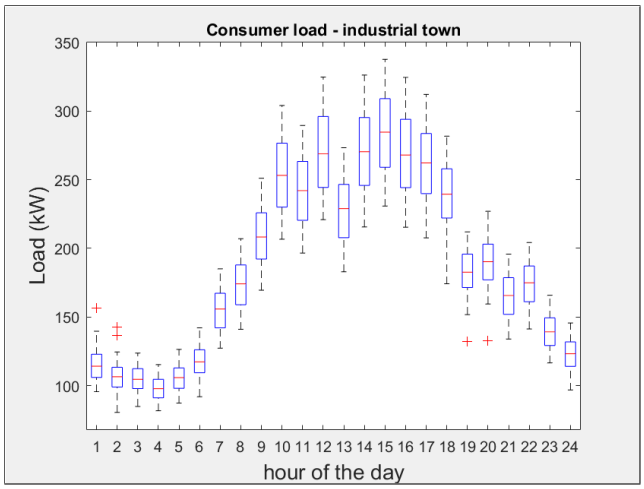

FIGURE 3.13 – Load depending on the hours of day

Figures 3.12 and 3.13 illustrate Consumer demand as a function of the hour of the day, in a somewhat industrialized village (kW).
The mean value and the standard deviation of the consumer load over the two years are 186.5kW and 65.4kW respectively. The consumer lad shows high variations over the hours.

If we consider the hypothesis of an agrarian village with small-scale industrial units, the power consumption curve has an increasing trend throughout the day (with peaks around midday) due to the increase in the intensity of industrial activities. At night, the power consumption curve has a downward trend, with minimal consumption due to low (or no) industrial activity. It is assumed that the minimum values observed are only the power consumption in the residential sector.

3.6 | Mathematical modeling the photovoltaic panel

The output power of a photovoltaic generator P_{pvg} depends fundamentally on two input variables, namely, solar radiation G and ambient temperature t_a [57, 73, 56], additionally, it is

characterized by operating parameters normally provided by the manufacturer. When deducing equations in the next step, all electric currents are in A, voltages in V, powers in W and temperatures in capital letter T in K, or temperature in lowercase letter t in °C.

3.6.1 | Parameters of the photovoltaic solar panel manufacturer

The photovoltaic panel is made of np parallel and ns series cells. The **input parameters** are characteristics of each *photovoltaic cell* or of the photovoltaic panel. The **characteristics of panel** are provided by the solar PV panel manufacturer :

— $Pmax$, the nominal power output (Wp : Watt peak at 1000 $\mathrm{W\,m^{-2}}$),
— Voc, the open-circuit voltage (V),
— Isc, the short-circuit current (A),
— $Vmpp$, the voltage at maximum power point (V),
— $Impp$, the current at maximum power point in (A),
— $kIsc$, the intensity current temperature coefficient, ($°C^{-1}$),
— $kVoc$, the voltage temperature coefficient ($°C^{-1}$),
— $kPmax$, the maximum power temperature coefficient ($°C^{-1}$),
— $tnmot$, the Nominal Operating Cell Temperature (K),
— ns, the number of series cells,
— np, the number of parallel cells,

These parameters are provided by the manufacturer under two conditions ass :

— *Nominal Operating Cell conditions :* $tnoc = 20°C$, for $Gnoc = 800\mathrm{W\,m^{-2}}$ solar irradiance.
— *Standard testing conditions :* $tstd = 25°C$, for $Gstd = 1000\mathrm{W\,m^{-2}}$ solar irradiance.

The table below illustrates in detail the electrical and thermal characteristics of the selected photovoltaic cell.

RECOM - Black Panther Mono crystalline module RCM-380-6MA		
Electrical characteristics		
Testing conditions	STC	NMOT
P_{max}, nominal power output (Wp at 1000 $watt.m^{-2}$)	380	284.2
V_{mpp}, maximum power voltage (V)	40.1	37.3
V_{mpp}, maximum power current (A)	9.48	7.62
V_{oc}, open-circuit voltage (V)	48.5	45.3
I_{sc}, short-circuit current (A)	9.93	8.02
Thermal characteristics		
kP_{max}, P_{max} temperature coefficient ($^0C^{-1}$)	-0.37%	
$kVoc$, Voc temperature coefficient ($^0C^{-1}$)	-0.34%	
kI_{sc}, I_{sc} temperature coefficient ($^0C^{-1}$)	+0.06%	
Operating temperature (^0C)	-40 to +85	
t_{noct}, Nominal Operating Temperature (NMOT, ^0C)	42 ± 2	
G, irradiance ($watt/m^{-2}$)	$Gstd = 1000$	$Gnoc = 800$
t, irradiance (^0C)	$tstd = 25$	$tnoc = 20$

TABLE 3.3 – Manufacturer characteristics of a photovoltaic panel (mono crystalline module). The panel performance declines linearly of 0.65% on 2-25 years. The module efficiency is 19.2%.

The photovoltaic cell parameter data provided by the manufacturer provide three notable points of the I-V characteristic to consider, namely :

— For $I = 0$, we have the Open-Circuit Voltage at $(V_{oc}, 0)$
— For $V = 0$, we have the Short-Circuit Current at $(0, I_{sc})$
— Power = P_{max} at (V_{mpp}, I_{mpp})

3.6.2 | Photovoltaic solar panel model

A simple photovoltaic cell can be represented by an electrical equivalent circuit as shown in Figure 3.14 below.

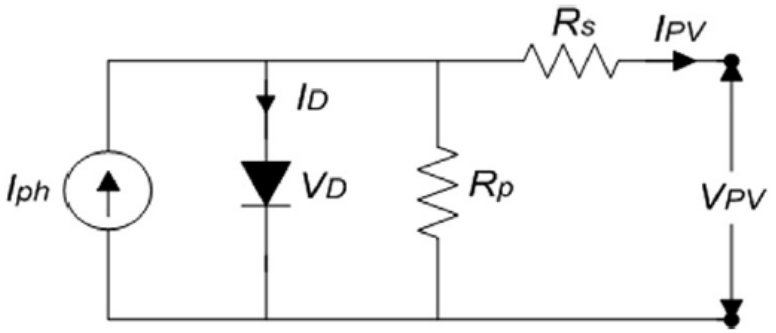

FIGURE 3.14 – The electrical equivalent circuit of a photovoltaic cell [3, 6].

It is important to highlight that the electrical circuit in figure 3.14 represents a simple photodiode (or photocell), a solar panel is composed of a set of photodiodes connected in series or in parallel. According to [6], the number of cells connected in parallel n_p is directly proportional to the photovoltaic current I_{ph} (the greater the number of photovoltaic cells connected in parallel, the greater the photovoltaic current), while, photovoltaic cells connected in series n_s are directly proportional with the output voltage of a photodiode V_{ph} (the greater the number of photovoltaic cells connected in series, the greater the output voltage of the photodiode).

The characteristic I-V equation deduced from the basic electrical circuit of a photovoltaic cell ilustrated in figure 3.14 bellow, can be expressed as [74] :

$$\boxed{I = Iph - I0\left[\exp\left(\frac{V + RsI}{ns.V_t.a}\right) - 1\right] - \frac{V + RsI}{Rp}}, \tag{3.7}$$

Where :
Iph is the photovoltaic current produced by solar irradiance, $I0$ is the reverse saturation current of the array (leakage current), Rs and Rp are the equivalent series and parallel electrical resistances of the array, and a is an ideality constant which depends on the technology used to produce the panels as ilustrated in the table 3.4 below [10] :

Technology	Value of "a"
Si-mono	1.2
S-poly	1.3
a-Si :H	1.8
a-Si :H tandem	3.3
a-Si :H triple	5
CdTe	1.5
CIS	1.5
AsGa	1.3

TABLE 3.4 – Diode ideality constant A as a function of the technology of the photo-voltaic cell [10, 11].

In equation 3.7, the parameter V_t represents the **temperature voltage** expressed as :

$$V_t = \frac{k_B \cdot Tc}{q} \tag{3.8}$$

where
$q = 1.60217646e-19\text{C}$ is the electron charge, $k_B = 1.3806503e-23\text{J K}^{-1}$ is the Boltzmann constant. T_c is the temperature of the cell (supposed to be the junction temperature).
The photocell converts solar radiation s into photovoltaic current I_{ph}, however, it is influenced by the ambient temperature T_a. The temperature of the photovoltaic cell T_C can be expressed as :

$$Tc = Ta + (t_{nmot} - t_{noc}) \cdot \frac{G}{G_{noc}}, \tag{3.9}$$

Where :
G is the solar irradiation, $Gnoc$ and $tnoc$ are the solar irradiation and the temperature in the nominal operating condition, and t_{nmot} is the operating temperature.

The solar panels are connected in series, which allows increasing the voltage in order to meet the minimum operating requirements of the inverter. If the solar modules were connected in parallel, the positive terminal of one module is connected to the positive terminal of another module, which increases the amperage of the system, that's why we highlight equations for solar panels connected in series.

3.6.2.1 | Remarkable points

The $I-V$ characteristic of the photovoltaic panel pass through the remarkable points :

— $(0, Isc)$, therefore :

$$I_{sc} = Iph - I0\left[\exp\left(\frac{Rs.Isc}{ns.Vt.a}\right) - 1\right] - \frac{Rs.Isc}{Rp}, \tag{3.10}$$

— $(Voc, 0)$:

$$0 = Iph - I0\left[\exp\left(\frac{Voc}{ns.Vt.a}\right) - 1\right] - \frac{Voc}{Rp}. \tag{3.11}$$

— $(vmpp, impp)$ where the power is equal to $pmax$:

$$impp = I_{ph} - I0\left[\exp\left(\frac{v_{mpp} + R_s.i_{mpp}}{ns.Vt.a}\right) - 1\right] - \frac{vmpp + R_s \cdot i_{mpp}}{R_p}, \tag{3.12}$$

— Moreover the maximum of the $P-V$ characteristic occurs at the remarkable point $(vmpp, impp)$. The power is :

$$\boxed{P = V.I = V.Iph - V.I0\left[\exp\left(\frac{V + RsI}{ns.Vt.a}\right) - 1\right] - V.\frac{V + Rs.I}{Rp}}. \tag{3.13}$$

Therefore :

$$\begin{aligned} pmax &= vmpp.Iph - vmpp.I0\left[\exp\left(\frac{vmpp + Rsimpp}{ns.Vt.a}\right) - 1\right] \\ &\quad -vmpp.\frac{vmpp + Rs.impp}{Rp} \end{aligned} \tag{3.14}$$

— The maximum of $P-V$ curve occurs at the vanishing of the derivative dP/dV. The derivative $dP/dV = 0$ will provide extreme points, however, in this case only the maximum power is of interest, thus $P_{max} = max\left(\frac{dP}{dV} = 0\right)$, where $\frac{dP}{dV}$ is expressed as :

$$\begin{aligned} \frac{dP}{dV} &= -\frac{(Is.Rp.Vt + Is.Rp.V)\exp\left(\frac{V}{ns.Vt.a} + \frac{I.Rs}{Vt}\right)}{Rp.ns.Vt.a} - \\ &\quad \frac{(2V + I.Rs + (-Is - Iph).Rp)\, ns.Vt.a}{Rp.ns.Vt.a}. \end{aligned} \tag{3.15}$$

Therefore, we obtain :

$$0 = -\frac{(Is.Rp.ns.Vt.a + Is.Rp.vmpp)\exp\left(\frac{vmpp}{ns.Vt.a} + \frac{impp.Rs}{ns.Vt.a}\right)}{Rp.ns.Vt.a} - \frac{(2vmpp + impp.Rs + (-Is - Iph).Rp)\, ns.Vt.a}{Rp.ns.Vt.a} \tag{3.16}$$

Remark 3.1. Therefore, we have four equations that can be used to calculate the unknowns $(Iph, I0, Rs, Rp)$ and possibly a. These equations are not linear.

In the following we will use the above equations to find the unknowns. For this we will use Particle Swarm Optimization Method, bio-inspired algorithm that searches for an optimal solution in the solution space.i.e., iteratively optimizes a problem improving a candidate solution in relation to a known measure of quality. To find the intervals of search, firstly, we have to evaluate some approximated solutions.

3.6.3 | Approximated solution

In many papers, the above model is simplified using the condition $Rp \to \infty$. In Ref. [1], the approximated Eq. 3.7 if Rp tends toward infinity is given :

$$\boxed{I = I_{ph} - I0 \cdot \left[\exp\left(\frac{V + R_s \cdot I}{n_s \cdot V_t \cdot a}\right) - 1\right] - \underbrace{\frac{V + R_s \cdot I}{R_p}}_{=0}}, \quad \text{neglected term} \tag{3.17}$$

The equivalent circuit is shown in Fig. 3.15.

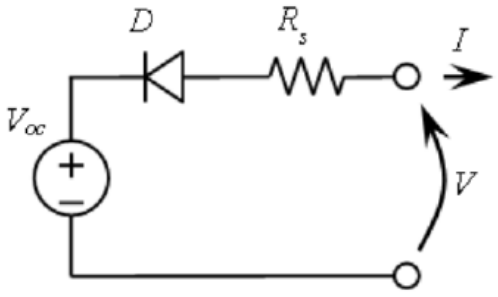

FIGURE 3.15 – Equivalent circuit of the simplified model of photovoltaic cell [1].

In this case, we obtain the simplification of Eq. 3.7 :

$$\boxed{I = I_{ph} - I_0 \cdot \left[\exp\left(\frac{V + R_s \cdot I}{n_s \cdot V_t \cdot a}\right) - 1\right]}. \tag{3.18}$$

The $V - I$ characteristic is therefore :

$$\boxed{V = n_s \cdot a \cdot V_t \ln\left(\frac{I_{ph}}{I_0} + 1 - \frac{I}{I_0}\right) - R_s \cdot I} \tag{3.19}$$

The simplified equation is consistent with the constraints of the $I - V$ and $P - V$ characteristics going through the *remarkable points* :

— $0 = I_{ph} - I_0 \left[\exp\left(\frac{V_{oc}}{n_s \cdot V_t \cdot a}\right) - 1\right]$, from which, we deduce the necessary condition :

$$\boxed{I_0 = \frac{I_{ph}}{\exp\left(\frac{V_{oc}}{n_s \cdot V_t \cdot a}\right) - 1}}. \tag{3.20}$$

— $I_{sc} = I_{ph} - I_{ph}\frac{\exp\left(\frac{R_s \cdot I_{sc}}{n_s \cdot V_t \cdot a}\right) - 1}{\exp\left(\frac{V_{oc}}{a \cdot V_t}\right) - 1}$. then :

$$\boxed{Iph = I_{sc}\frac{\exp\left(\frac{V_{oc}}{n_s \cdot V_t \cdot a}\right) - 1}{\exp\left(\frac{V_{oc}}{n_s \cdot V_t \cdot a}\right) - \exp\left(\frac{R_s \cdot I_{sc}}{n_s \cdot V_t \cdot a}\right)}}. \tag{3.21}$$

If $\frac{R_s \cdot I_{sc}}{n_s \cdot V_t \cdot a} \to 0$, then $I_{ph} = I_{sc}$: This equation is often used in the literature as a prior condition, however, its origin still causes intense debate. To find this equality, we have to consider the condition $\lim_{Rs \to 0}$ while Rs is small but not negligible. Actually, $\lim_{Rs \to 0} \Rightarrow I_{ph} = I_{sc}$.

— The remarkable point of $I - V$ characteristic : $(impp, vmpp)$.

$$impp = Iph - I0 \left[\exp\left(\frac{vmpp + Rs.impp}{ns.Vt.a}\right) - 1\right], \tag{3.22}$$

that we rewrite using previous results :

$$\boxed{i_{mpp} = I_{sc}\frac{\exp\left(\frac{V_{oc}}{n_s \cdot V_t \cdot a}\right) - \exp\left(\frac{v_{mpp} + R_s . i_{mpp}}{n_s . V_t \cdot a}\right)}{\exp\left(\frac{V_{oc}}{n_s \cdot V_t \cdot a}\right) - \exp\left(\frac{R_s \cdot I_{sc}}{n_s \cdot V_t \cdot a}\right)}} \tag{3.23}$$

Remark 3.2. The maximum power $pmax$ can be expressed by using the $I-V$ characteristic :

$$p_{max} = v_{mpp} \cdot I_{ph} - v_{mpp}.\frac{I_{ph}}{\exp\left(\frac{V_{oc}}{n_s \cdot V_t \cdot a}\right) - 1}\left[\exp\left(\frac{v_{mpp} + R_s.i_{mpp}}{n_s \cdot V_t \cdot a}\right) - 1\right] \tag{3.24}$$

We can conclude that $p_{max} \neq v_{mpp} \cdot i_{mpp}$. Note that the values of i_{mpp}, v_{mpp} and p_{max} are indicated in the manufacturer data-sheet.

— Finally, the maximum of power is reached if its derivative vanishes. Therefore :

$$0 = I_{ph} + I_0 - I_0 \exp\left(\frac{v_{max} + Rs \cdot i_{mmpp}}{n_s \cdot V_t \cdot a}\right)\left(1 + \frac{v_{mpp}}{n_s \cdot a \cdot Vt}\right) \tag{3.25}$$

This approximation gives an explicit equation of the perfect photovoltaic panel, by removing the resistances from the model. The voltage can be calculated for $Rp \to \infty$:

$$V = n_s \cdot a \cdot Vt \ln\left[\exp\left(\frac{V_{oc}}{n_s \cdot a \cdot V_t}\right) + \frac{I}{I_{sc}}\left(1 - \exp\left(\frac{V_{oc}}{n_s \cdot Vt \cdot a}\right)\right)\right] \tag{3.26}$$

$$= \boxed{V_{oc} + n_s \cdot a \cdot Vt \ln\left[1 - \frac{I}{I_{sc}} + \frac{I}{I_{sc}} \exp\left(-\frac{V_{oc}}{n_s \cdot V_t \cdot a}\right)\right]} \tag{3.27}$$

The influence of R_p and R_s was studied [75]. Actually, the typical value of Rp and Rs are given in Ref. [75] as well as an iterative method to determine their values from the parameters. The minimum of Rp was evaluated from the slope of the line segment between the short-circuit and the maximum-power points of the cell electrical characteristic :

$$\min(R_p) = \frac{v_{mpp}}{I_{sc} - i_{mpp}} - \frac{V_{oc} - v_{mpp}}{i_{mpp}}. \tag{3.28}$$

This minimum could help to check the validity of the assumption $R_p \to \infty$.

This last equation gives :

$$R_s = -\frac{v_{mpp}}{i_{mpp}} + \frac{n_s \cdot a \cdot V_t}{i_{mpp}} \ln\left(\frac{(I_{ph} + I_0) \cdot n_s \cdot a \cdot V_t}{I0(v_{mpp} + n_s \cdot a \cdot V_t)}\right) \tag{3.29}$$

3.6.4 | Approximated equation : if $R_p \to \infty$

The present approach consists in considering the limit of the $I-V$ characteristic from the beginning of calculations. We will get different results from those.

Moreover, Rs appearing in linear form in Eq. 3.29 as well as argument of exponential, another assumption is required to calculate analytically these quantities :

$$\frac{I_{sc}.R_s}{n_s \cdot a \cdot V_t} << 1 \quad \Rightarrow \quad \exp\left(\frac{I_{sc} \cdot R_s}{n_s \cdot a \cdot Vt}\right) \approx 1. \tag{3.30}$$

This condition may be simply expressed as $\boxed{Rs \to 0}$. Under this condition, Eqs. 3.31-3.32 do not involve exponential of Rs anymore. The following equations are no more coupled by Rs :

$$I_{ph} \approx \frac{I_{sc}\left[\exp\left(\frac{V_{oc}}{n_s \cdot aVt}\right) - 1\right]}{\exp\left(\frac{V_{oc}}{n_s \cdot a.V_t}\right) - 1} = I_{sc} \tag{3.31}$$

$$I_0 \approx \frac{I_{sc}}{\exp\left(\frac{V_{oc}}{n_s a.V_t}\right) - 1} \tag{3.32}$$

$$R_s = -\frac{v_{mpp}}{i_{mpp}} + \frac{n_s \cdot a \cdot V_t}{i_{mpp}} \ln\left(\frac{(I_{ph} + I_0) \cdot n_s \cdot a \cdot V_t}{I0(v_{mpp} + n_s \cdot a \cdot Vt)}\right) \tag{3.33}$$

The additional assumption [1] :

$$\exp\left(-\left(\frac{V_{oc}}{n_s \cdot a \cdot V_t}\right)\right) << 1 \tag{3.34}$$

is used to simplify the second equation : and therefore the $I - V$ characteristic.

$$I0 \approx Isc.\exp\left(-\left(\frac{Voc}{ns.a.Vt}\right)\right) \tag{3.35}$$

$$\tag{3.36}$$

This set of equations can be used to calculate the $I - V$ characteristic, provided the assumptions validity check.

$$I = Isc - Isc\left[\exp\left(\frac{V - V0 + RsI}{ns.Vt.a}\right) - 1\right]. \tag{3.37}$$

with :

$$\begin{aligned} Rs &= -\frac{vmpp}{impp} + \frac{ns.a.Vt}{impp} \ln\left(\frac{\left(1 + \exp\left(-\left(\frac{Voc}{ns.a.Vt}\right)\right)\right).ns.a.Vt}{\exp\left(-\left(\frac{Voc}{ns.a.Vt}\right)\right)(vmpp + ns.a.Vt)}\right) \\ &\approx \frac{Voc - vmpp}{impp} + \frac{ns.a.Vt}{impp} \ln\left(\frac{ns.a.Vt}{vmpp + ns.a.Vt}\right) \end{aligned} \tag{3.38}$$

The $V - I$ characteristic is therefore :

$$V = ns.a.Vt \ln\left(\frac{Isc - I}{Isc \exp\left(-\left(\frac{Voc}{ns.a.Vt}\right)\right)} + 1\right) - Rs.I \tag{3.39}$$

$$= Voc + ns.a.Vt \ln\left(1 - \frac{I}{Isc} + \exp\left(-\left(\frac{Voc}{ns.a.Vt}\right)\right)\right) - Rs.I \tag{3.40}$$

$$\approx Voc + ns.a.Vt \ln\left(1 - \frac{I}{Isc}\right) - Rs.I \tag{3.41}$$

Let us detail the relationship between the manufacturer data and the quantities in Eq. 3.7. In the case of the RCM-380-MA panel (Tab. 3.3), the module is mono-cristalline and therefore $a = 1.2$.
$Vt.a$ can be calculated independently of the manufacturer data.
$I0$ is the reverse saturation current of the diode (leakage current) :

$$I_0 = \frac{Isc}{\exp\left(\frac{Voc}{ns.a.Vt}\right) - 1}\left(\frac{Tc}{Tnoc}\right)^3 \exp\left[\frac{q \cdot Eg}{k_B \cdot a}\left(\frac{1}{Tnoc} - \frac{1}{T_c}\right)\right], \tag{3.42}$$

with I_{sc} the short-circuit current and Eg is the gap energy of the semiconductor (about 1.12eV), $q = 1.60217646e - 19\text{C}$ is the electron charge, $k_B = 1.3806503e - 23\text{J K}^{-1}$ is the Boltzmann constant, V_t is the thermal voltage, a is the diode ideality constant. The gap energy of the semiconductor Eg can be expressed as a function of the maximum operating temperature (see Eq. (7) in Ref. [75]). However, another way to define I_0 as a function of the manufacturer datasheet has been proposed.

3.6.5 | Overview of the model in Ref. [1]

In Ref. [3], the implicit equation 3.7 has been solved by using specific methods such as maximum power point tracking (MPPT) technique. These methods are time consuming, therefore we will turn us to a more simple model (simplified model of photovoltaic panel) close to that proposed in Ref. [1].

$$I = I_{ph} - I_0\left[\exp\left(\frac{V + R_s \cdot I}{n_s.V_t.a}\right) - 1\right] - \frac{V + R_s \cdot I}{R_p},$$

Iph is the photovoltaic current produced by solar irradiance G (W m^{-2}). I_{sc} is *the nominal short-circuit current*, given in the manufacturer datasheet [75, 1] :

$$I_{ph} = I_{sc}. \tag{3.43}$$

The dependence of the photo-current to the solar irradiation will be introduced later. To overpass the introduction of additional quantity Eg and to connect the $(I-V)$ characteristic to the manufacturer data, a remarkable point $(Voc, 0)$ is replaced in Eq. 3.7. The first assumption is $\boxed{Rp \to \infty}$. The consequences are :

— $Iph = Isc$

with :

$$0 = I_{sc} - I0\left[\exp\left(\frac{Voc}{ns.Vt.a}\right) - 1\right] - \frac{Voc}{Rp}. \tag{3.44}$$

The additional term Voc / Rp is neglected to get explicit equation and to solve it in explicit form [75] :

$$I_0 = \frac{Isc - \frac{Voc}{Rp}}{\exp\left(\frac{Voc}{ns.Vt.a}\right) - 1} \approx \frac{I_{sc}}{\exp\left(\frac{V_{oc}}{n_s \cdot V_t \cdot a}\right) - 1}. \tag{3.45}$$

The $I-V$ characteristic is therefore :

$$I = I_{sc} - \frac{I_{sc}}{\exp\left(\frac{V_{oc}}{n_s \cdot V_t \cdot a}\right) - 1}\left[\exp\left(\frac{V + R_s \cdot I}{n_s \cdot V_t \cdot a}\right) - 1\right].$$

Additional assumption is made in Ref. [1] :

$$\boxed{\exp\left(-\frac{V_{oc}}{n_s \cdot V_t \cdot a}\right) << 1}.$$

Therefore :

$$I = I_{sc}\left[1 - \exp\left(\frac{V - V_{oc} + R_s \cdot I}{n_s \cdot V_t \cdot a}\right)\right].$$

3.6.6 | The temperature dependence

The temperature dependence of $I0$ is given with slight modification of Eq. (6) in [75] for $kIsc$). Voc is replaced by $Voc(1 + k \cdot Voc \cdot (t_c - t_{noc}))$ and Isc by $I_{sc}(1 + k \cdot I_{sc} \cdot (tc - tnoc)) \cdot G/Gnoc$, where $Gnoc$, $kIsc$ and $tnoc$ are given by the manufacturer, and ta is the ambient temperature.

$$I0 \approx \frac{Isc(1 + k \cdot Isc(tc - tnoc))}{\exp\left(\frac{Voc(1+k \cdot V_{oc}(t_c - t_{noc}))}{ns \cdot V_t \ a}\right) - 1} = \alpha Isc. \tag{3.46}$$

Therefore, the characteristic $I-V$ with $Rp \to \infty$ becomes :

$$\begin{aligned} I \;\approx\; & \mathbf{Isc}(1+\mathbf{kIsc}(tc-\mathbf{tnoc}))\frac{G}{\mathbf{Gnoc}} - \\ & \frac{\mathbf{Isc}(1+\mathbf{kIsc}(tc-\mathbf{tnoc}))\frac{G}{\mathbf{Gnoc}}}{\exp\left(\frac{\mathbf{Voc}(1+\mathbf{kVoc}(tc-\mathbf{tnoc}))}{\mathbf{ns.a.Vt}}\right)-1}\left[\exp\left(\frac{V+Rs.I}{\mathbf{ns}\frac{\mathbf{k_B T}}{\mathbf{q}}.\mathbf{a}}\right)-1\right] \end{aligned} \tag{3.47}$$

where the quantities written in boldface are known (manufacturer data, Tabs. 3.3 for example). The input parameters of this equation are the cell temperature tc, the solar irradiation G, and the variables are the current I and the voltage V. Knowing G and tc, a single couple (V, I) should be found.

Remark 3.3. This equation differs from Eq. (6) in Ref. [75], as the units of kI and kV in manufacturer data are $°C^{-1}$.

Rs and Rp are series and parallel electrical resistances (Ω). Two problems clearly appear in this equation. The first one is the implicit characteristic of the PV cell : the electric current appears in the exponential function as well as in linear terms of this equation. The second one is the lack of indication on Rs (and Rp values in manufacturer data). However, the remarkable points of the $I-V$ characteristic are used to calculate these quantities.

— We have already used the point $(Voc, 0)$ to deduce Is under the additional assumption

$$\frac{Voc}{Rp} << Isc - I0\left[\exp\left(\frac{Voc}{ns.Vt.a}\right)-1\right].$$

This assumption is consistent with the large value of Rp.

— The $I-V$ characteristic pass through the short-current circuit point $(Isc, 0)$. Therefore, we deduce :

$$\mathbf{Isc} \;=\; \mathbf{ff.Isc} - \mathbf{fi.Isc}\left[\exp\left(\frac{Rs.\mathbf{Isc}}{\mathbf{ns}\frac{\mathbf{k_B T}}{\mathbf{q}}.\mathbf{a}}\right)-1\right] - \frac{Rs.\mathbf{Isc}}{Rp} \tag{3.48}$$

with

$$\alpha = (1+\mathbf{kIsc}(tc-\mathbf{tnoc}))\frac{G}{\mathbf{Gnoc}}$$

and :

$$\beta = \frac{(1+\mathbf{kIsc}(tc-\mathbf{tnoc}))}{\exp\left(\frac{\mathbf{Voc}(1+\mathbf{kVoc}(tc-\mathbf{tnoc}))}{\mathbf{ns.a.Vt}}\right)-1}.$$

This equation is implicit in Rs and cannot be analytically solved.

— The power characteristic reach a maximum value through at $(Impp, Vmpp)$. Therefore, we deduce an explicit equation in Rp but implicit in Rs :

$$\begin{aligned}\frac{dVI}{dV}(Impp, Vmpp) &= -\frac{\beta Isc(vmpp + ns.a.Vt)\gamma}{Rp.ns.a.Vt} + \\ &\quad (\alpha+\beta)Isc - \frac{2vmpp + Rs.impp}{Rp} \\ &= 0, \end{aligned} \tag{3.49}$$

with $\gamma = \exp\left(\frac{vmpp+Rs.impp}{ns.a.Vt}\right)$. If we suppose that $pmax = impp.vmpp$ [3], we get another implicit equation, involving γ :

$$pmax = vmpp\left(-Isc.\beta.\gamma + Isc.\alpha - \frac{vmpp + Rs.impp}{Rp}\right) \tag{3.50}$$

These two equations can be solved to find Rs and Rp with an iterative method as proposed in Ref. [3]. A relationship between Rp and Rs is :

$$Rp = -\frac{a \cdot V_t \cdot v_{mpp}^2}{Isc.v_{mpp}^2\beta\gamma - ns.a.Vt(\beta.Isc.v_{mpp} + p_{max})} \tag{3.51}$$

$$= \frac{n_s \cdot a \cdot V_t \cdot v_{mpp}}{-I_{sc}.v_{mpp} \cdot \beta \cdot \gamma + n_s \cdot a \cdot V_t \cdot (\beta.I_{sc} + i_{mpp})} \tag{3.52}$$

$$= \frac{n_s \cdot a \cdot V_t \cdot v_{mpp}}{n_s \cdot a \cdot V_t \cdot i_{mpp} + I_{sc}.\beta(n_s \cdot a \cdot V_t - v_{mpp} \cdot \gamma)} \tag{3.53}$$

where Rs is hidden in γ, and $pmax = impp.vmpp$ was used in Eq. 3.53. We will give a simpler in the following subsection.

However, the goal of this study is to provide quick algorithms to evaluate the power produced by photovoltaic arrays. Consequently, we use some additional approximations to get analytical results and explicit equations.

3.6.7 | Rigorous simplified model

The assumptions of the simplified model used in Ref. [1] were : $Iph = Isc$, $\exp\left(-\frac{Voc}{ns.Vt.a}\right) << 1$ and $Rp \to \infty$. The equivalent circuit is shown in Fig. 3.15, page 61.

In this section, we will show that the underlying hypothesis $Rs \to 0$ ***is actually used to get the simplified model. Indeed, the model in Ref. [1] is a fitting of the ideal diode characteristic,***

and Rs ***is reintroduced after. Therefore,*** $ns.a.Vt$ ***will also be evaluated from the remarkable points of the characteristic.***

The influence of these resistances was studied [75]. Actually, the typical value of Rp and Rs are given in Ref. [75] as well as an iterative method to determine their values from the parameters.

3.6.7.1 | Analysis of the simplified I-V characteristic

If Rp value is large enough, the characteristic equation assuming $Iph = Isc$ becomes :

$$\boxed{I = I_{sc} - I_0 \left[\exp\left(\frac{V + R_s \cdot I}{n_s \cdot V_t \cdot a}\right) - 1\right] - \underbrace{\frac{V + R_s \cdot I}{R_p}}_{=0}^{\text{neglected term}},}$$

$I0$ is calculated in the same manner as in the full model, by using the $(0, Voc)$ remarkable point of the characteristic, without including the temperature dependence :

$$I_0 = \frac{Isc}{\exp\left(\frac{Voc}{ns.Vt.a}\right) - 1}. \tag{3.54}$$

Therefore :

$$I = I_{sc} - \frac{I_{sc}}{\exp\left(\frac{V_{oc}}{n_s \cdot V_t \cdot a}\right) - 1}\left[\exp\left(\frac{V + R_s \cdot I}{n_s \cdot V_t \cdot a}\right) - 1\right]. \tag{3.55}$$

The voltage is deduced to get simple calculations of the $I - V$ characteristic :

$$\begin{aligned} V &= n_s \cdot V_t \cdot a \ln\left[\exp\left(\frac{V_{oc}}{n_s \cdot V_t \cdot a}\right)\left(1 - \frac{I}{I_{sc}}\right) + \frac{I}{I_{sc}}\right] - R_s \cdot I \qquad (3.56)\\ &= n_s \cdot V_t \cdot a \ln\left[\exp\left(\frac{V_{oc}}{n_s \cdot V_t \cdot a}\right)\left(1 - \frac{I}{I_{sc}} + \frac{I}{I_{sc}}\exp\left(-\frac{V_{oc}}{n_s \cdot V_t \cdot a}\right)\right)\right] - R_s \cdot I \\ &= V_{oc} + n_s \cdot V_t \cdot a \ln\left[1 - \frac{I}{I_{sc}} + \frac{I}{I_{sc}}\exp\left(-\frac{V_{oc}}{n_s \cdot V_t \cdot a}\right)\right] - R_s \cdot I \qquad (3.57)\end{aligned}$$

The $I - V$ characteristic in Eq. 3.57 pass over the remarkable points $(V_{oc}, 0)$. On the contrary, $(0, I_{sc})$ does not belong to the curve as equation

$$0 = V_{oc} + n_s \cdot V_t \cdot a\left(-\frac{V_{oc}}{n_s \cdot V_t \cdot a}\right) - R_s \cdot I_{sc},$$

is verified only if the series resistance R_s vanishes. Therefore, the simplified model does not handle this remarkable point. The error on voltage for $I = I_{sc}$ is $-R_s \cdot I_{sc}$. We must verify that this quantity is small enough to reduce the error value.

3.6.7.2 | The electric power

The electric power is :

$$P = V \cdot I = V \left\{ I_{sc} - \frac{I_{sc}}{\exp\left(\frac{V_{oc}}{n_s \cdot V_t \cdot a}\right) - 1} \left[\exp\left(\frac{V + R_s \cdot I}{n_s \cdot V_t \cdot a}\right) - 1 \right] \right\} \tag{3.58}$$

$$\approx V \cdot I_{sc} \cdot \left[1 - \exp\left(\frac{V - V_{oc} + R_s \cdot I}{n_s \cdot V_t \cdot a}\right) \right]. \tag{3.59}$$

The electric power is close to that given in Eq. (2) of Ref. [3], where the term $-V_{pv}/N_s$ must be removed and "the value of R_s and R_p can be neglected".

The output power is multiplied by the fill factor ff which evaluates the maximum power produced by a solar panel :

$$ff = \frac{p_{max}}{V_{oc} \cdot I_{sc}}. \tag{3.60}$$

This unit less coefficient is a measure of the squareness of the $I - V$ characteristic.

The electric power is of interest as it opens the way of using additional quantities from the manufacturer sheet : p_{max}, v_{mpp} and i_{mpp}.

3.6.7.3 | Calculation of the series resistance R_s

The power is maximum at the (i_{mpp}, v_{mpp}) point : $\frac{dP}{dV}(i_{mpp}, v_{mpp}) = 0$, therefore, we obtain a first value for the series resistance R_s :

$$\boxed{Rs_1 = \frac{V_{oc} - v_{mpp}}{i_{mpp}} + \frac{n_s \cdot V_t \cdot a}{i_{mpp}} \ln\left[\frac{n_s \cdot V_t \cdot a}{n_s \cdot V_t \cdot a + v_{mpp}}\right]} \tag{3.61}$$

The $I - V$ characteristic :

If we state that maximum of power $\max(P) = pmax$ as we want to use this manufacturer data, we get a second form for Rs :

$$\boxed{Rs_2 = \frac{V_{oc} - v_{mpp}}{i_{mpp}} + \frac{n_s \cdot V_t \cdot a}{i_{mpp}} \ln\left[1 - \frac{p_{max}}{v_{mpp} \cdot I_{sc}} + \frac{p}{v_{mpp} \cdot I_{sc}} \exp\left(-\frac{V_{oc}}{n_s \cdot V_t \cdot a}\right)\right]} \tag{3.62}$$

Both expressions of Rs may be compatible only if the arguments of the logarithm functions are equal :

$$1 + \frac{p_{max}}{i_{sc} \cdot v_{mpp}} \left(\exp\left(-\frac{V_{oc}}{n_s \cdot V_t \cdot a}\right) - 1 \right) = \frac{n_s \cdot V_t \cdot a}{n_s \cdot V_t \cdot a + v_{mpp}} \tag{3.63}$$

Moreover, if we assess that the $I-V$ curve pass through (i_{mpp}, v_{mpp}), we get :

$$\boxed{Rs_3 = \frac{V_{oc} - v_{mpp}}{i_{mpp}} + \frac{n_s \cdot V_t \cdot a}{i_{mpp}} \ln\left[1 - \frac{i_{mpp}}{I_{sc}} + \frac{i_{mpp}}{I_{sc}} \exp\left(-\frac{V_{oc}}{n_s \cdot V_t \cdot a}\right)\right]} \tag{3.64}$$

Rs_3 is consistent with Rs_1 only if $pmax = impp.vmpp$. Therefore, the assumption in Ref. [75] is rather a condition of consistence of the remarkable points.

This first simplified model does able to check if the electric power reaches a maximum value for $(vmpp, impp)$ and if the $I-V$ characteristic pass through this point. Moreover, implicit equations prevent us to get simple expressions of resistances. Therefore, a supplementary assumption is put to the front in the following.

Remark 3.4. If we replace Iph and $I0$ by their approximated expression (for $Rp \to \infty$ and $Rs \to 0$) in the non approximated $I-V$ equation :

$$I = Iph - I0\left[\exp\left(\frac{V + RsI}{ns.Vt.a}\right) - 1\right] - \frac{V + RsI}{Rp},$$

and if we solve this equation at $(Voc, 0)$ point : $Rp = \frac{Voc}{Iph + I0\left(1 - \exp\left(\frac{Voc}{ns.a.Vt}\right)\right)}$, we obtain infinite Rp. This result is consistent with the fact that we consider the assumptions on the resistances from the beginning of the thought process. On the contrary, using the $(Is, 0)$ point gives :

$$\boxed{Rp = Rs\frac{1 - \exp\left(\frac{Voc}{ns.a.Vt}\right)}{\exp\left(\frac{Isc.Rs}{ns.a.Vt}\right) - 1}}. \tag{3.65}$$

3.6.7.4 | Further simplification

It's clear that the assumption $\exp\left(-\frac{V_{oc}}{n_s \cdot V_t \cdot a}\right) << 1$ leads to simplifications of equations, toward the ideal diode model ($R_p \to \infty$ and $R_s \to 0$) :

$$\exp\left(-\frac{V_{oc}}{n_s \cdot V_t \cdot a}\right) << 1 \Rightarrow \frac{1}{\exp\left(\frac{V_{oc}}{n_s \cdot V_t \cdot a}\right) - 1} \approx \exp\left(-\frac{V_{oc}}{n_s \cdot V_t \cdot a}\right).$$

This simplification is legitimate, $n_s \cdot V_t \cdot a$ being much smaller than V_{oc}.
The inequality 3.34 helps to simplify Eqs. 3.55, page 69 and 3.57, page 69 :

$$I \approx I_{sc} - \frac{I_{sc}}{\exp\left(\frac{V_{oc}}{n_s \cdot V_t \cdot a}\right) - 1}\left[\exp\left(\frac{V + R_s \cdot I}{n_s \cdot V_t \cdot a}\right) - 1\right].$$

becomes :

$$I \approx I_{sc} - I_{sc}.\exp\left(-\frac{V_{oc}}{n_s \cdot V_t \cdot a}\right)\left[\exp\left(\frac{V+R_sI}{n_s \cdot V_t \cdot a}\right)-1\right] \quad (3.66)$$

$$\approx I_{sc} - I_{sc}.\left[\exp\left(\frac{V-V_{oc}+R_s \cdot I}{n_s \cdot V_t \cdot a}\right) - \exp\left(-\frac{V_{oc}}{n_s \cdot V_t \cdot a}\right)\right] \quad (3.67)$$

$$\approx \boxed{I_{sc}\left[1-\exp\left(\frac{V-V_{oc}+R_sI}{n_s \cdot V_t \cdot a}\right)\right]} \quad (3.68)$$

By the same token [1] :

$$V \approx V_{oc} + n_s \cdot V_t \cdot a \ln\left[1-\frac{I}{I_{sc}}+\frac{I}{I_{sc}}\exp\left(-\frac{V_{oc}}{n_s \cdot V_t \cdot a}\right)\right] - R_s.I \quad (3.69)$$

$$\approx \boxed{V_{oc} + n_s \cdot V_t \cdot a \ln\left(1-\frac{I}{I_{sc}}\right) - R_s \cdot I} \quad (3.70)$$

Again, using remarkable points of the characteristic gives :

— at $(V_{oc}, 0)$: $V_{oc} \approx V_{oc} + n_s \cdot V_t \cdot a \ln\left(1-\frac{0}{I_{sc}}\right) - R_s.0 = V_{oc}$.

— at $(0, I_{sc})$: $0 \approx V_{oc} + n_s \cdot V_t \cdot a \ln\left(1-\frac{I_{sc}}{I_{sc}}\right) - R_s \cdot I_{sc}$. This equation cannot be verified, the present approximation leads to infinite value for the logarithm function (before this approximation the error was $R_s \cdot I_s$). The $I-V$ characteristic gives : $I_{sc} = I_{sc}\left[1-\exp\left(\frac{-V_{oc}}{n_s \cdot V_t \cdot a}\right)\right] \approx I_{sc}$, therefore, we have to beware of the $V-I$ characteristic, whereas the $I-V$ is more efficient.

— at (v_{mpp}, i_{mpp}) :

+ $dP/dV(i_{mpp}, v_{mpp}) = 0$, therefore :

$$R_s = Rs'_1 = \frac{V_{oc}-v_{mpp}}{i_{mpp}} + \frac{n_s \cdot V_t \cdot a}{i_{mpp}} \ln\left[\frac{n_s \cdot V_t \cdot a}{n_s \cdot V_t \cdot a + v_{mpp}}\right] \quad (3.71)$$

which is identical to Rs_1 (Eq. 3.61, page 70).

+ $p_{max} = \approx impp\left(V_{oc} + n_s \cdot V_t \cdot a \ln\left(1-\frac{i_{mpp}}{I_{sc}}\right) - R_s.i_{mpp}\right)$, therefore :

$$Rs = Rs'_2 = \frac{V_{oc}-v_{mpp}}{i_{mpp}} + \frac{n_s \cdot V_t \cdot a}{i_{mpp}} \ln\left[1-\frac{i_{mpp}}{I_{sc}}\right]. \quad (3.72)$$

which is Rs_2 (Eq. 3.62, page 70) :

$$Rs_2 = \frac{V_{oc}-v_{mpp}}{i_{mpp}} + \frac{n_s \cdot V_t \cdot a}{i_{mpp}} \ln\left[1+\frac{i_{mpp}}{I_{sc}}\left(\exp\left(-\frac{V_{oc}}{n_s \cdot V_t \cdot a}\right)-1\right)\right].$$

by applying the assumption $\exp\left(-\frac{V_oc}{Vt.a}\right) << 1$ (Eq. 3.34, page 64).

Again, we expect the equality for the power passing through (i_{mpp}, v_{mpp}) and reaching a maximum value at this point :

$$1 - \frac{i_{mpp}}{I_{sc}} = \frac{n_s \cdot V_t \cdot a}{n_s \cdot V_t \cdot a + v_{mpp}}$$

This equality is verified if we set :

$$n_s \cdot a \cdot V_t = v_{mpp} \left(\frac{I_{sc}}{i_{mpp}} - 1 \right) \tag{3.73}$$

Consequently, to prevent the different values of Rs, we give up the physical definition of the thermal voltage Vt to the benefit of a parameter, which affords to a best fitting by using manufacturer data.

Let us note that the derivative of electric power was with respect to I in Ref. [1] while the maximum is reached in the $I - V$ characteristic (function of V). Let us summarize the method used to model the photovoltaic panel.

Theorem 3.1. *To my knowledge, this calculation is new, and brings some rigor to the approximate reasoning of the references [3, 1, 75].*

- $I_{ph} = I_{sc}$ *and* $I_0 = \frac{1}{\exp\left(\frac{V_{oc}}{n_s \cdot V_t \cdot a}\right)}$ *are obtained for* $R_p \to \infty$ ***and*** $R_s \to 0$.
- *The final* $I - V$ *and* $V - I$ *characteristics also require* $\exp\left(-\frac{V_{oc}}{n_s \cdot V_t \cdot a}\right) << 1$:

$$I \approx I_{sc} \left[1 - \exp\left(\frac{V - V_{oc} + R_s I}{n_s \cdot V_t \cdot a} \right) \right]$$

$$V \approx V_{oc} + n_s \cdot V_t \cdot a \ln\left(1 - \frac{I}{I_{sc}}\right) - R_s \cdot I$$

- $n_s \cdot V_t \cdot a$ *is replaced by* $V_T = v_{mpp}\left(\frac{I_{sc}}{i_{mpp}} - 1\right)$ *and* $p_{max} = i_{mpp} \cdot v_{mpp}$ *to handle that the* $I - V$ *curve pass through* (i_{mpp}, v_{mpp}), *that* p_{max} *is the maximum power* P, *and that* $dP/dI(i_{mpp}, v_{mpp}) = 0$.
- *Using the* $(I_s, 0)$ *point gives :*

$$R_p \approx R_s \frac{\exp\left(\frac{V_{oc}}{n_s \cdot a \cdot V_t}\right)}{1 - \exp\left(\frac{I_{sc} \cdot R_s}{ns.a.Vt}\right)}.$$

Remark 3.5. Again, if we replace I_{ph} and I_0 by their approximated expression (for $R_p \to \infty$ and $R_s \to 0$) in the non approximated $I - V$ equation :

$$I = I_{ph} - I_0 \left[\exp\left(\frac{V + R_s \cdot I}{n_s \cdot V_t \cdot a}\right) - 1\right] - \frac{V + R_s \cdot I}{R_p},$$

and if we solve this equation at $(V_{oc}, 0)$ point : $R_p = \frac{V_{oc}}{I_{ph} + I0\left(1 - \exp\left(\frac{V_{oc}}{n_s \cdot a \cdot V_t}\right)\right)}$, we obtain infinite Rp. This result is consistent with the fact that we consider the assumptions on the resistances from the beginning of the thought process.

3.6.8 | Summary of the assumptions and results : Algorithm

The restrictive assumptions, used to get a simplified analytical model of the photovoltaic panel are following :

- $Iph = Isc$ the photon-current is the inverse saturation current for any value of the solar irradiance. Indeed, we cannot verify its validity. It is broadly used as a first statement. *The underlying assumption is* $Rs \approx 0$.
- $R_p \to \infty$ or $\frac{V_{oc}}{R_p} << I_{sc} - I_0 \exp\left(-\frac{V_{oc}}{n_s \cdot V_t \cdot a}\right)$ to get I_0 (Eq. 3.46, page 66).
- $\exp\left(-\frac{V_{oc}}{n_s \cdot V_t \cdot a}\right) << 1$,
- $n_s \cdot V_t = n_s \cdot k_B \cdot T \cdot a/q$ is replaced by $VT = v_{mpp}\left(\frac{I_{sc}}{i_{mpp}} - 1\right)$, to heed the maximum power data from manufacturer.

Numerical tests of validity.

- We evaluate $\exp\left(-\frac{V_{oc}}{VT}\right)$ from manufacturer data sheet (Tab. 3.3, page 57 : in standard conditions $Vmpp = 40.1$V, $I_{mpp} = 9.48$A, $V_{oc} = 48.5$V, $I_{sc} = 9.93$A : $VT = 1.90$V, therefore, $\exp\left(-\frac{Voc}{VT}\right) = 8.6e-12$ is much less than 1.
- We could compare VT to $ns.k_B.T/q$ to evaluate the closeness of the fitting parameter to the physical value : $VT = 1.90$V and $n_s \cdot k_B.T_{std}/q = 0.2$. The release of this parameter appears to be critical to adjust the $I - V$ characteristic to the maximum power data. The discrepancy is due to the hard assumptions used to calculate Iph, I_0 and R_s : $R_p \to \infty$ and $R_s \approx 0$.
- The assumption of large R_p can be checked from Eq. 3.53, page 68.

Under these assumptions, the useful equations are following.

- The temperature of the cell : $T_c = T_a + (t_{nmot} - t_{noc})\frac{G}{Gnoc}$, Eq. 3.9, page 59.

— Temperature dependence of V_{oc} : V_{oc} is replaced by : $V_{oc} \cdot (1 + kVoc(t_c - t_{noc}))$.
— Temperature dependance of P_{max} : P_{max} is replaced by : $P_{max} \cdot (1 + kPmax(t_c - t_{noc}))$.
— Temperature and solar irradiance dependence of I_{sc} : I_{sc} is replaced by : $I_{sc} \cdot (1 + kI_{sc}(t_c - t_{noc})).G/G_{std}$.
— The replacement of the thermal voltage (Eq. 3.73, page 73) :

$$VT = v_{mpp}\left(\frac{Isc}{i_{mpp}} - 1\right).$$

— The series resistance R_s :

$$R_s = \frac{V_{oc} - p_{max}/i_{mpp}}{i_{mpp}} + \frac{VT}{i_{mpp}} \ln\left(1 - \frac{i_{mpp}}{I_{sc}}\right)$$

— The voltage of the solar panel (Eq. 3.70, page 72) :

$$V \approx V_{oc} + VT \ln\left(1 - \frac{I}{I_{sc}}\right) - R_s \cdot I$$

— The solar panel current :

$$I \approx Isc\left[1 - \exp\left(\frac{V - Voc + RsI}{VT}\right)\right]$$

— The output electrical power of the solar panel :

$$P = V.I \approx I.\left(Voc + VT \ln\left(1 - \frac{I}{Isc}\right) - Rs.I\right)$$

— The parallel resistance to check the validity of assumptions (Eq. 3.65, page 71) :

$$Rp = Rs\frac{\exp\left(\frac{Voc}{ns.a.Vt}\right) - 1}{1 - \exp\left(\frac{Isc.Rs}{ns.a.Vt}\right)}.$$

The slope of the line segment between the short-circuit and maximum power remarkable points gives the minimum of Rp (Eq. (11) in Ref. [75]) :

$$\min(Rp) = \frac{vmpp}{Isc - Imp} - \frac{Voc - vmpp}{impp}$$

The characteristic of a photovoltaic grid : an association of $Ns \times Np$ panels is :

$$I = Np.Iph - Np.I0\left[\exp\left(\frac{V + Rs\frac{Ns}{Np}I}{Ns.Vt.a}\right) - 1\right] - \frac{V + Rs\frac{Ns}{Np}I}{Rp\frac{Ns}{Np}} \tag{3.74}$$

Under the strong assumptions $Rp \to \infty$ and $Rs \to 0$, the values of power overestimate the grid production :

$$\max(P) = V.Np\left(Iph - I0.\exp\left(\frac{V}{Ns.a.Vt}\right)\right). \tag{3.75}$$

3.6.9 | Comparison of models

The model proposed in Ref [1] is based on the same assumptions as ours, but works on the $V-I$ characteristic instead of the $I-V$. Therefore, the derivative of P in relation to the voltage instead of the electric current. The maximum of electric power is therefore :

$$pmax = impp\left(Voc + Vt\ln\left(1-\frac{impp}{Isc}\right) - Rsimpp\right) \tag{3.76}$$

$$\left.\frac{dVI}{dI}\right|_{I=impp} = vmpp + \frac{Vtimpp}{impp - Isc} - Rs.impp = 0. \tag{3.77}$$

The solutions of this system of linear equations are :

$$Vt|_{I=impp} = \frac{(2Vmp - Voc)(Isc - Imp)}{Imp + (Isc - Imp)\ln\left(1-\frac{Imp}{Isc}\right)} \tag{3.78}$$

$$Rs|_{I=impp} = \frac{Vmp}{Imp} - \frac{2Vmp - Voc}{Imp + (Isc - Imp)\ln\left(1-\frac{Imp}{Isc}\right)}. \tag{3.79}$$

Table 3.5 summarize the common equations and the differences between our model and that in Ref. [1].

	Model A Our calculation	Model B Ref [1]
(I,V)	$I \approx Isc\left[1-\exp\left(\frac{V-Voc+RsI}{VT}\right)\right]$	
(V,U)	$V \approx Voc + VT\ln\left(1-\frac{I}{Isc}\right) - Rs.I$	
Iph	Isc	
Isc	$Isc(1+kIsc(tc-tnoc)).G/Gstd$	
$I0$	$Isc(1+kIsc(tc-tnoc)).G/Gstd$	
Voc	$Voc(1+kVoc(tc-tnoc)).\frac{Tc}{Tstd}$	$Voc(1+kVoc(tc-tnoc)).\frac{Tc}{Tstd}$ $+VT.\log(G/Gstd)$
Rs	$Rs = \frac{Voc-pmax/impp}{impp} + \frac{VT}{impp}\ln\left(1-\frac{impp}{Isc}\right)$	$Rs = \frac{Vmp}{Imp} - \frac{2Vmp-Voc}{Imp+(Isc-Imp)\ln\left(1-\frac{Imp}{Isc}\right)}$
Rp	$Rp = Rs\frac{\exp\left(\frac{Voc}{ns.a.Vt}\right)-1}{1-\exp\left(\frac{Isc.Rs}{ns.a.Vt}\right)}$	-
VT	$VT = vmpp\left(\frac{Isc}{impp}-1\right)$	$VT = \frac{(2vmpp-Voc)(Isc-impp)}{impp+(Isc-impp)\ln\left(1-\frac{impp}{Isc}\right)}$
$\max(P)$	$\frac{dP}{dV}=0$	$\frac{dP}{dI}=0$

TABLE 3.5 – Comparison between of our model and that in Ref. [1].

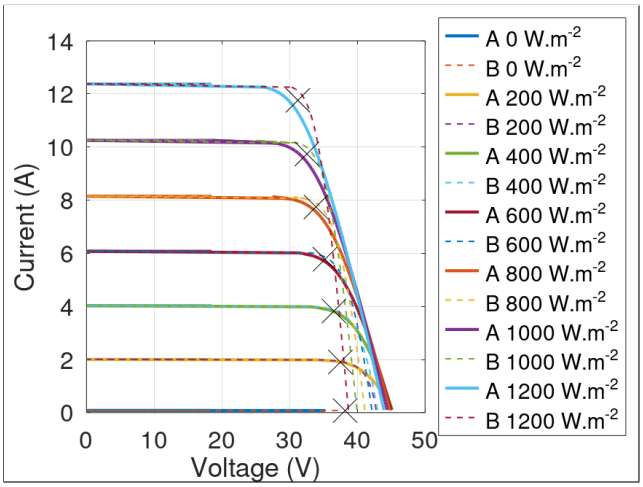

FIGURE 3.16 – I-V characteristic of RECOM

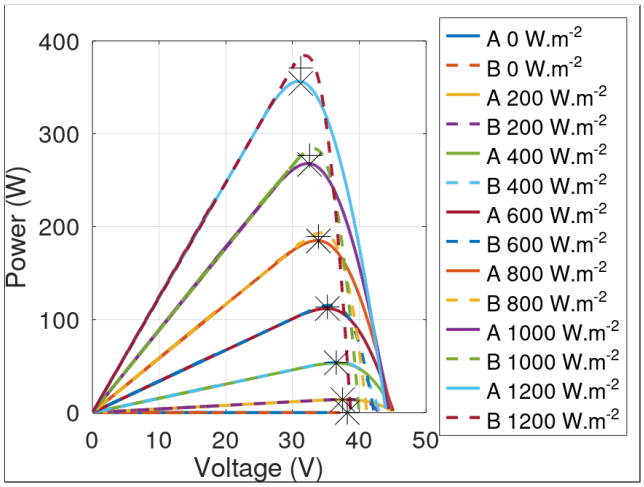

FIGURE 3.17 – P-V characteristic of RECOM

Figure 3.16 referring to $I-V$ Characteristic function of the RECOM photovoltaic panel (Tab. 3.3, page 57) and figure 3.17 referring to electrical power provided by RECOM solar panel, illustrate the Comparison between the results of our model and that in Ref. [1]. $pmax.ff$ and $impp.vmpp.ff$ are drawn with "x" and "$+$".

The characteristics are close to those in manufacturer data-sheets. There is a slight discrepancy between both models. Our model give curves that pass through $(impp, vmpp)$. However the model in Ref. [1] does not preserve this property of $I-V$ curves, the calculation using dP/dI instead of dP/dV.

3.7 | Analytical formulation using Lambert function

The extraction of electric parameters of photovoltaic panels has been an intensive research topic for many years, are quite complex equations to use common analytical methods. The basic principle of the method is based on the use of the Lambert function W_0.
The Lambert function (or omega function) relates :

$$y\exp(y) = x \Leftrightarrow y = W_0(x). \tag{3.80}$$

The tricks consists in identifying y and x in the phenomenon equation :

$$I = Iph - I0\left(\exp\left(\frac{V + Rs.I}{Vt}\right) - 1\right) - \frac{V + Rs.I}{Rp}.$$

In Ref. [76], Eq.(4) give the explicit solution for the current :

$$I = \frac{ns.Vt.a}{Rs} W_0\left(\frac{I0.Rs.Rp}{ns.Vt.a(Rp + Rs)} \exp\left(\frac{Rp.(V + I0.Rs)}{ns.a.Vt(Rp + Rs)}\right)\right) + \frac{V - I0.Rs}{Rp + Rs} \tag{3.81}$$

3.8 | PSO to relate of model and manufacturer parameters

The unknowns of the following model

$$I = Iph - I0\left(\exp\left(\frac{V + Rs.I}{\alpha Vt}\right) - 1\right) - \frac{V + Rs.I}{Rp}.$$

are Iph, $I0$, α, Rs and Rp in Ref. [77]. The inputs are the manufacturer data.
The particle swarm optimization is used to determine these parameters. To do this, we execute the following function which includes the remarkable points of the I-V characteristic. We define a fitness function which differs from that in [77].
We choose the interval of search as being the approximated solution from subroutine *SolarPanel.m* : $VT = 1.9386$V,, $voc = 44.8520$V, $Isc = 9.1295e-10$A, $Rs = 0.6281\Omega$, $isc = 10.1904$A. The domain of search is delimited by $1e-4$ and $1e4$ times these values. $c_1 = c_2 = 1.5$, Ω decreases linearly from 0.9 to 0.4 along the maximum of 3000 iterations. The end of descent uses the multidimensional unconstrained nonlinear minimization (Nelder-Mead) with the best result of PSO as starting point. 1000 realizations of the same algorithm gives a value of fitness function less than 1e-14.
The best result is : $Iph = 7.73$, $Is = 1.05e-25$, $Rs = 0.9831$, $ns.a = 29.41$ and $Rp > 1e+9$ (execution of ten times the 1000 realizations shows that this parameters is the less accurately determined). Therefore, the previously used assumptions of simplification of the model are valid : Rp is great enough to be considered as infinite, Rs is small, and $Is >> Iph$.

Figures 3.18 and 3.19 below illustrate the comparison of the model and manufacturer parameter curves.

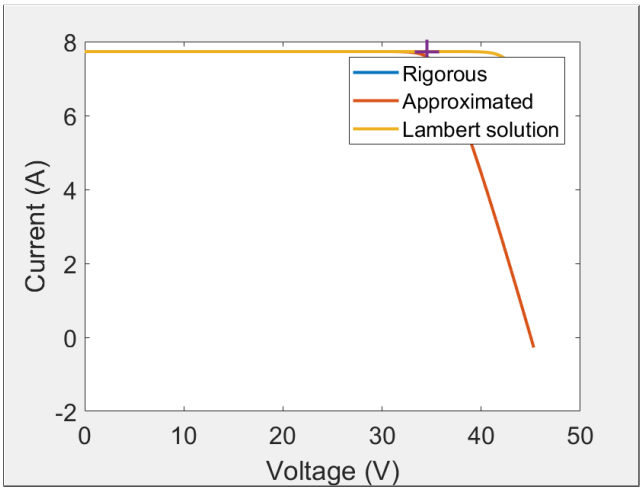

FIGURE 3.18 – Comparison of I-V characteristics

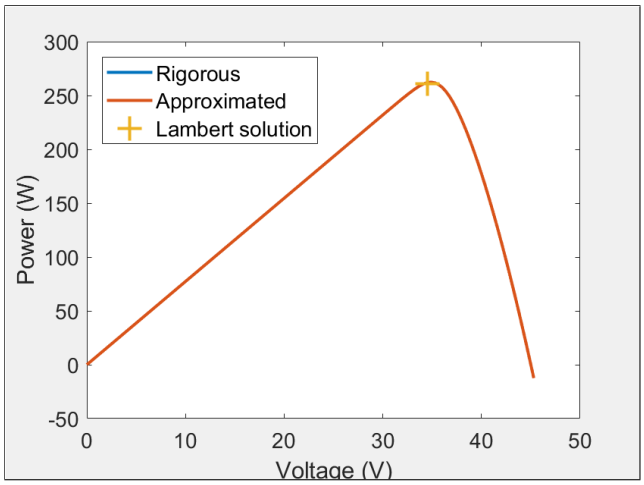

FIGURE 3.19 – Comparison of P-V characteristics

As a conclusion, the electric power produced by the panel cannot be approximated by :

$$P(V,I) = V.isc\left(\exp\left(\frac{V - voc + I.Rs}{ns.a.Vt}\right) - 1\right), \tag{3.82}$$

rather by :

$$P(V,I) = V.Iph + V.Is\left(1 - \exp\left(\frac{V + I.Rs}{ns.a.Vt}\right) - 1\right) \tag{3.83}$$

3.9 | Model of photovoltaic array (grid)

According to Ref. [75], the characteristic of $Ns \times Np$ association of panels (grid) is :

$$\boxed{I = Np.Iph - Np.I0\left[\exp\left(\frac{V + Rs\frac{Ns}{Np}I}{Ns.Vt.a}\right) - 1\right] - \frac{V + Rs\frac{Ns}{Np}I}{Rp\frac{Ns}{Np}}}. \tag{3.84}$$

The same reference gives the maximum power P produced by the photovoltaic grid, under the strong assumptions $Rp \to \infty$ and $Rs \to 0$ (there is no Joule loss) :

$$P = V.Np\left(Iph - I0.\exp\left(\frac{V}{Ns.a.Vt}\right)\right). \tag{3.85}$$

However, this definition of $I0$ is used in Refs. [1, 75] even if the calculation of Rs and Rp are proposed. This lack of rigor in the procedure may puzzle the reader. Therefore, a more realistic

model should be established by keeping the role of Rs, from the beginning of the calculations. The following subsection detail the corresponding calculations.

3.10 | Propagation of uncertainties

In this section we evaluate the influence of experimental uncertainties on the electrical power produced. Manufacturers' catalogs usually do not provide uncertainties about the parameters, so we assume two cases namely :

(i) Relative uncertainty u_r = 1 %

(ii) Relative uncertainty u_r = 10 %

For each of the assumed relative uncertainty values, we evaluated the propagation of uncertainty over the parameters contained in the manufacturers' data sheets, namely, temperature voltage V_T, open-circuit voltage v_{oc}, series resistance R_s, short circuit current i_{sc}, fill factor ff and maximum power P_{max}.

The results of modeling the propagation of uncertainty through the model of this thesis are compared with results of the modeling of uncertainty from the model in Ref. [7].

We use the method described in Ref. [78]. This is a simple Monte Carlo method, used to evaluate the variations of the outputs of a model, as a function of the variations of its inputs. If we suppose a relative uncertainty u_r on each of the parameters found in the manufacturer datasheet, we can calculate the uncertainty on the produced photovoltaic power P. We calculate 1000 sets of parameters by using uniform pseudo-random generation of values around the manufacturer parameters, within an interval which size is governed by u_r.

3.10.1 | For relative uncertainty $u_r = 1\%$

3.10.1.1 | Temperature voltage V_T

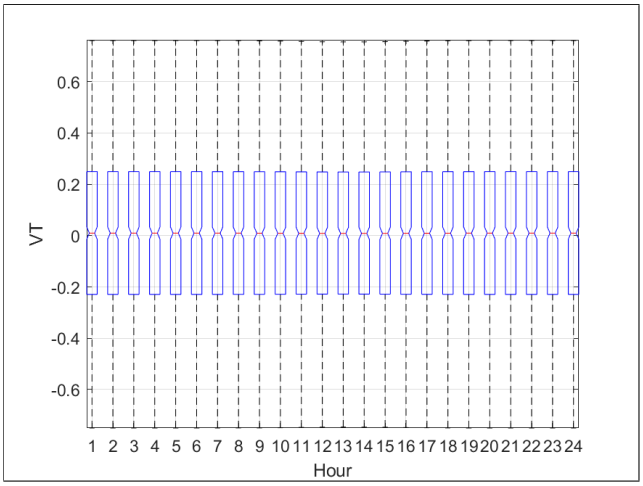

FIGURE 3.20 – Our model : temperature voltage V_T.

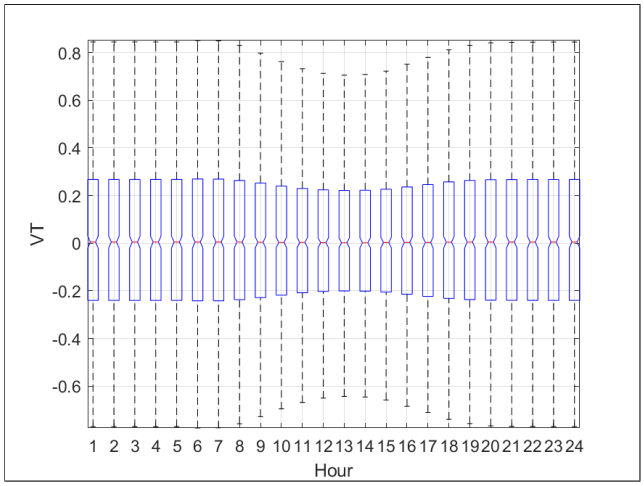

FIGURE 3.21 – Model in Ref. [7] : temperature voltage V_T.

The thermal voltage as the voltage produced within the P-N junction due to the action of temperature, in our model, the uncertainty seems to propagate uniformly throughout the 24 hours of the day, which is unlikely considering that the thermal voltage is caused by temperature and the temperature increases considerably during the daytime hours. See temperature variation in figure 3.4 page 44.
The hourly distribution of uncertainty propagation by the model in Ref. [7] is shown to be slightly different during the daytime hours, showing that the temperature rise during the daytime influences the temperature of the P-N junction, which we assume to be expected (or likely) considering the definition and concept of thermal voltage.

3.10.1.2 | Open-Circuit Voltage V_{oc}

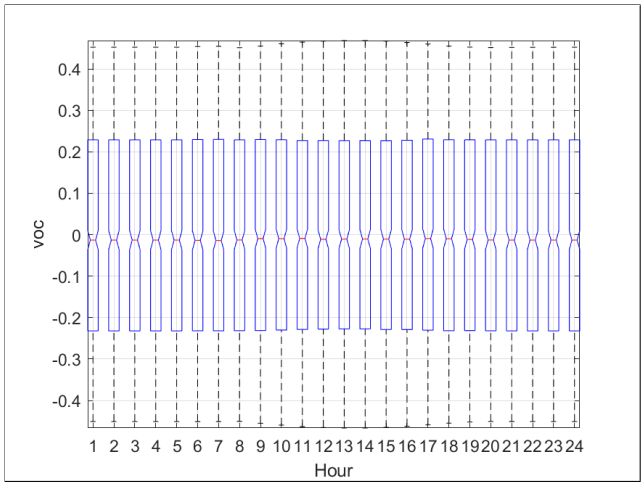

FIGURE 3.22 – Our model : open-Circuit Voltage V_{oc}.

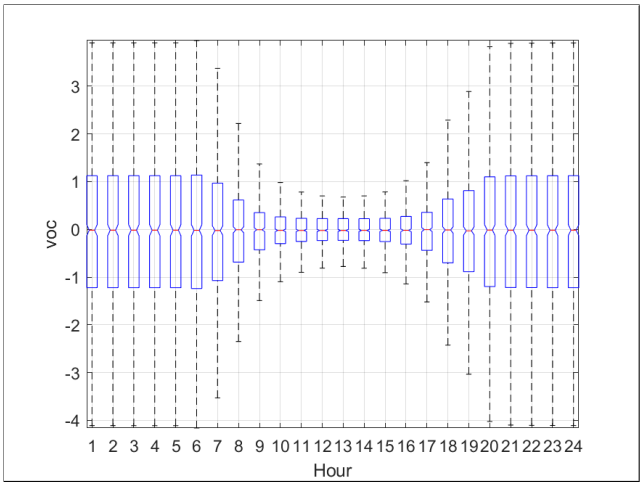

FIGURE 3.23 – Model in Ref. [7] : open-Circuit Voltage V_{oc}.

Open circuit voltage in a photocell occurs when no current flows through the cell, in this case it happens at night the solar radiation is unavailable, therefore there is no current flowing in the photocell. The propagated uncertainty is expected to have different distributions between the daytime and nighttime period as in the model of Ref. [7]. In our model, the hourly propagated uncertainty distribution appears to have a constant influence.

3.10.1.3 | Series Resistance R_s

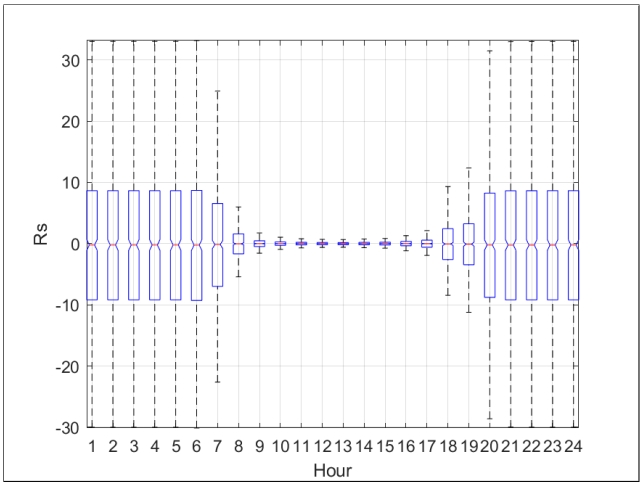

FIGURE 3.24 – Our model : series Resistance R_s.

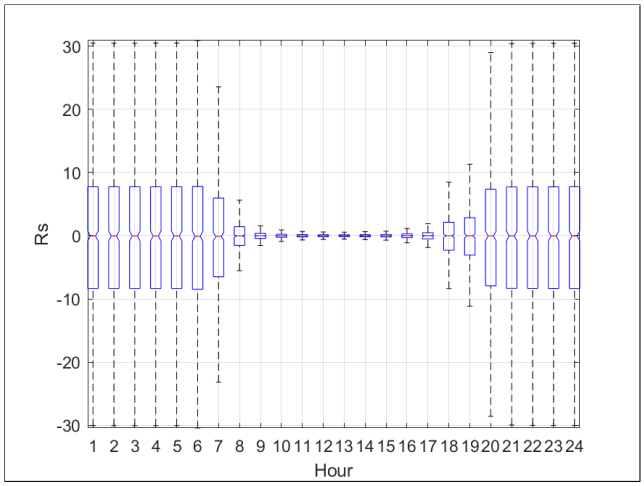

FIGURE 3.25 – Model in Ref. [7] : series Resistance R_s.

One of the main causes of resistance in a photovoltaic cell is the movement of current between the emitter and the base of the solar cell which is only possible during daytime hours, for that reason, It is expected that the propagation of uncertainty has a totally opposite distribution in the night period (without photocurrent) and in the day period (with photocurrent) as shown in figures 3.24 and 3.25.

3.10.1.4 | Short-Circuit Current I_{sc}

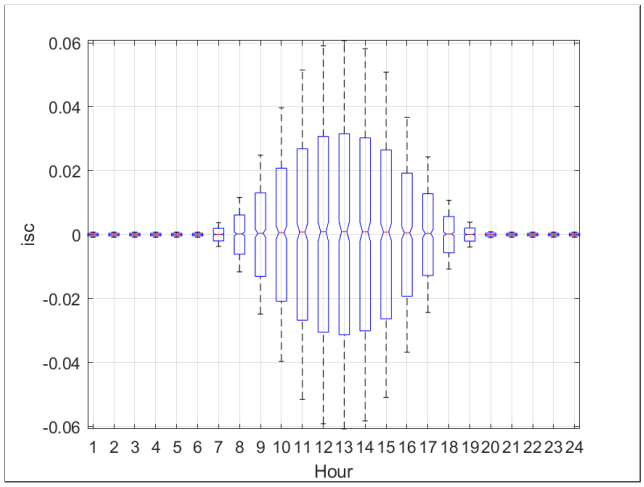

FIGURE 3.26 – Our model : short-Circuit Current I_{sc}.

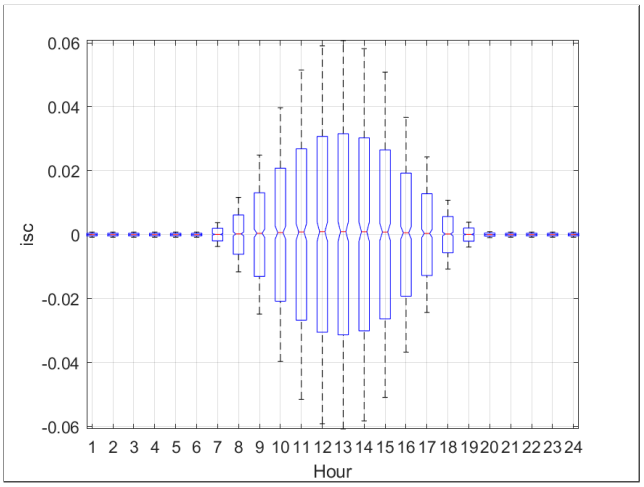

FIGURE 3.27 – Model in Ref. [7] : short-Circuit Current I_{sc}.

Short-circuit current expresses an excessive amount of current flowing through the circuit, is the opposite of open-circuit where resistance tends to infinity. The hourly propagation of uncertainty varies according to the hourly variation of solar radiation illustrated in figure 3.3 on page 43. Observing the hourly distribution of the propagation of uncertainty in figures 3.26 and 3.27, we can say that the greater the solar radiation, the greater the probability of generating the photovoltaic current and, therefore, the greater the uncertainty and vice versa.

3.10.1.5 | Fill factor ff

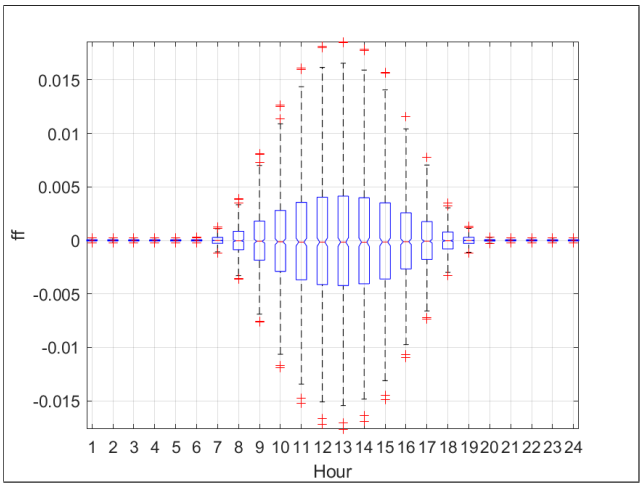

FIGURE 3.28 – Our model : fill factor

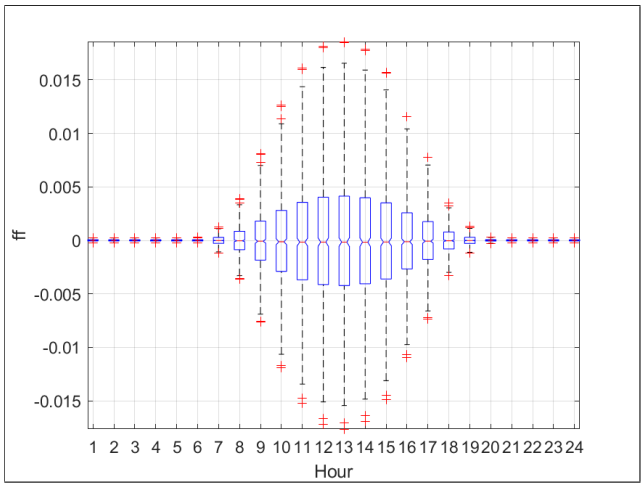

FIGURE 3.29 – Model in Ref. [7] : fill factor

The fill factor is essentially the measure of efficiency of the photovoltaic module, expressed by the ratio between the maximum power obtained, and the product of the short circuit current and the open circuit voltage. The fill factor, by definition and concept, should follow the same pattern of variation in relation to the power produced and therefore the existing uncertainty should vary in the same trend.

3.10.1.6 | Maximum Power P_{max}

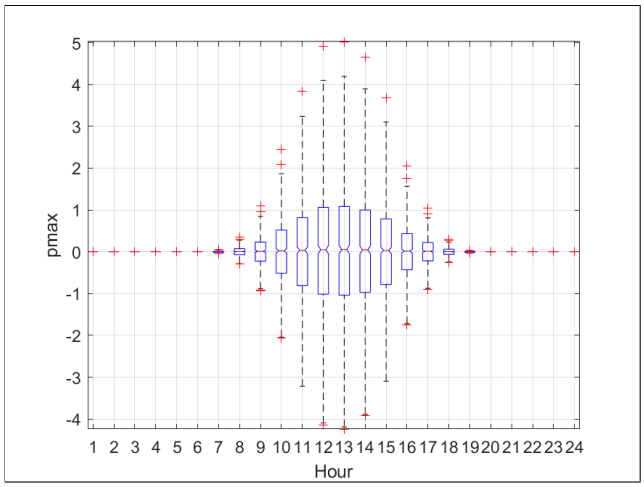

FIGURE 3.30 – Our model : maximum Power P_{max}

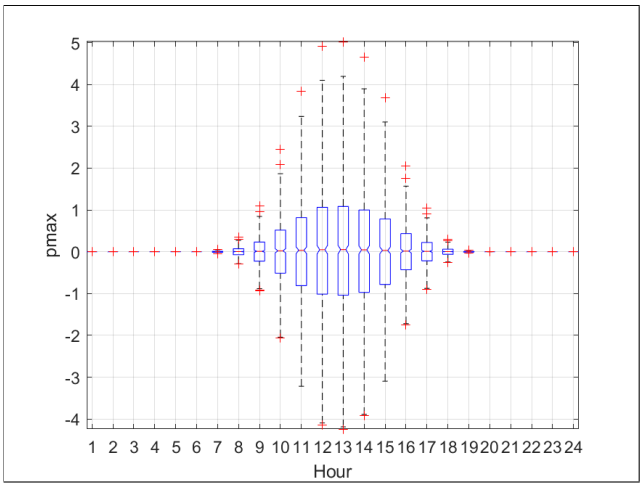

FIGURE 3.31 – Model in Ref. [7] : maximum Power P_{max}

The maximum power of a photovoltaic solar panel varies according to the intensity of the available solar radiation whose uncertainty propagates through the system and influences the power produced, thus, the uncertainty about the maximum power varies in the same trend as the maximum power.

The figures illustrated and discussed above refer to the propagation of uncertainty based on a reference uncertainty $u_r = 1\%$. The model of propagation of uncertainty is presented below considering reference uncertainty $u_r = 10\%$.

3.10.2 | For relative uncertainty $u_r = 10\%$

3.10.2.1 | Temperature Voltage V_T

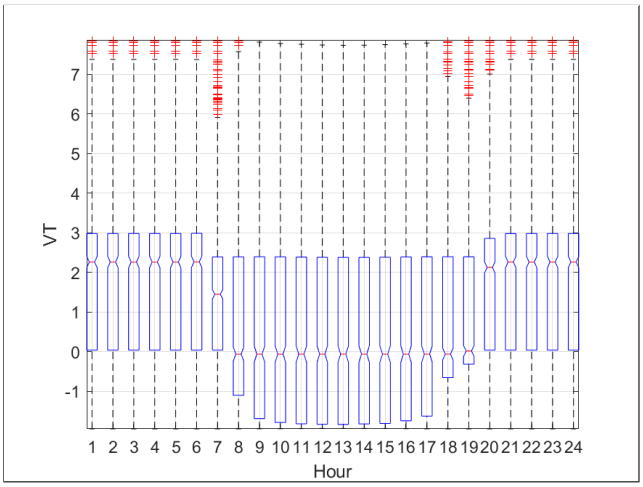

FIGURE 3.32 – Our model : temperature Voltage V_T.

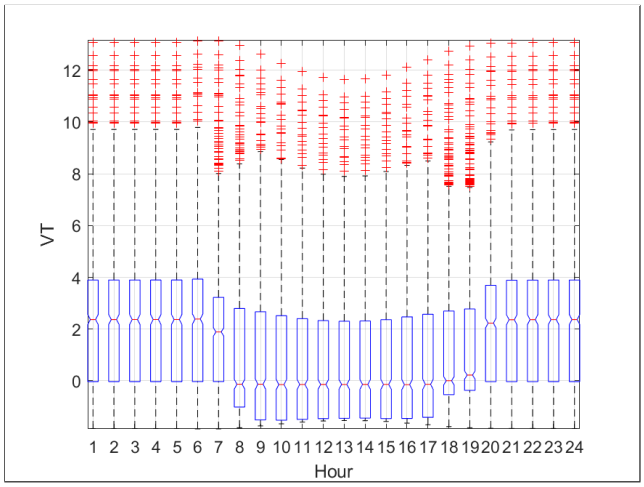

FIGURE 3.33 – Model in Ref. [7] : temperature Voltage V_T.

Comparing figures 3.20 and 3.21 and figures 3.32 and 3.33, it is observed that the increase in the uncertainty of reference, from $u_r = 1\%$ to $u_r = 10\%$, changes the response of the thermal voltage mainly in the daytime hours in the presence of solar radiation. Since the thermal voltage is caused by temperature, it is expected that there will be a change in the behavior of the uncertainty due to the increase in ambient temperature in the daytime period (see ambient temperature variation, figure 3.4 , page 44).

3.10.2.2 | Open-Circuit Voltage V_{oc}

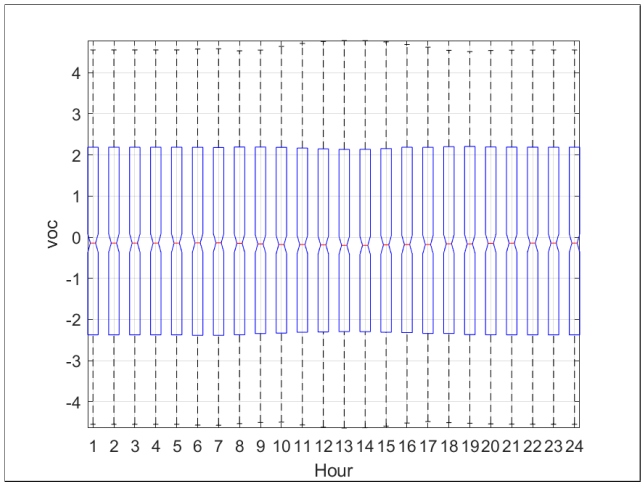

FIGURE 3.34 – Our model : open-Circuit Voltage V_{oc}.

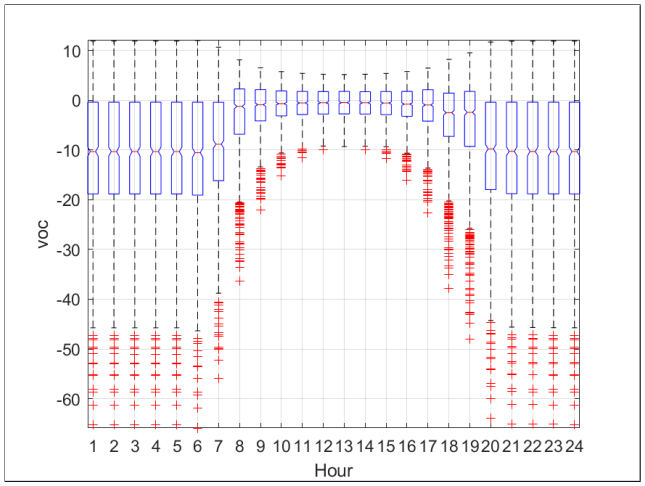

FIGURE 3.35 – Model in Ref. [7] : open-Circuit Voltage V_{oc}.

There is a significant change in the open circuit voltage response in the Ref. [7] model when the reference uncertainty is increased, however, our model shows an apparent "immunity" to the increase in the reference uncertainty. A more in-depth study is necessary to determine the cause of the non-change in the propagation of the uncertainty of the open circuit voltage, even increasing the reference uncertainty. The attempt to simplify the complex equations of the operating parameters of photovoltaic solar panels is generally done using the assumption method as presented in Ref. [7].
The difference in the behavior of the open-circuit voltage response can be explained by the slight difference between equation 3.70 deduced in this thesis, and equation (6) presented in Ref. [7].

3.10.2.3 | Series Resistance R_s

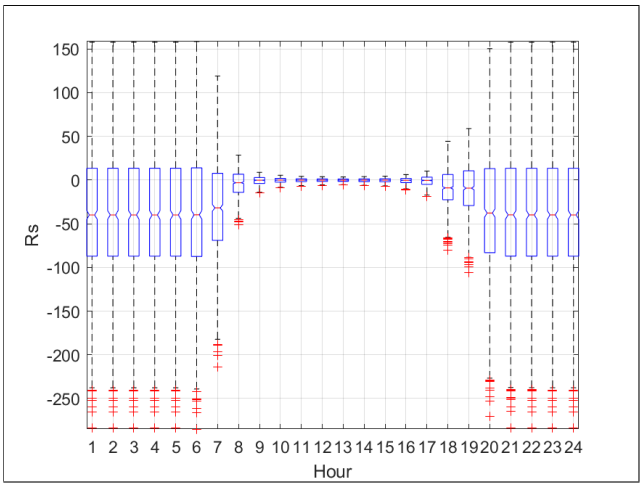

FIGURE 3.36 – Our model : series Resistance R_s.

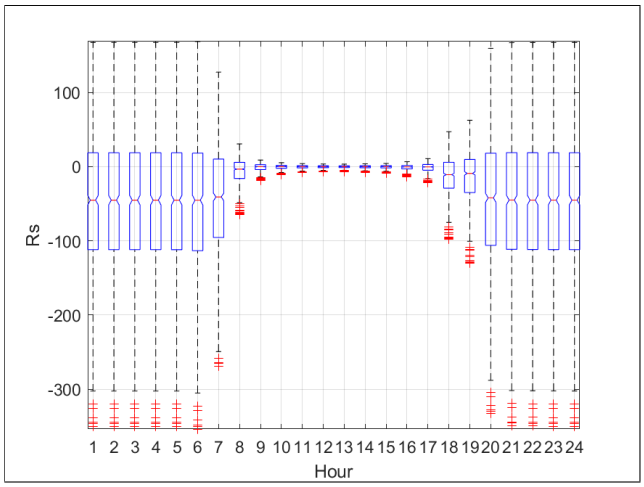

FIGURE 3.37 – Model in Ref. [7] : series Resistance R_s.

Increasing the reference uncertainty influences the uncertainty propagated through the series resistance. Knowing that the series resistance arises by the flow of current, it is noted that the uncertainty exists within the limits of the presence of solar radiation (daytime) when the generation of photovoltaic power is possible.

3.10.2.4 | Short-Circuit Current I_{sc}

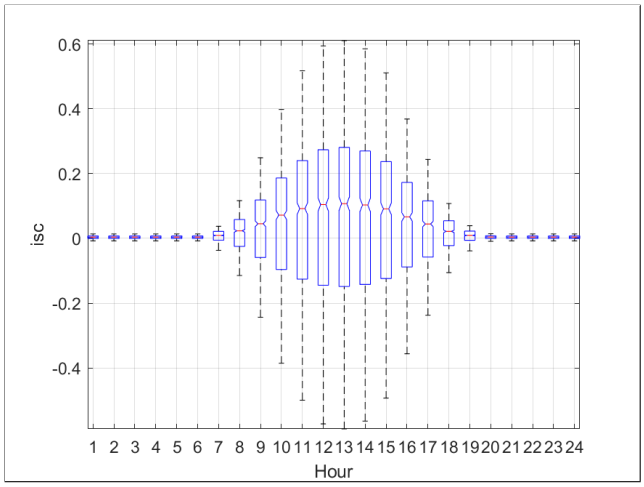

FIGURE 3.38 – Our model : short-Circuit Current I_{sc}.

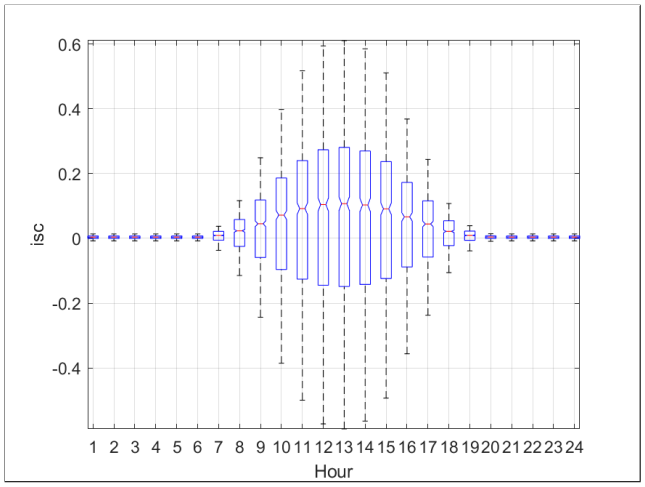

FIGURE 3.39 – Model in Ref. [7] : short-Circuit Current I_{sc}.

The increase in the reference uncertainty slightly influences the short-circuit current within the limits of the period in which there is solar radiation for power generation.

3.10.2.5 | Fill factor ff

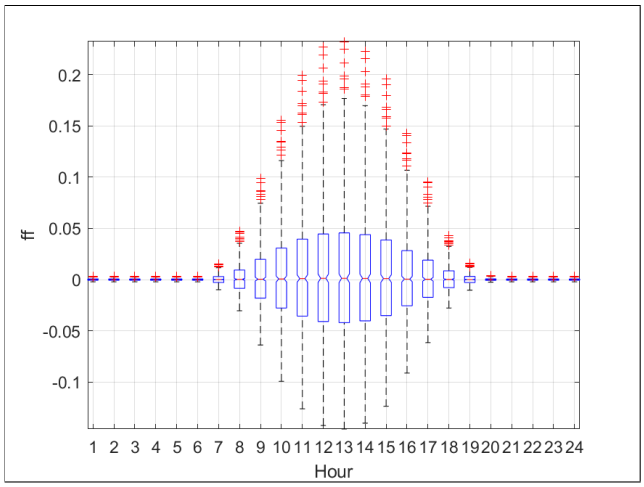

FIGURE 3.40 – Our model : fill factor ff.

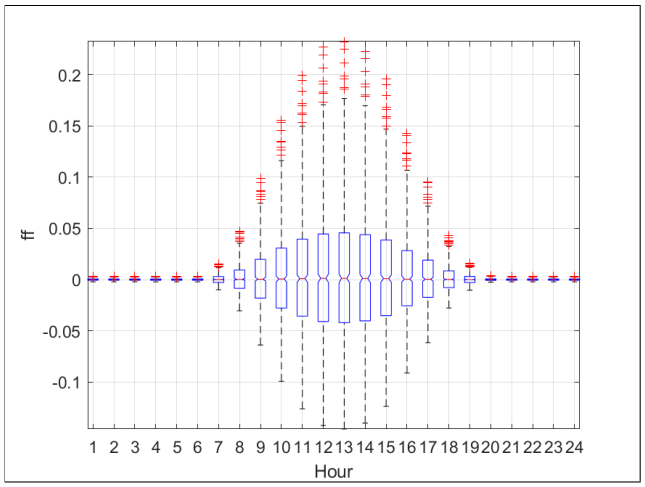

FIGURE 3.41 – Model in Ref. [7] : fill factor ff.

The notable impact of the increase in reference uncertainty on the fill factor is the emergence of a substantial number of outliers in the hourly distribution of the propagation of uncertainty, indicating that when considering the uncertainty about the fill factor, it is important to take into account the possible influence of extreme uncertainty that can significantly influence the fill factor.

3.10.2.6 | Maximum Power P_{max}

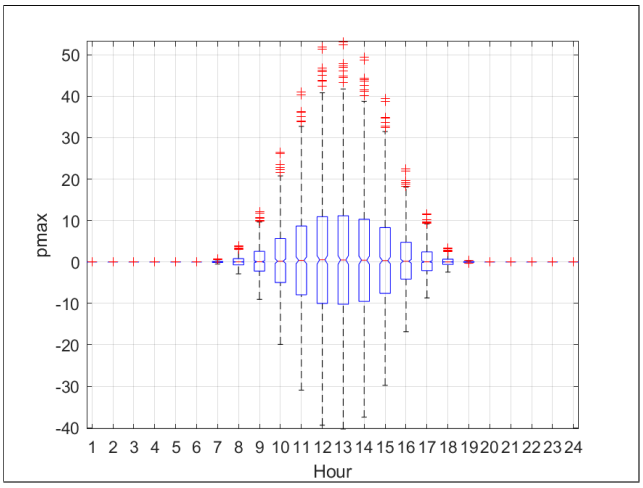

FIGURE 3.42 – Our model : maximum Power P_{max}.

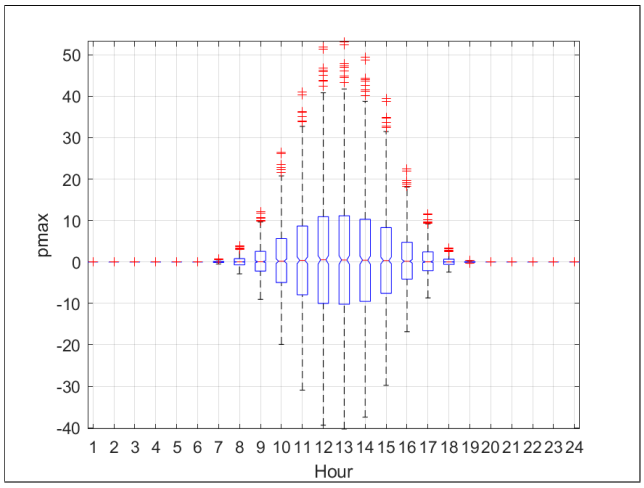

FIGURE 3.43 – Model in Ref. [7] : maximum Power P_{max}.

The hourly distribution of the propagation of uncertainty about the output power demonstrates greater intensity of the uncertainty expressed by the increase of outliers. An increasing number of outliers can mean that the greater the reference uncertainty about the parameters, the greater the propagation of uncertainty, and the impact of such propagated uncertainty will certainly influence the maximum power that the system can produce.

3.10.3 | General comment on section 3.10

In uncertainty modeling we assume two levels of reference uncertainty namely, $u_r = 1\%$ and $u_r = 10\%$. The increment of the reference distribution from $u_r = 1\%$ to $u_r = 10\%$ considerably influences the hourly distribution of uncertainty propagation, moreover, when the reference uncertainty is $u_r = 10\%$, there is a significant amount of outliers in the hourly

distribution of the propagated uncertainty, indicating that uncertainty exist and can reach extreme values influencing parameters, imposing high risk of leading to poor decision making.

3.11 | Improvements of the photovoltaic panel model

The output power of the solar cell is send to a DCDC converter that shapes the electric signal for its practical use. Therefore, the influence of this device should be investigated. It is also clear that the electric power delivered by the photovoltaic panel depends on the angle of incidence of light upon. The useful solar irradiance decreases by increasing incidence angle of the light on the panel. Therefore, the position of the sun with regards to the fixed panel must be evaluated. If this angle of incidence is calculated, the transmittance by the glass blade over solar cells and the shadow effect by the edges of the gridlines of the solar cells can be evaluated. Finally, the influence of the photovoltaic panel aging should be evaluated for realistic and sustainable purposes.

3.12 | The DC-DC converter

The DC-DC converter operates as an adapter between the photovoltaic panel and the load. In Refs. [2, 3], authors proposed calculation of the optimal duty ratio of the DC-DC handle the fact that the electric resistance of the panel and of the load must be equal to get a power transfer equal to $pmax$. The duty cycle (or duty ratio) for an ideal DC-DC converter is a function of the inductance resistance RL (main component of the DC-DC converter) :

$$\frac{Vo}{Vi} = \frac{D}{\frac{RL}{R(1-D)} + 1 - D} \tag{3.86}$$

$$\approx \frac{D}{1-D} \tag{3.87}$$

where Vi and Vo are the input and output voltage of the DC-DC converter, respectively, and Ro the resistance of the load. If the small resistance of the inductor is neglected, we obtain :

$$D = \frac{Vo}{Vo + Vi}. \tag{3.88}$$

3.12.1 | Duty ratio deducted in Ref. [2]

In the ideal case (no joule loss in the DC-DC converter) : $Vo.Io = Vi.Ii$, therefore :

$$\frac{Ii}{Io} \approx \frac{D}{1-D}$$

Consequently, the ratio of resistances is (Eq. (7) in Ref. [2]) :

$$\frac{Ro}{Ri} \approx \left(\frac{D}{1-D}\right)^2. \tag{3.89}$$

If $Ri = Rs$, the output resistance of the photovoltaic panel, we have, for given Ro :

$$\frac{Ro}{Rs} \approx \left(\frac{D}{1-D}\right)^2. \tag{3.90}$$

We deduce the optimum D :

$$D \approx \frac{\sqrt{Ro}}{\sqrt{Ro}+\sqrt{Rs}}. \tag{3.91}$$

The duty ratio D for the DC-DC converter should be adjusted the optimum. The optimal expression of D depends on the DC-DC converter type (Tab. 3.6 is that in Ref. [**?**] with our notations for the model of photovoltaic panel).

DC-DC converter	D for any Po	D when $Po = pmax$	Required
Buck-boost	$D = \frac{\sqrt{Ro}}{\sqrt{Ro}+\sqrt{Rs}}$	$D = \frac{Vo}{Vo+vmpp}$	None
Boost	$D = 1 - \frac{\sqrt{Rs}}{\sqrt{Ro}}$	$D = 1 - \frac{vmpp}{Vo}$	$Ro > vmpp/impp$
Buck	$D = \frac{\sqrt{Ro}}{\sqrt{Rs}}$	$D = 1 - \frac{Vo}{vmpp}$	$vmpp/impp > Ro$

TABLE 3.6 – Optimal duty ratio D for different DC-DC converters for load matching as a function of the output power Po. $Ro = Vo/Io$, Vo are output (or load) resistance and voltage, Rs is the input resistance (the series resistance of the photovoltaic panel), $vmpp$ is the optimal voltage [2]. $Rop = vmpp/impp$.

Switching at the optimal duty ratio guarantees that the power supplied to load is $pmax$. The Vo voltage and the Ro resistance are either that of the battery in charge mode (Rc) of that of the electric power grid (load). The buck-boost converter is the most efficient as it does not require a condition for operating, and the output voltage can be either greater or less than the source voltage.

If we consider the optimum duty-cycle of the buck-boost DC-DC converter : $D = Vc/(Vc + vmpp)$, with Vc the voltage of the battery in charge mode, the output power is $pmax$. A simple default choice is considering twice the electromotive force of the battery for Vc, as given by the study of the battery.
Therefore, the optimal D is $Dopt$:

$$Dopt = 2Ec/(2Ec + vmpp) \tag{3.92}$$

The optimum D being fixed, the transferred power efficiency through the DC-DC converter can be deduced.

3.12.2 | Duty ratio deducted in Ref. [3]

For buck-boost DC-DC- converter, the conversion ratio voltage is : $\frac{Vo}{Vi} = \frac{Io}{Ii} = \frac{D}{1-D}$. Consequently, the ratio of input to output power is :

$$\frac{Po}{Pi} = \left(\frac{D}{1-D}\right)^2 \tag{3.93}$$

If we set $D = Dopt$, the power efficiency of the DC-DC converter from N parallel is :

$$\eta_{DC-DC} = \left(\frac{2nb.Ec/(2nb.Ec + Np.vmpp)}{1 - 2nb.Ec/(2nb.Ec + Np.vmpp)}\right)^2 = 4\frac{nb^2.Ec^2}{Np^2.vmpp^2}, \tag{3.94}$$

Np being the number of parallel photovoltaic panels.
If we tune the DC-DC converter with $Dopt = Ec/(Ec + vmpp)$, we obtain $\eta_{DC-DC} = (nb.Ec/(Np.vmpp$
The best power efficiency is therefore obtained for a number of parallel batteries nb :

$$\boxed{\frac{1}{2}Np\frac{vmmp}{Ec} < nb < Np\frac{vmmp}{Ec}}. \tag{3.95}$$

3.13 | Model of solar position in the sky

The algorithm is described in Ref. [79]. The latitude and longitude of each of town considered in this study can be found at :

`https://latitude.to/satellite-map/mz/mozambique/297652/mecula-district.`

The decay of local times with regards to the UTC time used in calculations is retrieved from :

`https://24timezones.com/`

. In this study, we neglect the decay between the Earth rotation and the terrestrial dynamical time ΔUTC. This decay is derived from observation (US Naval Observatory) and is a fraction of second, positive or negative. Therefore it may be neglected compared to the UTC.
In modeling the position of the sun in the sky in relation to the geographical points considered in this study, we will take into account two parameters namely :

— θ, the topocentric zenith angle ($^\circ$), measured from the local vertical.
— Γ, the topocentric astronomers azimuth angle ($^\circ$), measured **westward from south**.

The NOAA web site gives the "azimuth angle measured clockwise to the point of horizon directly below the sun from the north and the elevation measured vertically from that point on the horizon up to the sun". Therefore the comparison can be made by using the topocentric azimuth angle $\Phi = \Gamma + 180$ in Ref. [79]. The angles are limited in the range $[0; 360]^\circ$.
The position of the sun will be considered in two geographical positions of Mozambique namely, in the province of Maputo and in the district of Mecula :

— **Maputo** is the capital and largest city in Mozambique, it is the main financial, corporate and commercial center in the country. Each province is administratively divided into relatively small territories called districts, as is the case with the district of Macula
— **Mecula** is a district located in Niassa province in northern Mozambique

The position of the sun measured in topocentric zenith angle θ (in $^\circ$) and topocentric astronomers azimuth angle Γ (in $^\circ$) for Maputo province and Mecula village both in Mozambique can be described by graphs 3.44 and 3.45 below :

3.13.1 | Sun position in Maputo province

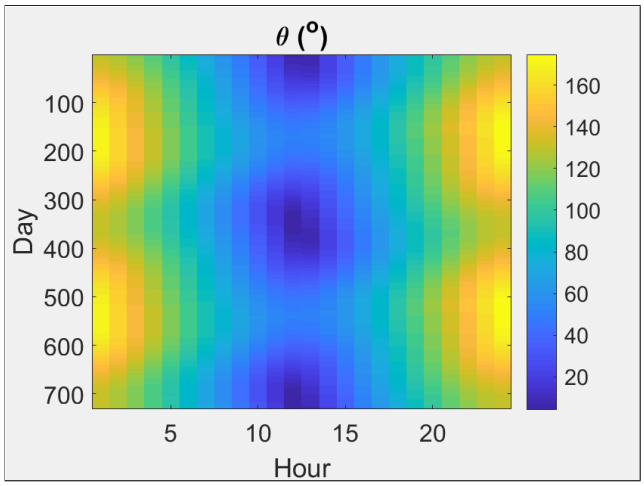

FIGURE 3.44 – Solar zenith angle θ in Maputo.

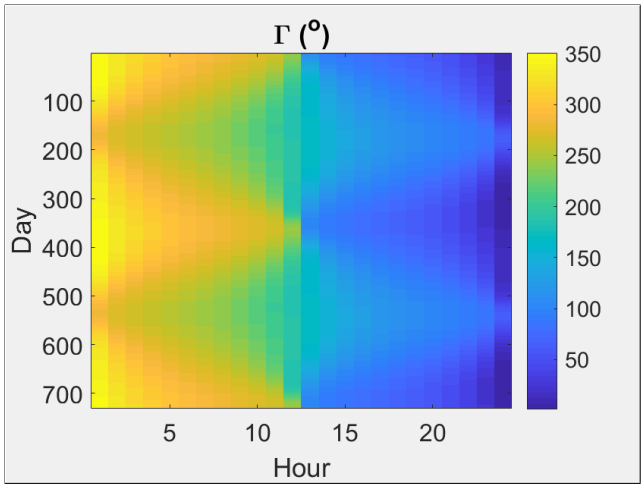

FIGURE 3.45 – Solar azimuth angle Γ in Maputo

Figures 3.44 and 3.45 illustrate the angles of sun illumination in Maputo province for each day and at each hour of the day during years 2019-2020.

3.13.2 | Sun position in Mecula district

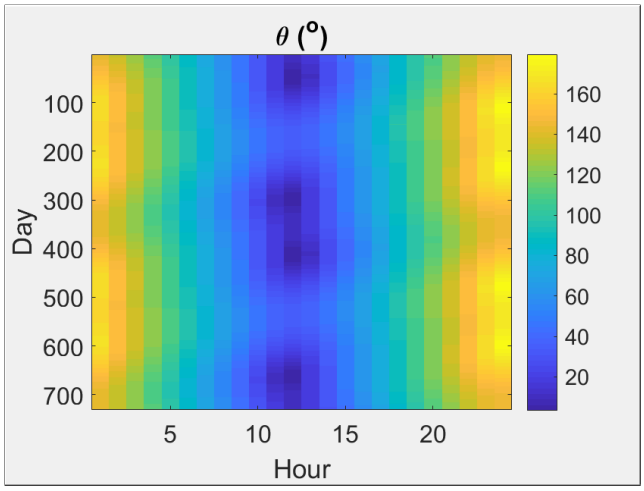

FIGURE 3.46 – Solar zenith angle θ in Mecula.

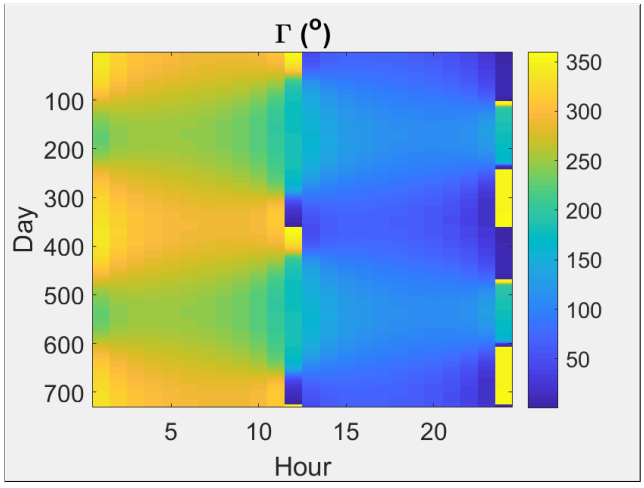

FIGURE 3.47 – Solar azimuth angle Γ in Mecula

Figures 3.46 and 3.47 illustrate the angles of sun illumination in Maputo province for each day and at each hour of the day during years 2019-2020.

3.13.3 | Comment on section figures 3.44,3.45, 3.46 and 3.47

According to [15] solar radiation on a global scale varies essentially as a function of the atmosphere, the geometry and the movement of the planet relative to the sun. At the local scale, the variation in solar radiation is mostly associated with the morphology of the terrain, such as variations in elevation, slope, exposure to the sun and shading. Mozambique has a high global radiation in the horizontal plane when compared to good places in Europe and Asia, being very close to some of the best places in the world, such as South Africa and California. Furthermore, Mozambique has a good solar resource, consistent throughout the territory and stable throughout the year.

3.13.4 | Optimization of the fixed panel orientation

The incidence angle I on a photovoltaic panel is deduced from :

$$I = \arccos\left(\cos(\theta).\cos(\omega) + \sin(\omega).\sin(\theta).\cos(\Gamma - \gamma)\right), \tag{3.96}$$

ω is the slope of the surface of photovoltaic panel surface measured from the horizontal plane, and γ is the surface azimuth rotation angle measured from south to projection of the surface normal on the horizontal plane, positive or negative if oriented east or west from south, respectively [79].
To improve the model, we include the transmittance of the overlying blade and the effect of shadowing of gridlines.

3.14 | The transmittance of the overlying blade

The transmittance of the overlying glass (or transparent medium) above the gridlines of the cell depends on the angle of incidence of light. The transmittance of plane wave through a glass blade of relative permittivity $\epsilon_2 \approx 2.25$ can be calculated from Fresnel coefficients [78]. The normal to the surface component of the incident wave vector is denoted w_1 in air and w_2

in glass : $w_1 = k_0 \cos(I)$, $w_2 = k_0\sqrt{\epsilon_2 - \sin^2(I)}$, with $k_0 = 2\pi/\lambda_0$, λ_0 being the wavelength of the incoming linearly polarized plane wave, under incidence angle I. The transmittance by the blade depends on the polarization of the light (s and p are the transverse electric and magnetic polarization respectively) :

$$T_s = \left|\frac{2w_1}{w_1 + w_2}\right|^2 . \left|\frac{2w_2}{w_2 + w_1}\right|^2 \tag{3.97}$$

$$T_p = \left|\frac{2\epsilon_2 w_1}{\epsilon_2 w_1 + w_2}\right|^2 . \left|\frac{2w_2}{w_2 + \epsilon_2 w_1}\right|^2 . \tag{3.98}$$

They are the product of transmittances by air-glass and glass-air single interfaces. Let us note the dependence on λ_0 only remains in the dispersion relation of ϵ_2. The sun light is unpolarized and therefore can be considered as an equal mix of these two perpendicular plane polarisation states. We consider unpolarized light impinging on the photovoltaic cell, even if its interaction with the atmosphere can lead to partially polarized light. The transmittance is calculated from 100,000 pseudo-random values r_s and r_p, following and uniform law of probability :

$$T_t = \frac{r_s T_s + r_p}{r_s + r_p} \tag{3.99}$$

The transmittance of unpolarized light by the glass blade is shown in Fig. 3.48.

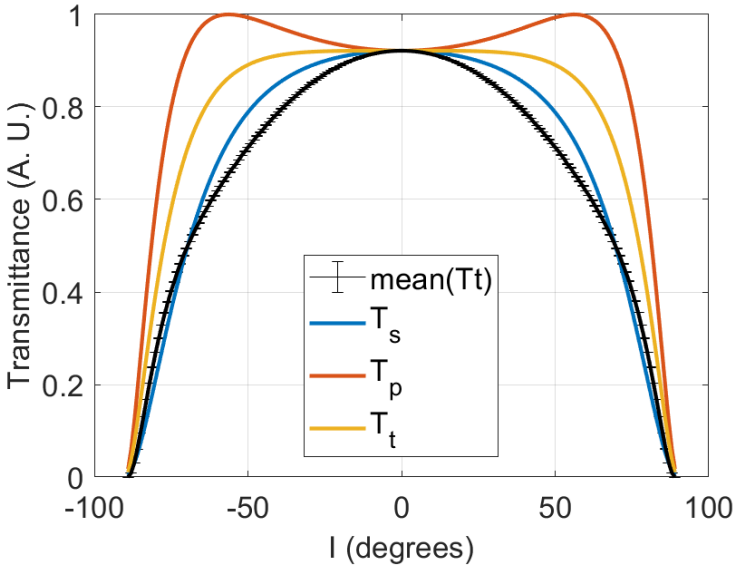

FIGURE 3.48 – Transmittance and Monte Carlo.

The spline fitting $\eta_p(I)$ of the result is used to calculate the effective solar radiation as a function of the incidence angle of sun light.

3.15 | The shadowing effect of the gridlines of cells

The electric power produced by the photovoltaic panel depends on the solar illumination and on the angle of incidence of the solar light on the panel. The angular dependence of the solar cell efficiency is commonly considered following a cosine law of the light incidence angle I. Authors of Ref. [80] gives an improved formula of the efficiency and distinguish the cases of illumination parallel and perpendicular to the cell gridlines. The efficiency is not sensitive to illumination incidence angle parallel to the gridlines. On the contrary, in the upright case of incidence, they identify three contributions : the classical cosine function loss, a sine function loss due to the reflected light from the gridlines, and a tangent function loss due to the shading effect. They fitted experimental data and obtained :

$$\eta_\perp = 1.81\% \sin(I) + 27.07\% \cos(I) - 1.86\% \tan(I), \tag{3.100}$$

where 27.07% is the maximum efficiency of th investigated panel and I the incidence angle. We rewrite this equation as a function of the maximum efficiency η_{max} of the panel :

$$\begin{aligned} \eta_\perp &= \eta_{max} \left(\frac{1.81}{27.07} |\sin(I)| + \cos(I) - \frac{1.86}{27.07} |\tan(I)| \right) \\ &\approx \eta_{max} \left(0.067 |\sin(I)| + \cos(I) - 0.069 |\tan(I)| \right). \end{aligned} \tag{3.101}$$

According to Ref. [80], if the incoming light is along the gridlines, $\eta_\parallel = \eta_{max}$. The gridlines projection of alignment is along the vertical direction. Therefore, we have to consider both angle of incidence of light on the solar panel that depend on the panel orientation with the horizontal plane. The useful solar radiation which produces the photon-current Iph is deduced from formula 3.102 as follows :

$$G_{eff} = G \left[\eta_\perp |\sin(\Gamma - \gamma)| + \eta_\parallel |\cos(\Gamma - \gamma)| \right], \tag{3.102}$$

where $\Gamma - \gamma$ is the angle between the direction of light incidence and the gridlines of the panel.

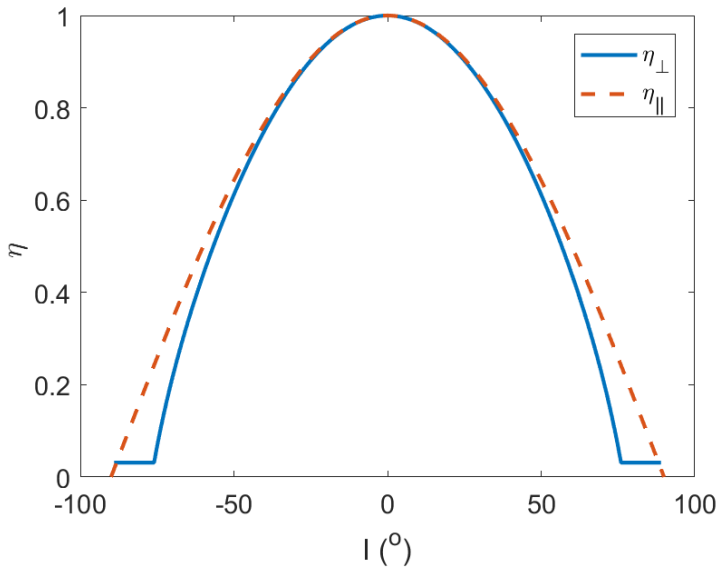

FIGURE 3.49 – Parallel and perpendicular efficiencies due to shadowing effect.

3.16 | The fitness function

The fitness function is the sum over hour of the solar irradiation G corrected with the shadowing effect and the angular dependence of the cover blade transmittivity :

$$F = \sum_{H} \left[G. \underbrace{\left(\eta_{\parallel} |\cos(\Gamma - \gamma)| + \eta_{\perp} |\sin(\Gamma - \gamma)| \right)}_{\text{shadowing effect}} . \underbrace{\eta_p(I)}_{\text{transmittance of non polarized light}} \right] \tag{3.103}$$

The maximum of illumination efficiency $\max(F(\omega, \gamma))$ is searched for every day of 2019 and 2020. The required accuracy on the panel orientation being less than the degree, we use a double loop on ω and γ with degree path of discretization.

3.17 | Parameters of the best orientation of the photovoltaic panel

3.17.1 | For Maputo province

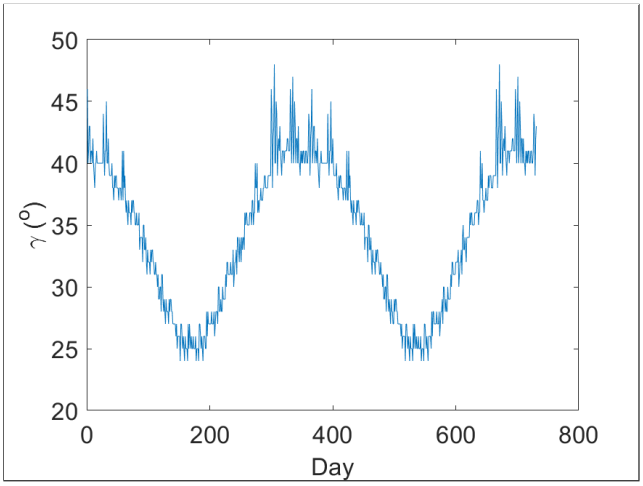

FIGURE 3.50 – Best γ : tilt of the PV panel relatively to the local horizontal plane

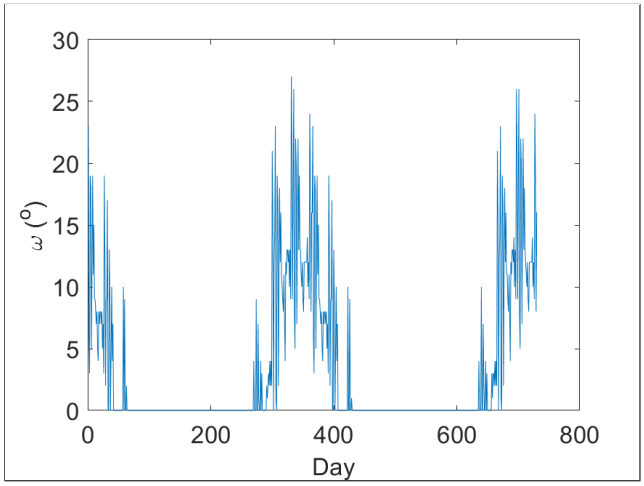

FIGURE 3.51 – Best ω : tilt of the PV panel relatively to the N-S direction.

Figures 3.50 and 3.51 illustrate the parameters of the best orientation of photovoltaic panel as a function of the day (2019-2020) for Maputo province (longitude $\sigma = 32.58322°$, latitude $\phi = -25.96553°$

3.17.2 | For Mecula district

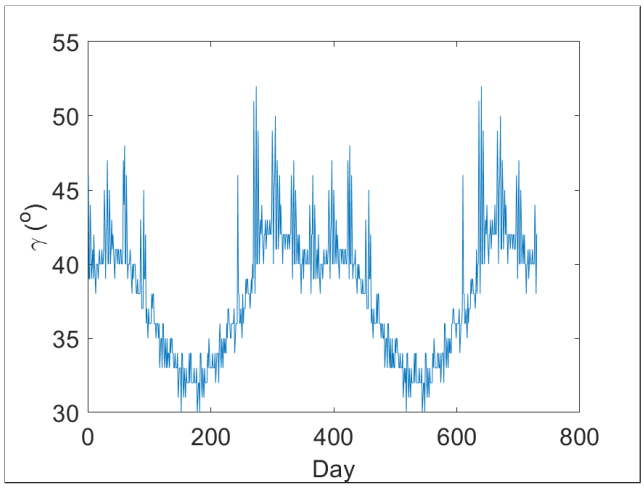

FIGURE 3.52 – Best γ : tilt of the PV panel relatively to the local horizontal plane

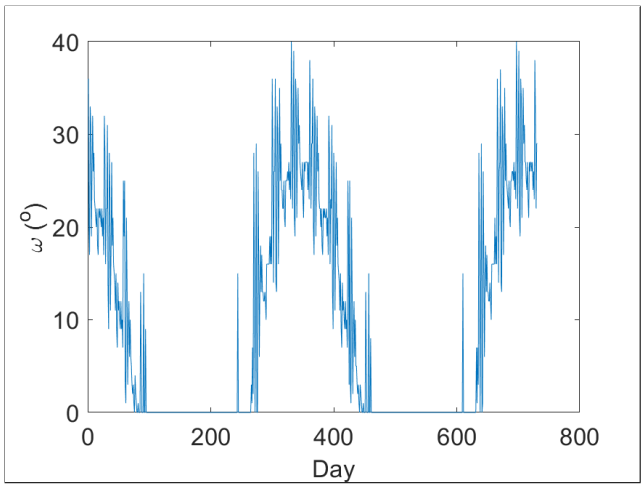

FIGURE 3.53 – Best ω : tilt of the PV panel relatively to the N-S direction.

Figures 3.52 and 3.53 illustrate parameters of the best orientation of photovoltaic panel as a function of the day (2019-2020) for Mecula town (longitude $\sigma = 37.667°$, latitude $\phi = -12.116°$

The best azimuth rotation angle γ varies from east to west for increasing day of year.
Near the equinox (March 20, 2019 and 2020, September 23, 2019 ; September 22 2020), γ is close to $\min(\gamma) + \max(\gamma))/2$ and is maximum or minimum at solstice days : June 21, 2019 ; June 20, 2020 ; December 22, 2019 ; December 21, 2020, respectively.
In case of static panel (that does not follow the sun trajectory), the best panel orientation also depends on the solar radiation G (W m^{-2}).
We deduce the best orientation of the panel, considering the maximum of the cumulative sum of G_{eff} over the two investigated years (2019-2020). For this calculation, we choose $\eta_{max} = 1$.

— Best ω (the slope of PV panel measured from the horizontal plane).

Maputo : the mean value of $\omega°$ is 3 with standard deviation of 6°. The most probable value is in [0,1]°. Therefore, the best value of the panel slope measured from horizontal plane is chosen to $\omega = 5°$. This little tilt could reduce the soiling of the photovoltaic panel without significant loss of efficiency.

Mecula : the mean value of $\omega°$ is 10 with standard deviation of 11°. The most probable value is in [0,1]°.

Therefore, the common value of the panel slope measured from horizontal plane is also chosen to $\omega = 5°$.

— Best γ (the azimuth rotation angle from south direction in the plane of the photovoltaic panel). $\gamma = 0$ correspond to gridlines parallel to the N-S direction.

Maputo : the mean value of $\gamma°$ is 34 with standard deviation of 6°. The most probable value is in [41,42]°.

Mecula : the mean value of $\gamma°$ is 38 with standard deviation of 4°. The most probable value is in [40,41]°.

Therefore, we choose $\gamma = 38°$ as a common value for the tilt of the photovoltaic gridlines relative to the N-S direction.

The common best solutions at Mecula and Maputo are $\omega \approx 5°$ and $\gamma \approx 38°$. Therefore, the ideal position of the panel a little bit tilted and headed south.

Remark 3.6. If we include the maximum production of the PV panel :

$$Tcell = Ta + (tnmot - tnoc)\frac{G}{Gstd}$$

$$pmax = pmax0.(1 + kpmax.(Tcell - tstd))\frac{G}{Gstd}$$

The result is the same, the maximum power being independent on the angle of incidence.

3.18 | Influence of the aging of photovoltaic panels

Experimental laws of aging have been established in [81, 82, 83]. The influence of external location and illumination of panels produces decrease of panel power production efficiency. Authors of Refs. [81, 82, 83] give the results of fitting of experimental data, as function of time t (years).

— The transmittance of the glass blade decreases from the initial transmittance $T(0)$ as :

$$T(t) \approx T(0) - 0.004t \tag{3.104}$$

— The produced maximum electric power decreases from the initial transmittance $T(0)$ as :

$$pmax(t) \approx pmax(0) - 0.12t \tag{3.105}$$

— The series resistance increases as :

$$Rs(t) \approx Rs(0) + 0.0012t \tag{3.106}$$

— The parallel resistance decreases as :

$$Rp(t) \approx Rp(0) + 0.018.t^2 - 2.352.t \tag{3.107}$$

This last law of aging is the most accurate (9 points for fitting against 5 more dispersed points for the others).

These results depends on the studied photovoltaic panel but the global behavior and their order of magnitude can be used to evaluate the effect of time on the production.

3.19 | Mathematical Modeling of the BESS

The battery parameters are normally provided by the manufacturer, in the modeling developed in this thesis, we consider the following parameters :

— I_{10} nominal battery current (A) : the current that can be delivered by the battery over 10 hours.

— C_{10} nominal capacity of the battery (A h) : the energy that ca be delivered by the battery over 10 hours, under constant current discharge regime.

— n_b number of battery elements, or cells (2 V) : in the following, we use the model introduced by Copetti ([63] CIE model : series of 2V cells, which characteristics are known by fitting experimental data).

— $V_{bat} = 2.n_b$ (V).

We suppose the dynamic regime of battery use (or floating charge model [64]). Indeed, each hour, the battery can simultaneously charged (intensity current I_c) and discharged (intensity current I_d). Therefore, the battery current is $I_{bat} = I_c - I_d$. Note that the control of each phase may improve the use of battery [63]. However, this regime simplify the model, by neglecting the hysteresis characteristic of charge and discharge (see discussion and figures (2) and (5) in [84]).

References [5, 4] are based on the Copetti model [63]. We use their numerical results to check the validity of our code. Copetti et al [63] discuss the charge or discharge currents expressed

as a function of n hours $I(C_n) = C_n/n$.
We suppose therefore, the relation between the current and the capacity given by :

$$I_{10}\frac{C_{10}}{10}, \tag{3.108}$$

C_{10} being the nominal capacity of the battery in a constant current discharge regime for 10 hours [4, (4) p. 4449]. **Consequently, the number of 2V cells in the battery that can be deduced from the battery voltage and either the nominal current or the nominal capacity are necessary to describe the battery.**
In this BESS modeling, we assume the following input parameters :

- C10 = 2000 : Nominal capacity of the battery : C10 = 1000 Ah ;
- I10 = 10 : Nominal current of the battery : I10 = 10 A
- nb = 24 : Number of cells in series nb = 24 for each battery
- Vbat=2.nb : Nominal voltage of each battery cell
  charge current intensity
- Discharge Current=26 A, from Ref. [5]
- maxload=(Discharge Current).(Vbat) : Watt
- DeltaT=20 : Temperature of the battery
- $\eta_{AC/DC}$=0.95 : Efficiency of rectifier between
  Wind-turbine and battery
- $\eta_{DC/AC}$=0.92 : Efficiency of inverter between
  Battery and consumer demand

Note that the model of battery is tedious and that we have to combine some requirements of models in various papers to increase the validity of our approach. For example, only some of them include the effect of temperature variations on the performance of batteries. The models of battery capacity and state of charges vary from one author to another. Authors include different electrical and chemical models to describe the battery behavior. Some models use dynamical evolution through differential equations, and coupled equations that require iterative resolutions. To get a reasonable complexity of the model and to reduce the computational time (for further repeated use of it), we choose a deterministic model that involves some approximations.
Approximation : The floating use of battery : the simultaneous charge and discharge in continuous mode of use, simplifies the time behavior of the battery by suppressing the influence of the time hysteresis (and characteristic time) of each change of mode. The discontinuity of

current due to the control of operating modes like in Ref. [63] may be neglected, in case of 1 hour of charge or discharge, at each time step.

3.20 | Battery intensity current

In dynamic regime of battery use (or floating charge), the battery current is deduced from both charge and load P_l [64] (kW) :

$$I_{bat} = \frac{1000 \cdot (n_{SC} P_{SC} + n_{WT} P_{WT} \eta_{AC/DC} - P_l / \eta_{DC/AC})}{V_{bat}}, \tag{3.109}$$

where :

— P_{SC} is the power produced by each of the n_{SC} solar-cells (kW),
— P_{WT} is the power produced by each of the n_{WT}wind-turbines (kW),
— $\eta_{DC/AC} = 0.95$ is the efficiency of the DC/AC converter (called "inverter" in [64]),
— $\eta_{AC/DC} = 0.92$ is the efficiency of the AC/DC converter (called "rectifier" in [64]).

We suppose a grid of n_{SC} identical solar-cells and n_{WT} wind-turbines. To test the codes, we have to adjust the power produced by wind-turbines and solar-cells, and used by consumer. We keep the time dependence of each power, but we impose the maximum value to compare to the results with those in Ref. [5].

3.21 | Battery voltage

Assuming the above definitions, we introduce the battery voltage as following, depending of the operating mode (d : discharge, c : charge, Eq. 3.109) :

$$V_d = n_b E_d - n_b R_d I_d \quad \text{if} \quad I_{bat} < 0 \tag{3.110}$$

$$V_c = n_b E_c + n_b R_c I_c \quad \text{if} \quad I_{bat} > 0 \tag{3.111}$$

These equations are the same as those in Refs. [63, 5, 4]. Some papers show different approach : polynomial fitting of V_{bat} as a function of SOC [64]. In Yahia paper [5], different cases for charge are introduced.

Operating type	Intensity current	Condition
Discharge	$I_{bat} < 0$	$V_d > 0.9V_N$
Strong discharge	$I_{bat} < 0$	$0.9V_N > V_d > 0.7V_N$
Deep discharge	$I_{bat} < 0$	$0.7V_N > V_d$

TABLE 3.7 – Operation area for discharge of the battery, V_N being the nominal voltage of the battery.

Obviously, these characteristic are those of each battery cell with nominal voltage 2 V. We must evaluate each unknown E_d, E_c (the electromotive forces) R_d and R_c (internal resistances) that depend on the operating mode and on :

— the capacity $C(T, C_{10}, I_{bat}, t)$, the amount of energy that can be restored by the battery (A h) (note the error in formula (3) in Laadissi paper [4]).

— the state of charge $SOC(C, T, I_{10}, C_{10}, I_{bat}, t)$, indicates how electric charges is stored in the cell at a given time t. SOC can be expressed in %.

t being the considered time of operation (charge or discharge), and T the temperature of the battery that can be influenced by the Joule loss deduced from R_d and R_c.
The following equations involve $\Delta T = T - 25°C$. ΔT is the heating of the battery and is generally set to an arbitrary but realistic value, between 5 and 45°C in [63].

3.22 | Joule loss

The battery Joule loss can be expressed as :

$$P_J = R_d I_d^2 \quad \text{if} \quad I_{bat} < 0 \tag{3.112}$$

$$P_J = R_c I_c^2 \quad \text{if} \quad I_{bat} > 0 \tag{3.113}$$

I_d and I_c are tables of positive values with size (day $\times$ hour = 731 $\times$ 24) to speed the calculations. $I_d = 0$ when $I_c \neq 0$ and conversely.
The maximum temperature elevation due to Joule loss is given by :

$$\Delta T_J = 3600 \cdot \frac{P_J}{mC_p} \tag{3.114}$$

m being the mass of the battery and C_p its mean thermal capacity.
It remains to calculate the capacity C of the battery, its SOC, and R_c, E_c, R_d, E_d. These quantities depend on the state of charge (SOC) and therefore on the charge and discharge efficiencies.

3.23 | Charge and discharge efficiencies

The efficiency of the battery during charge is supposed to be 100% [63, 64, 4], on the contrary, the efficiency in discharge mode is less than 100% : 90% in [64]. Due to Faradic process, the efficiency in charge and discharge are [63, 4, 5] :

$$\eta_c = 1 - \exp\left(\frac{20.73}{\frac{I}{I_{10}} + 0.55}(SOC - 1)\right). \tag{3.115}$$

$$\eta_d = 100\%. \tag{3.116}$$

In this case, the efficiency depends on SOC. In Ref. [64], the charge and discharge efficiencies are approximated by :

$$\eta_c = 90\% \tag{3.117}$$

$$\eta_d = 100\%. \tag{3.118}$$

We prefer using the first expression of the efficiencies, that depends on SOC and therefore on temperature. This efficiency dose not include the Joule losses.

3.24 | Battery capacity

The calculation of the battery capacity C is necessary to calculate the SOC. Copetti et al [63] give a typical fit of a 2V battery cell :

$$C = \frac{1.67C_{10}}{1 + 0.67\left(\frac{I_d}{I_{10}}\right)^{0.9}}(1 + 0.005\Delta T) \tag{3.119}$$

During discharge, C is limited by the current rate. Copetti uses I_d in this formula, even if the same notation I is used in all formula. Therefore, we suppose he means I_{bat} bu in discharge mode.

— $I_d = 0 \Rightarrow C = 1.67C_{10}(1 + 0.005\Delta T)$ (charge).
— $I_d < I_{10} \Rightarrow C > C_{10}(1 + 0.005\Delta T)$.
— $I_d = I_{10} \Rightarrow C = C_{10}(1 + 0.005\Delta T)$ with only temperature correction.

— $I_d > I_{10} \Rightarrow C < C_{10}(1 + 0.005\Delta T)$.

When the discharge current tends to zero, the maximum capacity that can be removed is about 67% over the capacity C_{10} at 25°C.

In Refs. [4, 5], the *mean value* of the discharge current is used.

If we suppose that the average is on one hour, we find again I_d.

$$\boxed{C = \frac{1.67 C_{10}}{1 + 0.67 \left(\frac{\bar{I}_d}{I_{10}}\right)^{0.9}} (1 + 0.005\Delta T)} \tag{3.120}$$

The **capacity** is a function of :

— ΔT The heating of the battery compared to the ambient temperature of 25°C. It is assumed to be identical for all elements of the battery.

— $\bar{I}_d$ the ***discharge*** *current.* (A).

Copetti et al [63] suppose it is valid for Fulmen EF2050 ($C_{10} = 50$A h), Varta Vb624 ($C_{10} = 100$A h) and ATSA Tudor ($C_{10} = 180$A h).

This formula is used in Refs. [63, 4, 5]. However, the capacity has no dependence on current intensity in [64]. Let us note that this formula depends on the used battery cell.

As T varies between 5 to 45°C, the temperature correction can be smaller or greater than 1.

We have to calculate the mean value of capacity expressed as :

$$C = C10\, 1.67/(1 + 0.67(Id/I10)^{0.9})\,(1 + 0.005.\Delta T) \tag{3.121}$$

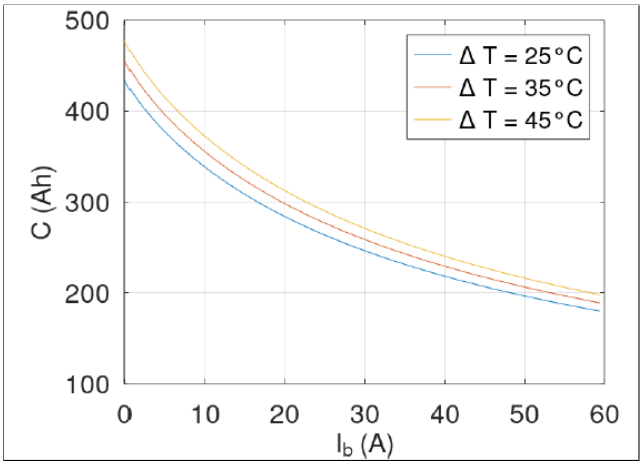

FIGURE 3.54 – Battery Capacity from our code

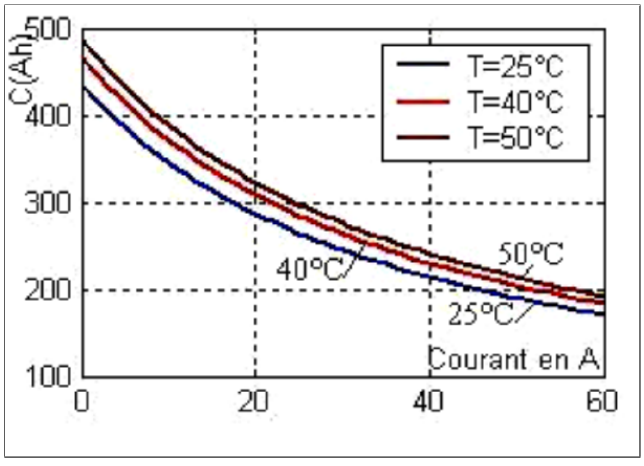

FIGURE 3.55 – Capacity from [5]

Figures 3.54 and 3.55 illustrate the Capacity of the battery, with $n_b = 24$ elements, $C_{10} = 260\text{A h}$, $I_{10} = 26\text{A}$, as a function of the average discharge current.

3.25 | Battery State-of-Charge (SOC)

The **state of charge** SOC of the battery is a function of the **capacitance** C_{bat} and the **amount of charge missing at the battery** Q_m which depends on the operating mode of the battery. The determination of SOC is critical to describe the behavior of the battery in charge and discharge operating modes, but tedious. Authors introduce different models for SOC.

— In Refs. [63, 5, 4], it is defined by :

$$SOC = 1 - \frac{I_d \times t}{C}. \tag{3.122}$$

The value of SOC **is therefore between** 0 **and** 1**.** Copetti et al relate C to the battery efficiency and $I_d t$ is the missing charge quantity in the battery.

— In Ref. [4], the definition of the SOC is the same but they introduce the total charge Q_{bat} in the battery, involving the faradic efficiency (**also depending on SOC**, Eq. 3.131), therefore we introduce the battery efficiency η_{bat} :

$$Q_{bat} = Q_{t-1} + \eta_{bat} \int_0^t I_{bat} dt, \tag{3.123}$$

where η_c depends on the operating mode of the battery. The integral boundary 0 is strange as the previous state Q_{t-1}. Therefore, we would rewrite :

$$Q_{bat}(t) = Q_{bat}(t-1) + \eta_{bat} \int_{t-1}^t I_{bat} dt, \tag{3.124}$$

This formula clarifies the role of the battery faradic efficiency in Copetti et al calculations. For one hour, the intensity current being constant, the charge in battery can be written :

$$Q_{bat}(t) = Q_{bat}(t-1) + \eta_{bat} I_{bat} t. \tag{3.125}$$

Therefore, the SOC is deduced :

$$SOC(t) = \frac{Q_{bat}}{C} = \frac{Q_{bat}(t-1) + \eta_{bat} I_{bat} t}{C}. \tag{3.126}$$

This formula handles the operating mode at time t.

— In Ref [64] introduce additional time dependence deduced from the self discharge rate $\sigma = 0.002$:

$$SOC(t) = SOC(t_0)\left[1 - \frac{\sigma}{24}(t - t_0)\right] + \int_{t_0}^{t} \frac{I_{bat}\eta_{bat}}{C} dt. \tag{3.127}$$

Considering constant current for $t - t_0 = 1\text{h}$:

$$\boxed{SOC(t) = SOC(t-1)\left[1 - \frac{\sigma}{24}\right] + \frac{I_{bat}\eta_{bat}}{C}.} \tag{3.128}$$

Again, I_{bat} is either negative in discharge mode, positive in charge mode. Therefore, this definition of SOC is iterative, includes the model of self-discharge mode and the battery capacity.

— In Ref. [85], the calculation of the charge depends on battery voltage and current. Therefore, it leads to autocoherent equations, these electrical characteristics depending on SOC or requires different fittings of the voltage and intensity. The same approach is proposed in Refs. [86, 64].

For coherence of the whole model of battery, we choose to pursue with the fitted data in Ref. [63] also used in Refs. [4, 5], but with the self discharge correction (Eq. 3.128) and the battery capacity in Eq. 3.120. The value of the battery efficiency is supposed to be a constant at this stage [64] :

$$\eta_{bat} = 1 \text{ in discharge mode} \tag{3.129}$$

$$\eta_{bat} = 0.90 \text{ in charge mode} \tag{3.130}$$

The electric energy loss in battery is due to faradic performance, relating the capacity to the battery to store energy (Laadissi [4] and Copetti [63] p. 286, citing reference 8). The efficiency of charge drops to zero at full charge. The charge efficiency is represented by the following function :

$$\eta_c = 1 - \exp\left(\frac{20.73}{\frac{I}{I_{10}} + 0.55}(SOC - 1)\right). \tag{3.131}$$

The numerical parameters are found by fitting this equation to actual data (tabular positive plates and low-antimony alloys) ([63], Eq. (5) p. 209).

To derive the state-of-charge formula, to include the state-of-charge that depends on the capacity as referred to in [63] requires a series of calculations as folowing :

$$\eta_{bat} = \eta_c(t-1) = 1 - \exp\left(\frac{20.73}{\frac{I}{I_{10}} + 0.55}(SOC(t-1) - 1)\right) \tag{3.132}$$

$$SOC(t) = SOC(t-1)\left[1 - \frac{\sigma}{24}\right] + \frac{I_{bat}\eta_{bat}}{C} \tag{3.133}$$

Therefore, we can deduce $SOC(t)$ from $SOC(t-1)$ and $\eta_c(t-1)$.
In our model, we consider time and day evolution. Consequently, we should consider the SOC and η_c at the beginning of a given day equal to the SOC and η_c at then end of previous day. The data used should therefore cover all the hours of the day. If we consider only a period of the day (between 6 AM and 7 PM), we must suppose that during the night, the wind-turbine produce the energy that is necessary to answer to the consumer demand.

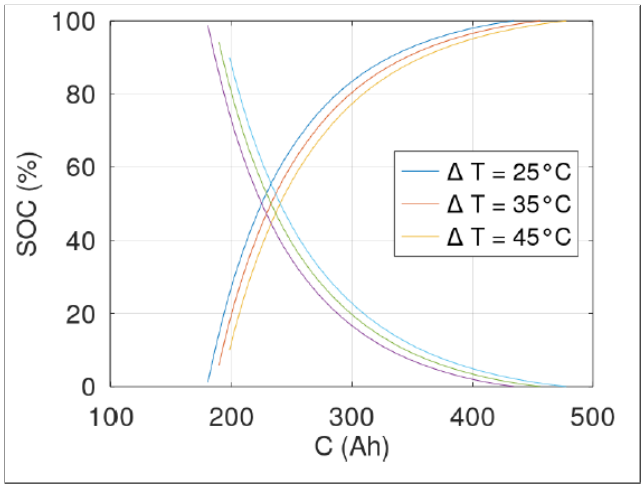

FIGURE 3.56 – Battery SoC of this thesis

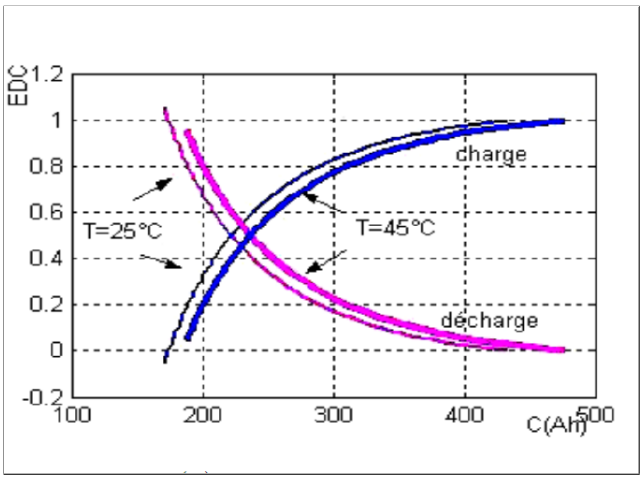

FIGURE 3.57 – Battery SoC from [5]

Figures 3.56 and 3.57 illustrate the State of charge of the battery, with $n_b = 24$ elements, $C_{10} = 260$A h, $I_{10} = 26$A, as a function of capacity, for $t = 3$h.
SOC can be calculated easily at any point during the discharge period, nevertheless during (re)charge it is more difficult. Generally, the efficient region is where SOC is below 0.7 and V_c is less than 2.3V per cell [63, p. 285]. Therefore, the charge efficiency efficiency η_c is given in Sec. 3.25 (Eq. 3.131).

3.26 | Discharge voltage, EMF and resistance

The battery voltage with n_b cells in **discharge** mode is :

$$V_d = n_b E_d - n_b R_d |I_d|, \tag{3.134}$$

with :

$$E_d = 2.085 - 0.12(1 - SOC) = 1.965 + 0.12\ SOC \tag{3.135}$$

$$R_d = \frac{1}{C_{10}} \left(\frac{4}{1 + |I|^{1.3}} + \frac{0.27}{SOC^{1.5}} + 0.02 \right) (1 - 0.007 \Delta T) \tag{3.136}$$

3.26.0.1 | Comparison with Ref. [5]

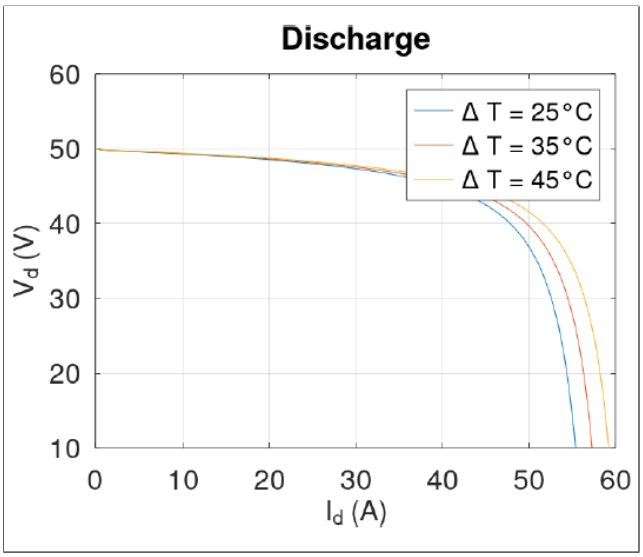

FIGURE 3.58 – Discharge voltage, V_d

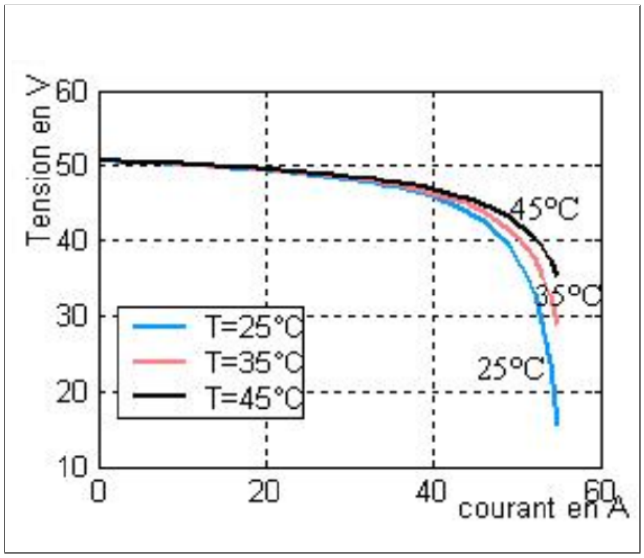

FIGURE 3.59 – Discharge voltage [5]

Figures 3.58 and 3.59 illustrate the Voltage of the battery, with $n_b = 24$ elements, $C_{10} = 260\text{A h}$, $I_{10} = 26\text{A}$, as a function of current.
The resistance of discharge (Eq. 3.136) is evaluated as a function of the state of charge (SOC) in Yahia paper. When the battery is fully charged, R_d is small and it increases with smaller SOC.

3.26.0.2 | Discharge Resistance R_d

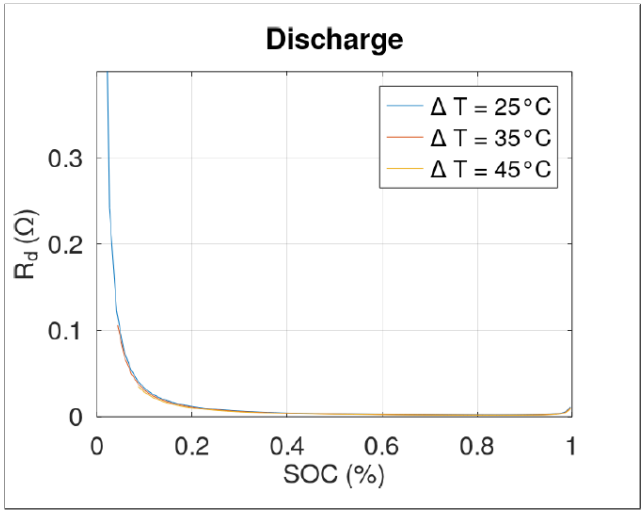

FIGURE 3.60 – Discharge resistance, R_d

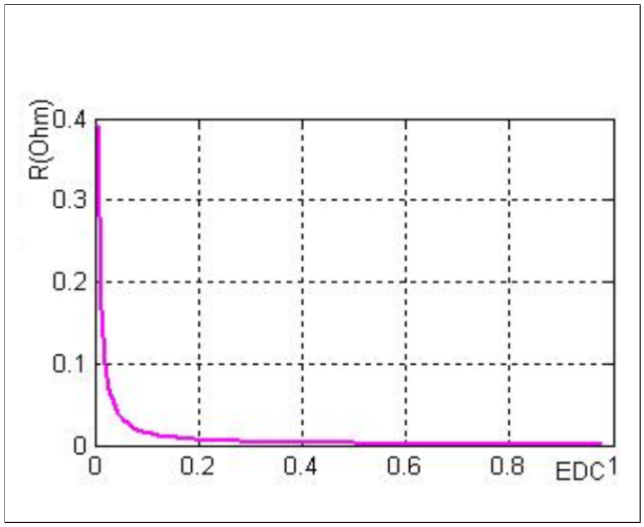

FIGURE 3.61 – R_d from [5]

Figures 3.60 and 3.61 illustrate the discharge resistance R_d of the battery, with $n_b = 24$ elements, $C_{10} = 260\text{A h}$, $I_{10} = 26\text{A}$, as a function of the state of charge.

3.26.0.3 | Discharge Voltage V_d

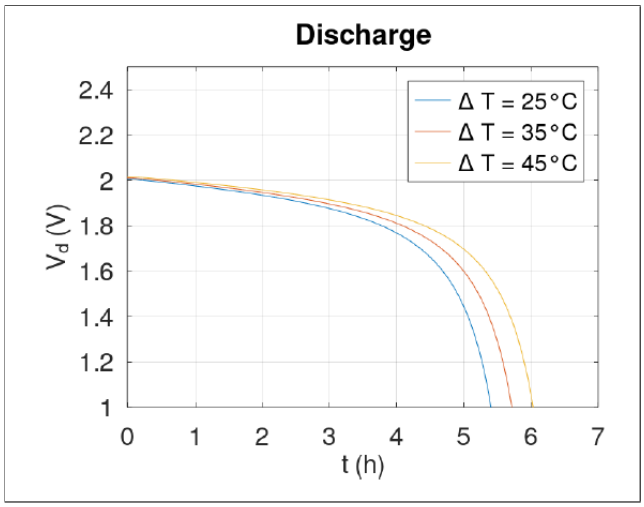

FIGURE 3.62 – Discharge voltage, V_d

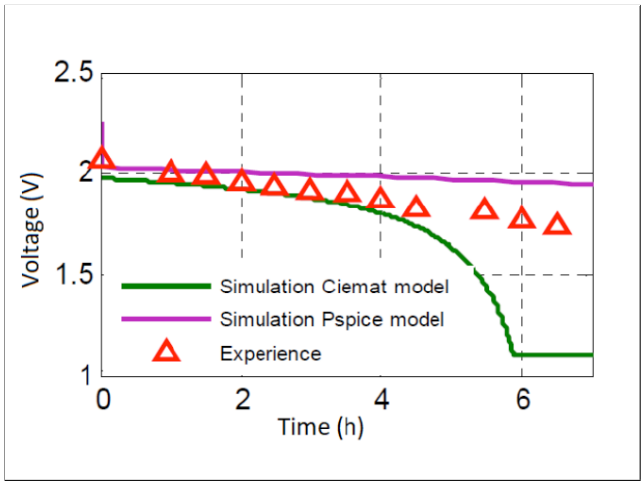

FIGURE 3.63 – V_d from [4]

Figures 3.62 and 3.67 illustrate discharge voltage with $n_b = 1$ element, $C_{10} = 62\,\mathrm{A\,h}$, $I_{10} = 10\mathrm{A}$, as a function of time. There is a difference between our results and those of Laadissi et al : for the discharge, they probably introduce a discharge threshold after 5.8 hour, that is not explained in the text and included in the formula they published. The global behavior is the same for shorter time. They do not mentioned the temperature elevation for CIEMAT calculations.

3.27 | Charge EMF, voltage and resistance

The battery voltage with n_b cells in **charge** mode is :

$$V_c = n_b \cdot E_c + n_b \cdot R_c \cdot I, \tag{3.137}$$

with :

$$E_c = 2 + 0.16 \cdot (SOC) \tag{3.138}$$

$$R_c = \frac{1}{C_{10}} \left(\frac{6}{1 + |I|^{0.86}} + \frac{0.48}{(1 - SOC)^{1.2}} + 0.036 \right) (1 - 0.0025\Delta T) \tag{3.139}$$

3.27.0.1 | Charge Voltage V_c

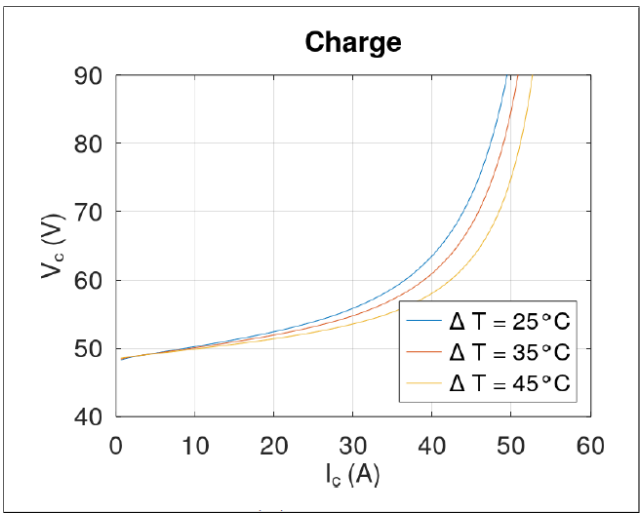

FIGURE 3.64 – Charge voltage, V_c

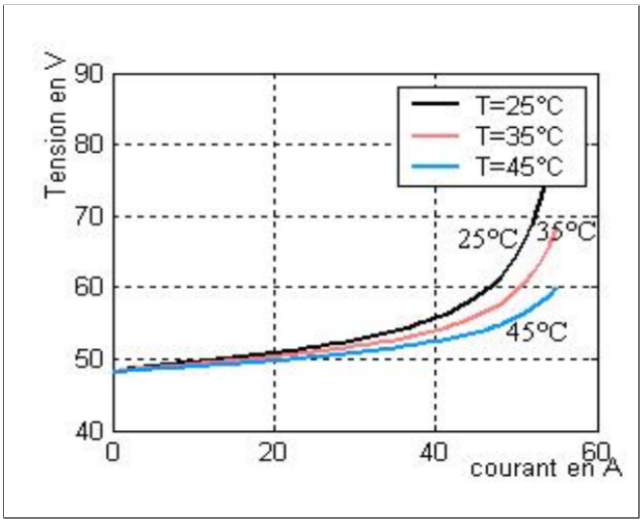

FIGURE 3.65 – V_c by [5]

Figures 3.64 and 3.65 illustrate Voltage of the battery, with $n_b = 24$ elements, $C_{10} = 260\text{A h}$, $I_{10} = 26\text{A}$, as a function of current. The resistance of charge (Eq. 3.139) is evaluated as a function of the state of charge (SOC) in Yahia paper. When the battery is fully charged, R_c is great and when the charge efficiency is small.

The charge may induce gassing process. It results in an increase of the final charge voltage V_{cc} with current intensity and with decreasing temperature. The gassing voltage V_g is :

$$V_g = \left(2.24 + 1.97 \ln\left(1 + \frac{I}{C_{10}}\right)\right)(1 - 0.002\Delta T). \tag{3.140}$$

The final charge voltage is :

$$V_{cc} = \left(2.45 + 2.011 \ln\left(1 + \frac{I}{C_{10}}\right)\right)(1 - 0.002\Delta T). \tag{3.141}$$

The overcharge phenomenon (gassing evolution) can be represented by an exponential function, suc as

$$V_c = V_g + (V_{cc} - V_g)\left(1 - \exp\left(\frac{Ah_r - 0.95C}{I\tau}\right)\right). \tag{3.142}$$

The time constant τ is :

$$\tau = \frac{17.3}{1 + 852\left(\frac{I}{C_{10}}\right)^{1.67}}. \tag{3.143}$$

Operating type	Intensity current	Condition	Charge efficiency
Charge	$I > 0$	$V < V_g$	$0 < \eta_c < 1$
Gassage	$I > 0$	$V_g < V < V_{cc}$	$0 < \eta_c < 1$
Saturation	$I > 0$	$V = V_{cc}$	$\eta_c = 0$

TABLE 3.8 – Operation area for charge of the battery.

3.27.0.2 | Charge Voltage as function of time $V_c(t)$

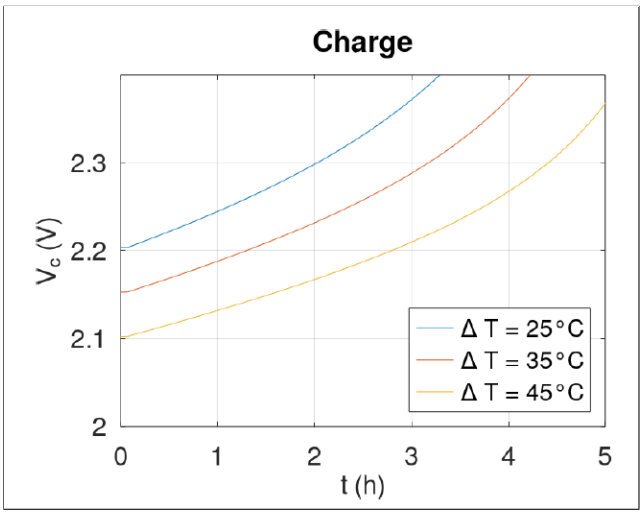

FIGURE 3.66 – Charge voltage $V_c(t)$

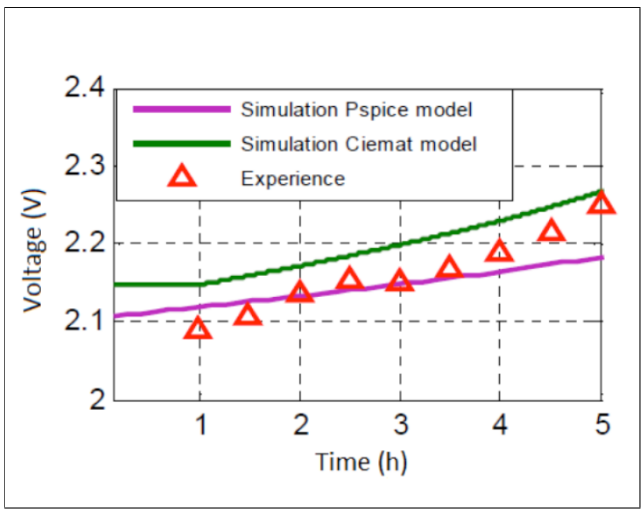

FIGURE 3.67 – $V_c(t)$ by [4]

There is a difference between our results and those of [4] as for the discharge, the curves are. The global behavior is the same for shorter time. They do not mentioned the temperature elevation for CIEMAT calculations.

3.28 | Range of Δt

The previous models of currents and voltages handle factor terms of the form $(1 - a\Delta t)$. The temperature correction cannot be negative number, the resistances being positives numbers.

— $I_c, V_c, R_c : a = 0.0025°\mathrm{C}^{-1}$,
— $I_d, V_d, R_d : a = 0.0007°\mathrm{C}^{-1}$,
— $V_g, V_{cc} : a = 0.002°\mathrm{C}^{-1}$.

Therefore, the maximum of a in the above equations being 0.0025, the maximum value of ΔT is :

$$\boxed{\max(\Delta T) = \frac{1}{0.0025} = 40°\mathrm{C}^{-1}} \tag{3.144}$$

If $\Delta T = 40°\mathrm{C}$, the charge voltage is a constant of the charge current. We have to control the temperature elevation we consider in the following.

Note : in Ref. [64], Zhou et al use about the same temperature coefficient, but with temperature in K instead of °C.

3.29 | Energy loss in battery : battery efficiency and temperature elevation

Two sources of energy loss are under consideration : faradic and Joule losses.

3.29.1 | Joule efficiency

The Joule energy loss is due to the resistances of charge R_c and discharge R_d, therefore, the battery efficiency due to Joule loss can be evaluated, in both operating modes :

$$\eta_r = \frac{E_d}{V_d} + \frac{E_c}{V_c} \tag{3.145}$$

The total efficiency of the battery being :

$$\eta_t = \eta_r . \eta_c \tag{3.146}$$

The global calculation of the relation between the input (from wind-turbines an solar-cells) power P_i and possible output (load) power P_o can be written :

$$P_o = \eta_t P_i = \eta_c \eta_r P_i \tag{3.147}$$

$$= \left[1 - \exp\left(\frac{20.73}{\frac{I}{I_{10}} + 0.55}(SOC - 1)\right) \times \left(\frac{E_d}{V_d} + \frac{E_c}{V_c}\right)\right] P_i \tag{3.148}$$

As P_o and the target P_i are known, we should deduce the characteristics of required batteries. (I_{10} and C_{10}).
Let us note that the Joule loss of energy contributes to temperature elevation of the battery. The temperature elevation of the battery (mass m and specific heat C_p) is :

$$\Delta T = 3600 \frac{R_c . I_c^2 + R_d I_d^2}{m C_p} - \Delta T(radiation) - \Delta T(convection) \tag{3.149}$$

The value of C_p must be found. The cooling by radiation and convection should be evaluated as well. In "Thermal management of Li-ion batteries using PCM- Metal foam composite : Experimental and numerical investigations" by EL IDI et al (`https://www.sft.asso.fr/DOIeditions/CFT2020/PDF/148_doi.pdf`), we find an order of magnitude of C_p : $C_p \approx$ 1500 or 2000J K^{-1} kg^{-1}. The mass of the battery can be found in technical notes.
Therefore, the temperature elevation due to Joule effect, including the heat loss by radiation and convection could be deduced.
The problem is that the temperature elevation is supposed to be known to calculate SOC, I_c, I_d... How to solve this auto-coherent problem ? With a loop of adjustment ? From a preliminary approximation ? Or it is too complicated and we suppose an arbitrary temperature elevation, like most of other authors ?

3.29.2 | Best conditions for keeping health of battery

In [5] it is atated that the voltage of the battery should be less than V_g (no gassing, Eq. 3.140, page 116) and greater than $0.7V_N = 1.4n_b$, with V_N the nominal voltage, [64] a working voltage range of 1.75-2.1V is recommended for discharge analysis, [63] the efficient region is where SOC is below 0.7 and V_c is less than 2.3V per cell, [87] using SOC calculation that are close to ours.
The battery life is extended if, at each time, SOC verify :

$$(1 - DOD)C_B \leq SOC(t) \leq C_B, \tag{3.150}$$

with DOD between 30% and 50% and

$$C_B = \frac{\text{Daily charge use} \times \text{Daily remaining self-sufficiency}}{DOD \times \eta_c} \tag{3.151}$$

This formula can be usefull to help select the battery characteristic.

3.30 | Battery parameters using input data from section 3.3

3.30.1 | Charge current I_c and discharge current I_d

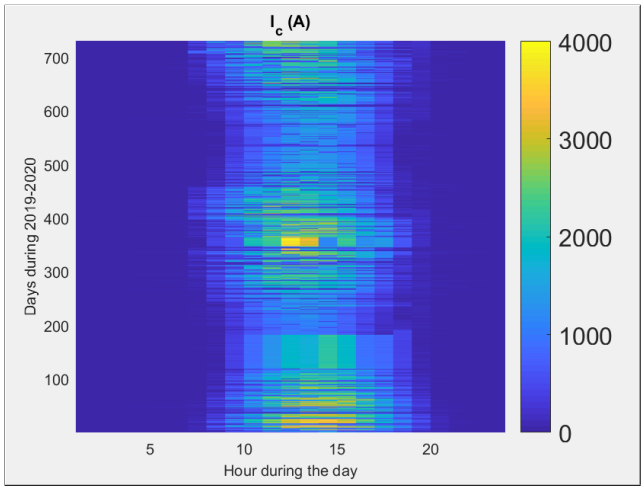

FIGURE 3.68 – Battery charging current, I_c

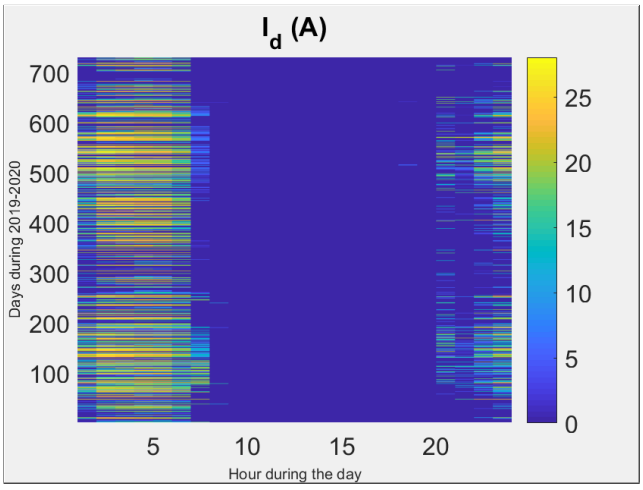

FIGURE 3.69 – Battery discharge current, I_d

Charging current is, by definition, the amount of electrical current passed from a source (generating or storage) to a device that consumes or stores energy. The purpose of a battery is to store energy and release it when needed in a controlled manner. The current delivered by the battery is the discharge current. In the case under analysis, the battery works as an auxiliary power source, which provides energy during generation interruptions and fluctuation of the produced power, but its main role is to assist wind turbine generators during the nights when photovoltaic solar panels cease due to unavailability of solar radiation.
It is expected (likely) that the rate of charging current will be high during the daytime period when the two generator subsystems (WTG and PVG) are in full operation to charge the batteries, while the rate of discharging current is expected to be more pronounced during the nights when the photovoltaic solar panels do not produce power, the battery begins to play its role in compensating the power to its fullest.

Charging current is more likely to occur during the day, while discharge current is more likely to occur at night.

3.30.2 | Battery capacity C_b

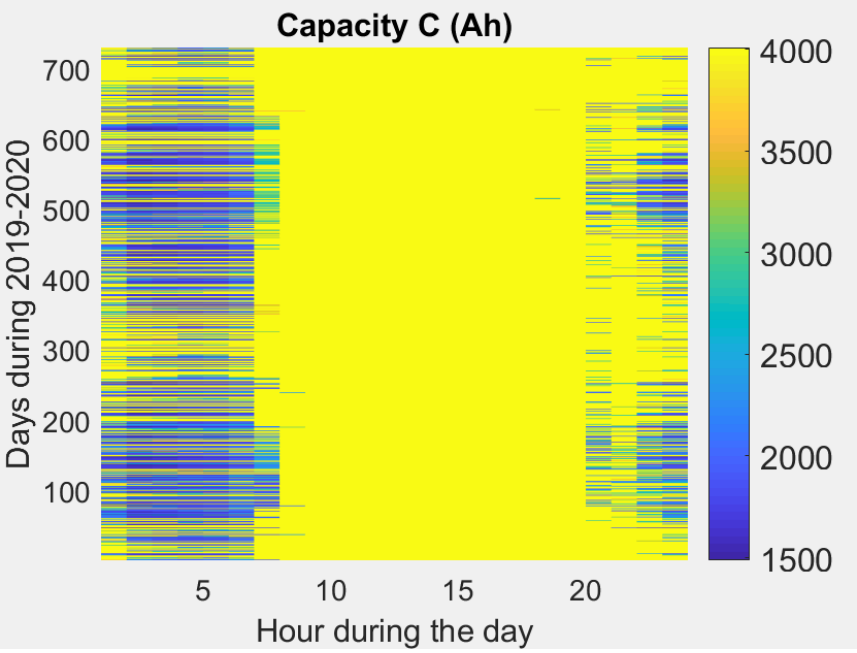

FIGURE 3.70 – Battery capacity C_b

The capacity of a battery expresses the amount of energy that can be stored and indicates the current that a battery can deliver over time. The maximum values of battery capacity are recorded in the daytime when the two subsystems (WTG and PVG) work simultaneously when we have high rates of charging current. It is expected (or likely) that the amount of charge stored in the battery will decrease during the nights when the battery assists the WTG farm to meet demand needs.

3.30.3 | Battery State-of-Charge *SOC*

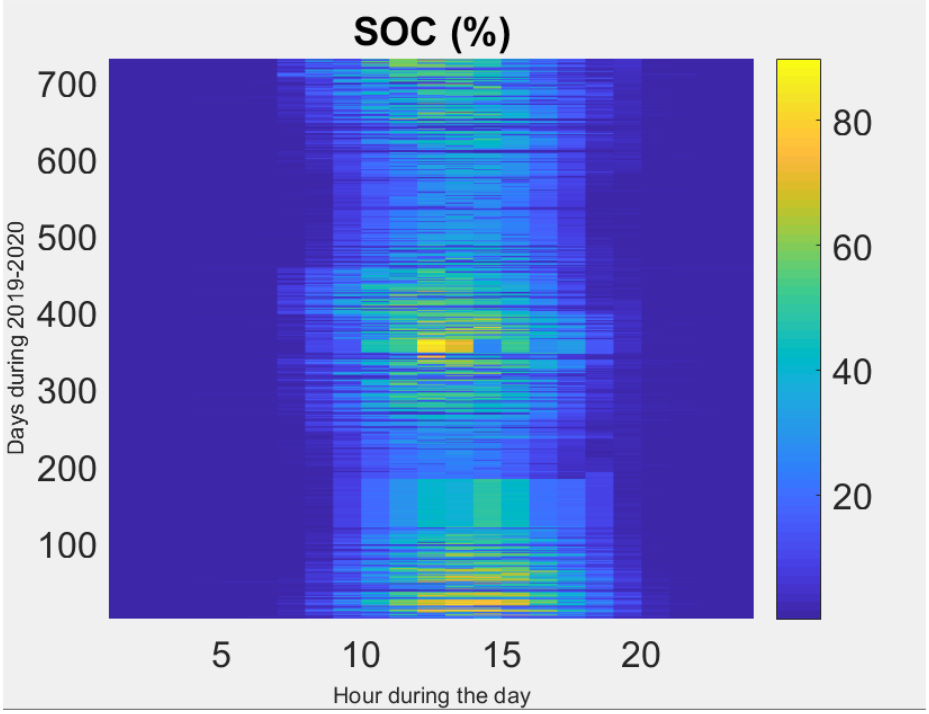

FIGURE 3.71 – Battery State-of-Charge *SoC*

State of charge (SoC) expresses the ratio between the available electrical charge and the battery capacity, indicating the capacity that is currently a function of the rated capacity. SoC is essential as it provides information on how long the battery can last before it needs to be charged.
We have observed that the SoC variation illustrated in Figure 3.71 is more likely to occur in the daytime period when the batteries can charge than in the nighttime period when the battery supplies power to demand.

3.30.4 | Charge voltage V_c and discharge voltage V_d

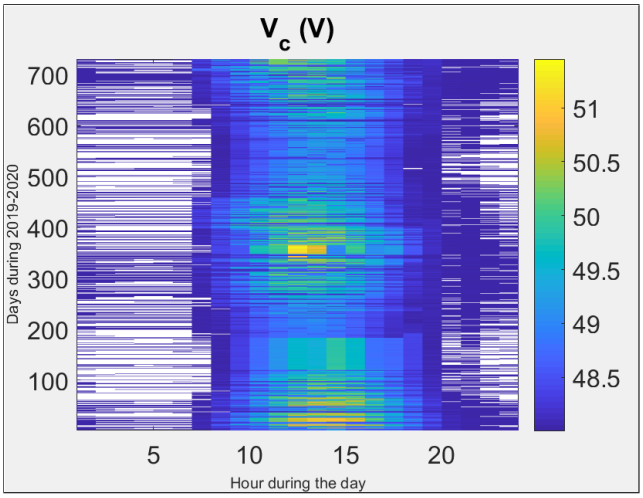

FIGURE 3.72 – Battery charging voltage, V_c

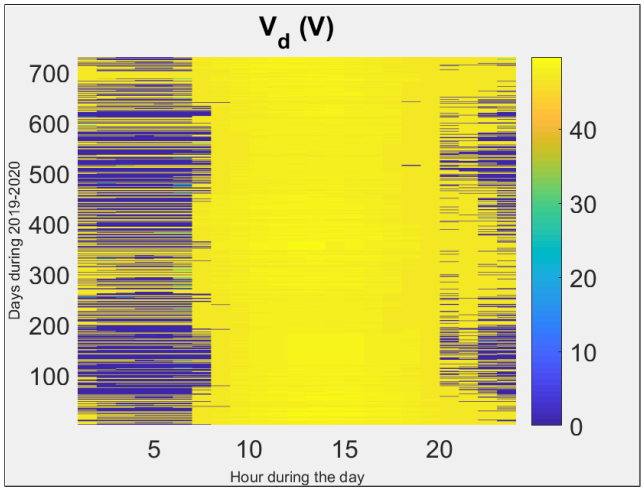

FIGURE 3.73 – Battery descharging voltage, V_d

Batteries with high internal resistance will take longer to fully charge, as well as losing energy during discharging. Batteries with the lowest internal resistance can usually be charged or discharged with higher currents, the desirable is that we have a lower resistance, knowing that the higher the internal resistance the less current the battery will be able to provide, and the higher the internal resistance the more the battery will heat up.

3.30.5 | Charging electromotive force E_c| Discharging electromotive force E_d

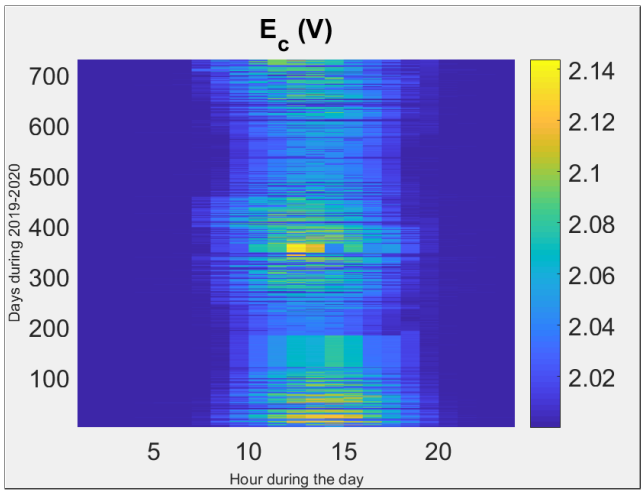

FIGURE 3.74 – Charging electromotive force, E_c

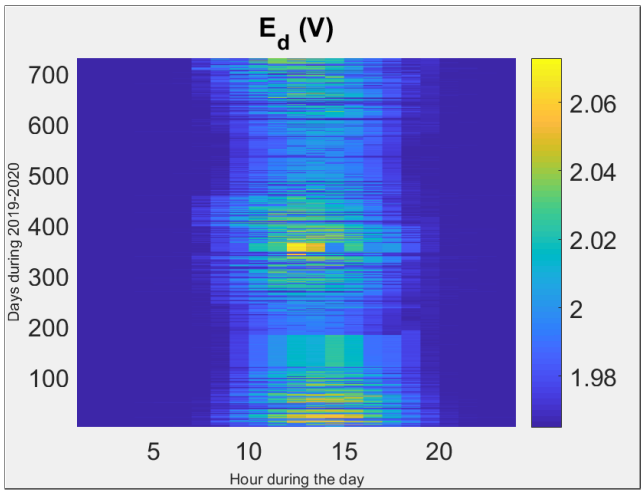

FIGURE 3.75 – Discharging electromotive force, E_d

Charging voltage expresses the amount of battery voltage when the battery is fully charged (or the voltage available at any point during the charging process) while the amount of battery voltage available at any point while the battery is discharging. The maximum values of the charge voltage are reached in the day period, although very rarely, however, the discharge voltage is predominantly high during most of the day, but with greater incidence during the day period when the batteries are highly charged.

3.30.6 | Charging power P_c and discharging power P_d

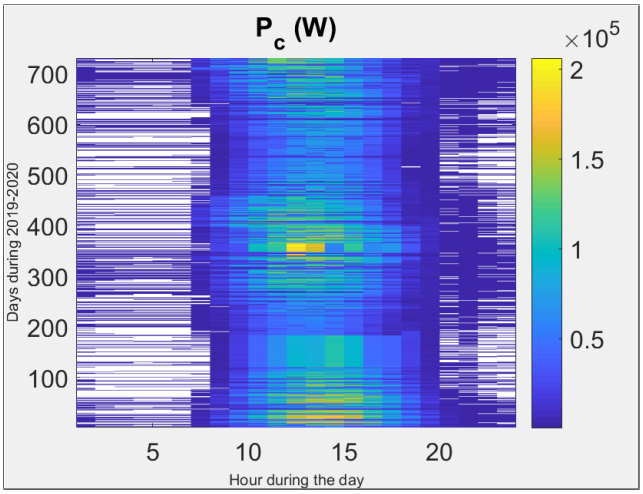

FIGURE 3.76 – Battery charging power, P_c

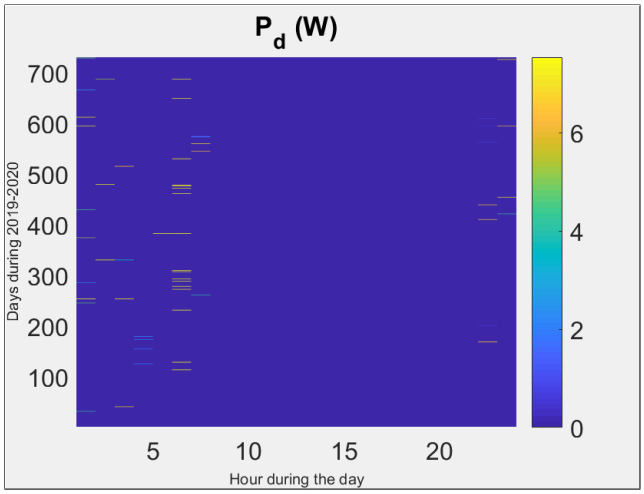

FIGURE 3.77 – Battery discharge power, P_d

The power supplied to the battery per unit of time is much more likely in the daytime hours when the two subsystems are operating at full, than in the nighttime hours, including during intermittence and fluctuation intervals of the produced power. The amount of energy that charges the battery per unit of time is very low during night time hours.

3.30.7 | Comments on the results of modeling the battery parameters

In general, the variation of the weather state over the hours of the day influences the behavior of the battery operating parameters. Furthermore, the parameters are influenced by night effect (no solar radiation, no power production by photovoltaic solar panels) and day effect (with solar radiation for power production by photovoltaic solar panels).

Taking into account the persistence of uncertainty related mainly to the variable availability of RES, it is desirable that we have charged batteries to compensate for fluctuations in power generation. The results of the modeling of the battery operating parameters demonstrate that the parameters are influenced not only by the variation of the input data over the hours of the day, but also by the period of day,i.e., during the day (with available solar radiation) and at night (no solar radiation available), known that a photovoltaic solar panel can only generate power during the day when there is availability of solar radiation and during the night the

generation is null.

The results demonstrate the charging current shows higher daytime numbers meaning faster charging speeds, while the discharge current shows higher nighttime values meaning faster discharging speed.

3.31 | Hybrid microgrid optimization

The microgrid of interest is classified as Isolated Hybrid Battery-Solar-Wind Power Generation System (HBSWPGS), a name justified by its configuration as illustrated in Figure 3.1 on page 38. The microgrid as a power generation system in a hybrid configuration, is composed of a farm with a certain number nWT (or nWTG) of wind turbine generators, and another farm with a certain number nPV (or nPVG) photovoltaic generators (or photovoltaic solar panels). The composition of the hybrid microgrid includes an Energy Storage System composed of a certain number nB of batteries, whose function is summarized in the following description :

(i) When the power produced is greater than the power demanded (when there is excess power production), the surplus production (or surplus power) is stored in the batteries within the limit of the storage capacity.

(ii) When the power produced is less than the power demanded (when there is a power production deficit), the production deficit must be compensated by the batteries within the limits of the available power.

(iii) The role of batteries in RES-based power generation systems includes mitigating the effects of fluctuating output power, system overload, and peak consumption.

The optimization of the microgrid as a whole is based on the premise that it must be able to produce and supply power at a sustainable cost, thus, in the optimization we include the subsystems acquisition cost component assuming :

(a) Estimated cost of a wind turbine is 8000 $.

(b) Estimated cost of a photovoltaic solar panel is 2000 $.

(c) Estimated cost of a battery is 250 $.

The total cost of each piece of equipment includes operating costs (example : transport, storage, taxes and fees) estimated at 15% of the purchase price.

The method of optimization is simply a triple nested loops on nWT, nSP and nB. The space of search are $nWT \in \{0;...;10\}$, $nSP \in \{0;...;300\}$, $nB \in \{0;...;300\}$. For each triplet of numbers, the number of hours for which the produced power is less than the demand and stored. The rate of consumer demand satisfaction is calculated.

During the microgrid optimization process, we evaluate the microgrid price by researching the best configuration at the lowest possible cost, which means, the purpose is to determine the microgrid that provides power and satisfies the demand needs at a low and sustainable cost, for this, we optimized two microgrids for two types of consumer demand : one is typical of agrarian region, the other of industrial. We compare the optimization parameters of the two systems as shown below. In the next subsections, we give the solar radiation, the useful solar radiation for the previously determined best orientation of fixed solar panels in Maputo, with polarization and shadowing corrections, and the electric power produced by solar panel. We also plot the wind speed and the power produced by wind turbines. Then, the two consumer demands are shown.

3.31.1 | Solar irradiance and power produced by photovoltaic panel

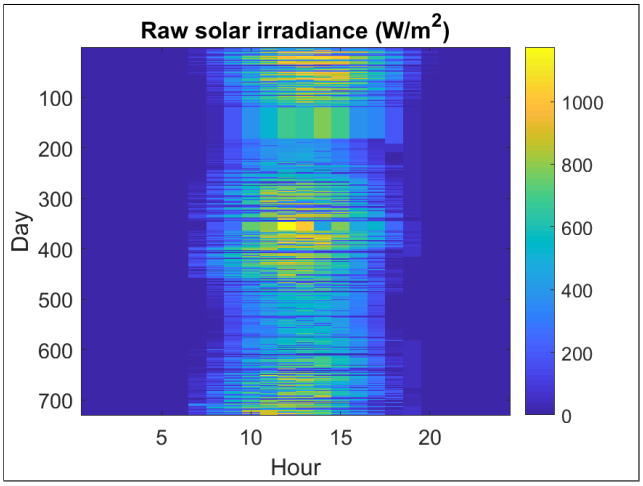

FIGURE 3.78 – Raw solar irradiance.

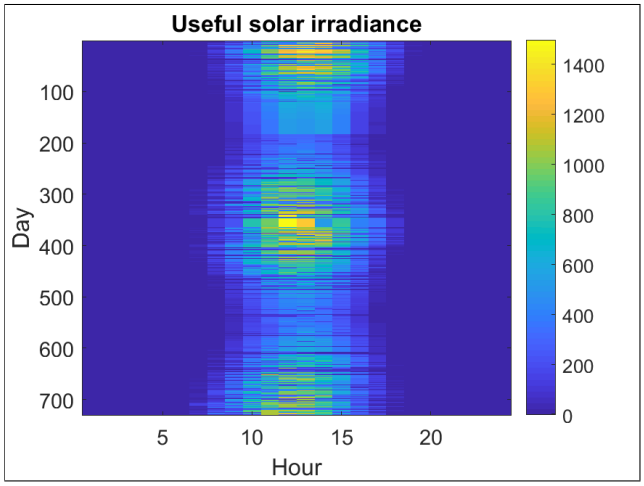

FIGURE 3.79 – Useful solar radiation.

The useful solar irradiance is reduced when the angle of incidence is far from the normal one : in winter, and at sunrise and sunset.

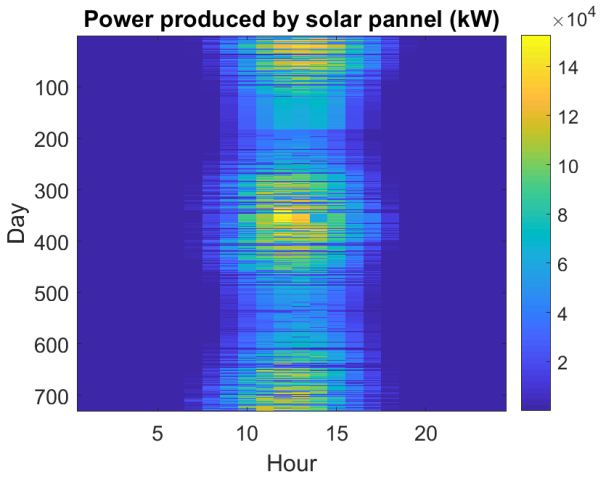

FIGURE 3.80 – Power produced by PVG.

The power produced by solar panels follows the useful solar irradiance.

3.31.2 | Wind speed and power produced by wind turbine generator

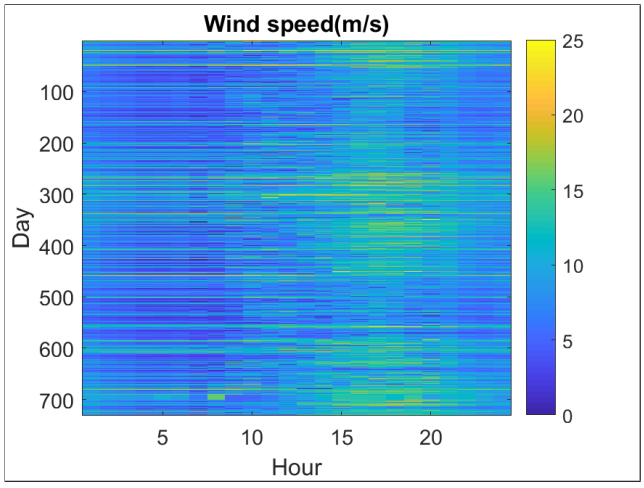

FIGURE 3.81 – Wind speed.

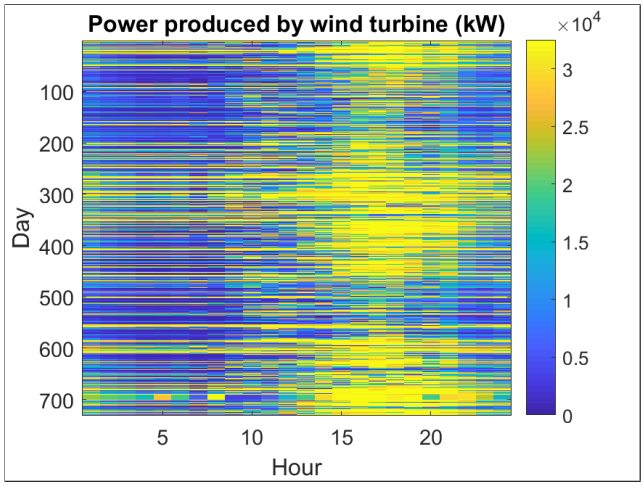

FIGURE 3.82 – Power produced by WTG.

The power produced by wind turbines roughly follows to the wind speed, even if the conversion is not linear.

3.31.3 | Model of power demand (consumption)

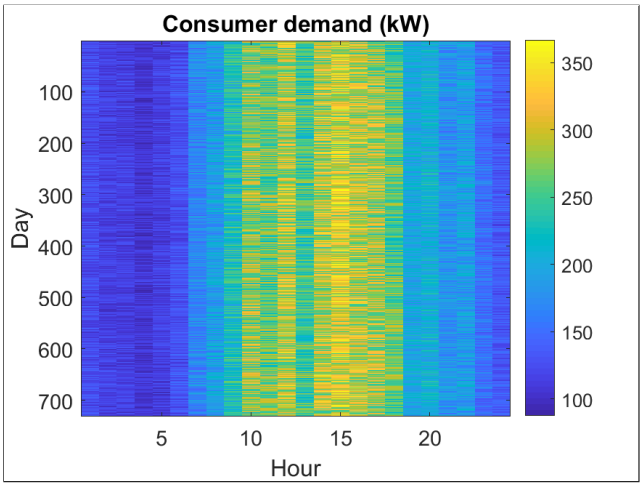

FIGURE 3.83 – Industrial power demand.

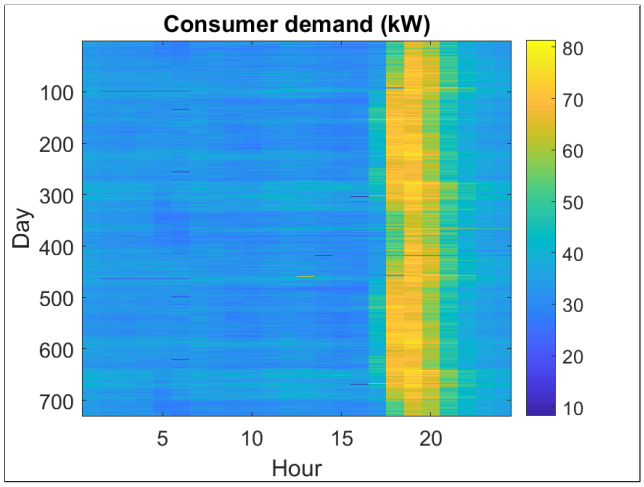

FIGURE 3.84 – Agrarian power demand.

The model of power demand (consumer load) is mainly along the working day in the industrial case, but on the evening in agrarian case. Moreover, it is 4.75 times higher. The agrarian case corresponds to an individual usage of electricity, whereas the industrial one involves an additional and major demand along the day.
As previously mentioned in section 3.3, Mozambique has medium-low intensity wind speed availability, without significant variations in its hourly average, however, solar radiation during the hours of the day varies a lot with peaks around noon hours, therefore, the availability and unavailability of solar radiation during the day and during the night respectively, determines the performance of the system hourly.
The pattern of demand (or consumption) of power in a context of a basically agrarian district (such as Mecula), presents peaks of consumption (or demand) outside peak generation hours, as illustrated in figures 3.10, 3.12, 3.83 e 3.84, which highlights the importance of Energy Storage Systems (ESS) that must supply the generation deficit by photovoltaic solar panels due to the unavailability of solar radiation during the night

3.31.4 | Optimization results

We give the results of microgrid optimization in four cases.

Case 1 combination of the three devices : solar panels, wind turbines and batteries,
Case 2 combination of the two devices : wind turbines and batteries,
Case 3 combination of the two devices : solar panels and batteries,
Case 4 combination of the two devices : solar panels and wind turbines.

The solution is not unique, therefore, in tables, the number of batteries, wind turbines and solar panels are given assuming the lower cost of microgrid.

3.31.4.1 | Case 1 : wind turbines, solar panels and batteries

Characteristic	Industrial	Agrarian
Price	82.512$	61.525$
Failures (h)	0	0
Wind turbines	6	4
Solar panels	1	0
Batteries	87	86

TABLE 3.9 – Best microgrid, including wind turbines, solar panels and batteries.

Discussion about case 1

(i) High cost, mainly wind turbines.

(ii) No failure in demand serving.

(iii) About the same microgrid type in both cases.

(iv) The wind speed should be carefully measured in location to assess the results.

3.31.4.2 | Case 2 : solar panels and batteries

Characteristic	Industrial	Agrarian
Price	-$	1.165.525$
Failures (h)	-	303
Wind turbines	0	0
Solar panels	-	497
Batteries	-	78

TABLE 3.10 – Best microgrid, including solar panels and batteries (no wind turbine).

Discussion about case 2 :

(i) No solution for the industrial case.

(ii) High cost and wide required surface to implement the photovoltaic panels.

(iii) 303 hours of failure in the agrarian case.

(iv) Required caring of photovoltaic panels surface.

(v) No noise pollution by wind turbines.

3.31.4.3 | Case 3 : wind turbines and batteries

Characteristic	Industrial	Agrarian
Price	94.587$	61.525$
Failures (h)	1	0
Wind turbines	6	4
Solar panels	0	0
Batteries	137	86

TABLE 3.11 – Best microgrid, including wind turbines and batteries.

Discussion about case 3

(i) The failure probability is counterbalanced by the increase of wind turbines and batteries.

(ii) No solar panel maintenance (regular cleaning requires by its quasi horizontal position)

(iii) Wide grid of batteries : possible problem due to aging.

3.31.4.4 | Case 4 : wind turbines and solar panels

Characteristic	Industrial	Agrarian
Price	1.196.000$	772.800$
Failures (h)	1125	312
Wind turbines	10	10
Solar panels	480	500
Batteries	0	0

TABLE 3.12 – Best microgrid, including wind turbines and solar cells (no battery).

Discussion about case 4

(i) The batteries are necessary to serve the demand.

(ii) High cost of such microgrid.

(iii) Wide grid of solar panels.

3.31.5 | Global discussion

Batteries appears to be useful in the investigated cases. The best solution appears to be a combination of batteries, wind turbines and solar panels.

If we tolerate a given rate of fails in satisfying the consumer demand, the cost of microgrid can be adjusted accordingly. For example, the best microgrids are the following as a function of the number of tolerated fails, nB being the number of batteries, nWT that of wind turbines and nSP that of solar panels.

Agrarian : 1 hour over the two years : $nB = 86$, $nWT = 4$, $nSP = 0$, cost : 61.525\$.
Industrial : 1 hour over the two years : $nB = 87$, $nWT = 6$, $nSP = 1$, cost : 82.512\$.
Agrarian : 24 hours over the two years : $nB = 78$, $nWT = 1$, $nSP = 0$, cost : 31.625\$.
Industrial : 24 hours over the two years : $nB = 100$, $nWT = 1$, $nSP = 0$, cost : 37.950\$.
Agrarian : 240 hours over the two years : $nB = 75$, $nWT = 1$, $nSP = 0$, cost : 30.762\$.
Industrial : 240 hours over the two years : $nB = 79$, $nWT = 1$, $nSP = 0$, cost : 31.912\$.

The increase of fail tolerance from 1 hour over two years to 240 leads only to about a half money-saving and corresponds mainly to a decrease of the number of batteries and wind turbines. Of course, these examples of data strongly depend on the price and type of considered devices. Moreover, the input data (wind speed, solar irradiance, and temperature) must be accurately known on a wide period of time.

3.32 | Probabilistic forecasting of output power generation

In RES-based microgrids, estimating the output power and forecasting the generation capacity of the microgrid is an important procedure when modeling or sizing a power generation farm. Normally, the estimation of the output power of a WTG or a PVG is carried out by the use of characteristic curves and deterministic models incapable of providing exact (or precise)

estimates of output power values, i.e., are not able to provide correct results under different conditions. To accommodate fluctuations in WTG and PVG output power due to variability and intermittence of wind speed and solar radiation in RES-based microgrids, probabilistic forecasting techniques for power generation will be included, that is, the WTG and PVG output power results obtained by deterministic models will be treated in terms of probabilistic modeling. The objective of probabilistic modeling is to include the stochastic component on the results obtained from deterministic modeling, thus including the impact of uncertainty [68].

3.32.1 | Probabilistic forecasting technique

According to [54] most probabilistic forecasting approaches are based on single models, however, it would be difficult to find a perfect single model for the forecasting task in different situations, thus, [88] states that model combination is more skillful than single models, as the model combination exploits the individual advantages of each single model to provide better results. In this context, [54] presented a Multi-model Combination (MMC) approach for probabilistic wind power forecasting whose formulation is used in this thesis as described in section 2.12.
The probabilistic multi-model combination (MMC) approach used in this thesis is based on the principle described in section 2.12, presented in two studies namely :

— The study of [68] suggests that we cannot find models that provide better results under different conditions, in addition, the study presents a model to improve the estimation accuracy of the output power of a WTG comparing deterministic models and probabilistic models, proving the superiority of probabilistic models.
— According to [54], many forecasting approaches are based on individual probabilistic models that are not perfect for all forecasting tasks. Thus, the principle of Multi-Model Combination (MMC) model is proposed to take advantage of particular abilities and superiorities of each individual probabilistic model participating in the combination.

3.33 | Diagram of probabilistic modeling of P_{wtg} and P_{pvg}

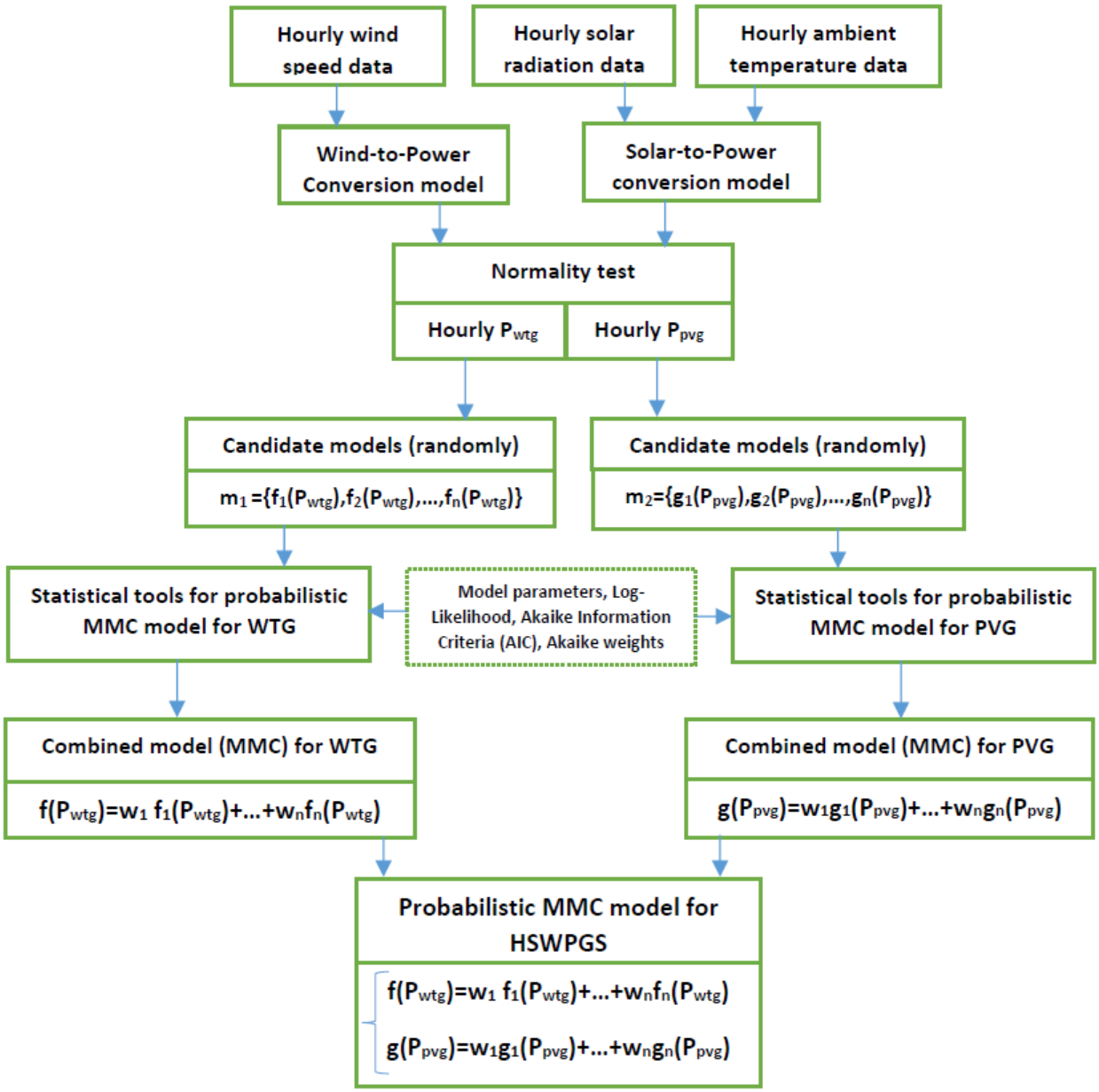

FIGURE 3.85 – Probabilistic Multi-Model Combination (MMC) model for HSWPGS.

The diagram in figure 3.85 illustrates a model based on the principle of an MMC model, idealized for application in an HSWPGS system whose operating principle is described in the following terms :

(i) **Input data**
The model depends entirely on environmental variables defined as input variables, namely wind speed v , solar radiation s and ambient temperature t_a.

(ii) **RES-to-Power Conversion**
Model contains a RES-to-Power conversion step in which wind speed is converted into WTG output power P_{wtg}, solar radiation and ambient temperature are converted into PVG output power P_{pvg}. Conversion equations are described in section 2.9.

— **Challenges and limitations of the deterministic part of the model**
P_{wtg} and P_{pvg} are variables of the estimated output power of the WTG and PVG respectively, obtained through parametric deterministic models in which the influence of uncertainty is not taken into account.

— **Strategy to reduce the challenges and limitations of the model**
Improving the accuracy of estimating (or forecasting) the output power of the WTG and PVG demands the use of probabilistic models that are presented in subsequent steps.

(iii) **Normality test**
In this model, the hourly data of the output power of the WTG and the PVG are taken as input variables (or input data) of the probabilistic model. Principle based on the study of [68].
Preliminary statistical analysis consists of testing normality, not as an end if the data show a normal distribution (or normality), but as a means of gaining knowledge about the statistical nature and behavior of the data, to make timely decisions on appropriate statistical procedures. In this thesis, the normality test was performed using the Anderson-Darling Test.

(iv) **Random candidate models**
The estimated output power data of the WTG and the PVG are consecutive series of hourly averages as illustrated in equations 3.5 and 3.6, where hourly data sets of P_{wtg} and P_{pvg} (one on each side) corresponding to the same hour are taken simultaneously.

Additionally, we have two sets m_1 and m_2 of individual probabilistic models $f(x)$ and $g(x)$ also called candidate models :

$$m_1 = \{f_1(x), f_2(x), \cdots, f_n(x)\} \tag{3.152}$$

and

$$m_2 = \{g_1(y), g_2(y), \cdots, g_n(y)\} \tag{3.153}$$

In sets m_1 and m_2 any individual probabilistic model with forecasting abilities can be a candidate.

The set of probabilistic models m_1 is tested on the data set P_{wtg}, and m_2 is tested on P_{pvg} for each specific hour h.

(v) **Computation of statistical parameters**

This step aims at the following :

— Compute the statistical parameters of each individual probabilistic model (or candidate probabilistic model) against the data on which such models are tested.

— Compute the Log-likelihood (Log-L(θ)) and the Akaike Information Criteria (AIC) as statistical parameters that provide the goodness-of-fit of each model in relation to the dataset on which such models are tested.

— Compute of Akaike weights ω_i : The weight with which each model participates in the combination

It is important to note that the AIC value alone for a single distribution (or individual distribution) does not tell us anything, that is, it does not provide useful information for formulating a statistically valid decision. The AIC value is only useful when compared to the AIC values of other models. AIC compares the relative "goodness-of-fit" of one model (distribution) versus that of other models. The distribution with the lowest AIC value is usually the model with the best goodness-of-fit. There is an inverse proportionality, the smaller the AIC value, the better the goodness-of-fit with respect to the data of interest [89].

The concept of the MMC model basically consists of combining several single models, each single model participates in the combination with a weight that is calculated as a function of the AIC value of each model respectively.

(vi) **Probabilistic multi-model combination model**

Using the AIC values of each single model in descending order, we consequently sort the

respective models in ascending goodness-of-fit order, and correspondingly (relative to the AIC value) we place the respective weights (Akaike weights), thus, we multiply each probabilistic model by its weight, as described in section 2.12.0.3.
Considering that it is a Hybrid Solar-Wind Power Generation System (HSWPGS), we will obtain two MMC model equations, one for forecasting and estimating the WTG output power and another for PVG expressed as :

$$\begin{cases} f(x) = \omega_1 \cdot f_1(x) + \omega_2 \cdot f_2(x) + \cdots + \omega_n \cdot f_n(x) \\ g(y) = \lambda_1 \cdot g_1(y) + \lambda_2 \cdot g_2(y) + \cdots + \lambda_n \cdot g_n(y) \end{cases}$$

Considering x = P_{wtg}, y = P_{pvg}, $f_n(x)$ corresponds to the family of models from set m_1, and $g_n(y)$ from family of models from set m_2.
In this stage of the diagram, we intend to use a probabilistic approach that allows quantifying global uncertainty, estimating output power, modeling Energy Storage Systems (ESS) considering sources of uncertainty.
In the section that presents the predictive modeling of the output power of the WTG, the PVG (modeling of photovoltaic cells), the behavior of the Energy Storage System system, and the propagation of uncertainty.

4

Conclusions

After an extensive deduction approach and an attempt to simplify modeling equations for the photovoltaic solar panel and use of battery modeling equations, the results obtained through mathematical modeling and graphic representation allow us to observe the behavior of the parameters as a function of the hourly variation of the weather state over the hours of the day.

4.1 | Strength of the approach

We summarize the strength of our approach.

(i) Easy improvements and adjustments of models and prices of wind turbines, solar panels and batteries : open models.

(ii) The transmittance and shadowing effect are included in the model of photovoltaic panels.

(iii) The latitude and longitude are addressed in the model of photovoltaic panels (optimization of the panel orientation).

(iv) Realistic consumer demand, wind speed, temperature, solar irradiation are considered.

(v) High speed of simulations : the optimization of microgrid requires less than 15 minutes on a standard laptop.

(vi) Possible evaluation of the influence of uncertainties of manufacturer parameters on the produced power.

(vii) Possible inclusion of the aging of the microgrid over years.

(viii) The whole model of microgrid can be used for statistical studies.

4.2 | Weaknesses of the present model

We summarize the weakness of our approach.

(i) Input data must be available (speed of wind, solar irradiance, temperature, consumer load). The characteristic of the measured spectrum of the solar irradiance should be known and adapted to the solar cells.

(ii) Strong dependence of the results on the input data. The possible evolution of input parameters, especially the climate change and increase of the consumer demand should be evaluated to design long time use of microgrid.

(iii) The whole environmental and societal footprints, including materials inputs and recycling costs are not integrated in the cost evaluation and the carbon footprint is not evaluated.

4.3 | Achieved Aims and Objectives

(i) We evaluated the uncertainty about the output power of the power generation subsystems as a function of hourly weather changes throughout the day.

(ii) We evaluated the uncertainty and sensitivity of the parameters of the photovoltaic solar panel as a function of hourly variations in the weather throughout the day.

(iii) We evaluated the behavior of the battery operating parameters in response to the night and day periods and as a function of the hourly variations of the weather throughout the day.

(iv) We optimize the microgrid configuration to find an option that ensures power supply at low and sustainable costs.

4.4 | Critique and Limitations

(i) The literature provides several studies on photovoltaic cell modeling, but the models appear to be quite complex. More simplified models are still necessary, in addition, the

deduction of the formulas of the parameters must always be accompanied by assumptions that can make the models of photovoltaic cells discrepant.

(ii) The battery modeling approaches available in the literature show that battery models are not yet perfect, and present a considerable level of complexity that demands increasing simplification.

4.5 | Final Remarks

The output power of the WTG and PVG calculated in this work are essentially deterministic, that is, such power does not include uncertainty, thus, a probabilistic modeling (use of probabilistic models) to model the output power is needed to obtain quantified uncertainty information. In this work, the purely probabilistic modeling was not conclusive, but the idea and the concept are properly formulated.

Bibliographie

[1] L. Cristaldi, M. Faifer, M. Rossi, and S. Toscani, "A simplified model of photovoltaic panel," in *2012 IEEE International Instrumentation and Measurement Technology Conference Proceedings*, 2012, pp. 431–436.

[2] E. I. Ortiz-Rivera, "Maximum power point tracking using the optimal duty ratio for dc-dc converters and load matching in photovoltaic applications," in *2008 Twenty-Third Annual IEEE Applied Power Electronics Conference and Exposition*. IEEE, 2008, pp. 987–991.

[3] R. Rajesh and M. Carolin Mabel, "A comprehensive review of photovoltaic systems," *Renewable and Sustainable Energy Reviews*, vol. 51, pp. 231–248, 2015. [Online]. Available : https://www.sciencedirect.com/science/article/pii/S1364032115005766

[4] E. M. Laadissi1, A. E. Filali, M. Zazi, and A. E. Ballouti, "Comparative study of lead acid battery modelling," *ARPN Journal of Engineering and Applied Sciences*, vol. 13, no. 15, pp. 4448–44 452, 2018. [Online]. Available : http://www.arpnjournals.org/jeas/research_papers/rp_2018/jeas_0818_7223.pdf

[5] A. O. M. Yahya, A. O. Mahmoud, and I. Youm, "Modélisation d'un systéme de stockage intégré dans un systéme hybride (pv / éolien / diesel)," *Revue des énergies renouvelables*, vol. 10, no. 2, pp. 205–214, 2007. [Online]. Available : https://www.asjp.cerist.dz/en/article/118229

[6] M. G. Villalva, J. R. Gazoli, and E. Ruppert Filho, "Modeling and circuit-based simulation of photovoltaic arrays," in *2009 Brazilian Power Electronics Conference*. IEEE, 2009, pp. 1244–1254.

[7] L. Cristaldi, M. Faifer, M. Rossi, and S. Toscani, "A simplified model of photovoltaic panel," in *2012 IEEE International Instrumentation and Measurement Technology Conference Proceedings*. IEEE, 2012, pp. 431–436.

[8] A. A. Teyabeen, F. R. Akkari, and A. E. Jwaid, "Mathematical modelling of wind turbine power curve," *International Journal of Simulation Systems, Science & Technology*, vol. 19, no. 5, pp. 1–13, 2018.

[9] ENERCON. (2006) Enercon product overview. [Online]. Available : https://pdf.directindustry.com/pdf/enercon/enercon-product-overview/20877-243513.html

[10] H. Essakhi, "modélisation et simulation d'un module photovoltaïque," *LASIME, ESTA Université Ibn Zohr, BP*, vol. 33, 2019.

[11] N. Pandiarajan, R. Ramaprabha, and R. Muthu, "Application of circuit model for photovoltaic energy conversion system," *International Journal of Photoenergy*, vol. 2012, 2012.

[12] T. Mohn, "It takes a village : Rural electrification in east africa," *IEEE Power and Energy Magazine*, vol. 11, no. 4, pp. 46–51, 2013.

[13] Z. Ding, M. Liu, W.-J. Lee, and D. Wetz, "An autonomous operation microgrid for rural electrification," in *2013 IEEE Industry Applications Society Annual Meeting*. IEEE, 2013, pp. 1–8.

[14] R. Nyakudya, T. Chikowore, S. Mhlanga, and L. Nyanga, "A decision support tool for rural electrification grid design," in *2013 IEEE International Conference on Industrial Technology (ICIT)*. IEEE, 2013, pp. 1443–1449.

[15] FUNAE. (2000) Renewable energy atlas of mozambique. [Online]. Available : https://gestoenergy.com/wp-content/uploads/2018/04/MOZAMBIQUE-RENEWABLE-ENERGY-ATLAS.pdf

[16] M. Manhique, D. Barchiesi, and R. Kouta, "Rural electrification in mozambique : Challenges and opportunities," in *E3S Web of Conferences*, vol. 294. EDP Sciences, 2021, p. 02004.

[17] B. S. Chouhan, K. Rao, and B. K. Saxena, "Reduction in carbon dioxide emissions due to wind power generation in india," in *2017 International Conference On Smart Technologies For Smart Nation (SmartTechCon)*. IEEE, 2017, pp. 257–264.

[18] T. Alexopoulos, D. Thomakos, and D. Tzavara, "Co 2 emissions, fuel mix, final energy consumption and regulation of renewable energy sources in the eu-15," in *2012 9th International Conference on the European Energy Market*. IEEE, 2012, pp. 1–8.

[19] M. Rusu, "Social cost of carbon : opportunities and environmental solutions," *Procedia Economics and Finance*, vol. 3, pp. 690–697, 2012.

[20] H. d. D. C. Fare, "Growth and co2 emissions : How do different countries fare ?" 2007.

[21] B. Li and N. Haneklaus, "The role of renewable energy, fossil fuel consumption, urbanization and economic growth on co2 emissions in china," *Energy Reports*, vol. 7, pp. 783–791, 2021.

[22] S. Vaz Jr, A. P. R. de Souza, and B. E. L. Baeta, "Technologies for carbon dioxide capture : A review applied to energy sectors," *Cleaner Engineering and Technology*, p. 100456, 2022.

[23] R. S. Dimitrov, "The paris agreement on climate change : Behind closed doors," *Global environmental politics*, vol. 16, no. 3, pp. 1–11, 2016.

[24] M.-C. C. Segger, "Advancing the paris agreement on climate change for sustainable development," *Cambridge International Law Journal*, vol. 5, no. 2, pp. 202–237, 2016.

[25] A. Verma, "Necessity of ecological balance for widespread biodiversity." 2017.

[26] G. Mutezo and J. Mulopo, "A review of africa's transition from fossil fuels to renewable energy using circular economy principles," *Renewable and Sustainable Energy Reviews*, vol. 137, p. 110609, 2021.

[27] M. Child and C. Breyer, "Transition and transformation : A review of the concept of change in the progress towards future sustainable energy systems," *Energy Policy*, vol. 107, pp. 11–26, 2017.

[28] V. Smil, *Energy transitions : global and national perspectives*. ABC-CLIO, 2016.

[29] Wikipédia, "Bibtex — wikipédia, a enciclopédia livre," 2022, [Online ; accessed 19-June-2022]. [Online]. Available : http://https://en.wikipedia.org/wiki/Energy_transition

[30] K. Isoaho and K. Karhunmaa, "A critical review of discursive approaches in energy transitions," *Energy Policy*, vol. 128, pp. 930–942, 2019.

[31] G. Notton, M.-L. Nivet, C. Voyant, C. Paoli, C. Darras, F. Motte, and A. Fouilloy, "Intermittent and stochastic character of renewable energy sources : Consequences, cost of intermittence and benefit of forecasting," *Renewable and sustainable energy reviews*, vol. 87, pp. 96–105, 2018.

[32] S. Ambec and C. Crampes, "Decarbonizing electricity generation with intermittent sources of energy," *Journal of the Association of Environmental and Resource Economists*, vol. 6, no. 6, pp. 1105–1134, 2019.

[33] G. Grote, *Management of uncertainty : Theory and application in the design of systems and organizations*. Springer, 2009.

[34] A. Pang, "Visualizing uncertainty in geo-spatial data," in *In Proceedings of the Workshop on the Intersections between Geospatial Information and Information Technology*. Citeseer, 2001.

[35] H. Gzyl, G. Molina, and E. ter Horst, "Assessment and propagation of input uncertainty in tree-based option pricing models," *Applied Stochastic Models in Business and Industry*, vol. 25, no. 3, pp. 275–308, 2009.

[36] B. Liu, "Why is there a need for uncertainty theory," *Journal of Uncertain Systems*, vol. 6, no. 1, pp. 3–10, 2012.

[37] E. Morse, J.-Y. Dantan, N. Anwer, R. Söderberg, G. Moroni, A. Qureshi, X. Jiang, and L. Mathieu, "Tolerancing : Managing uncertainty from conceptual design to final product," *CIRP Annals*, vol. 67, no. 2, pp. 695–717, 2018.

[38] G. J. Klir, "Uncertainty and information measures for imprecise probabilities : An overview." in *ISIPTA*, 1999, pp. 234–240.

[39] S. B. Suslick, D. Schiozer, and M. R. Rodriguez, "Uncertainty and risk analysis in petroleum exploration and production," *Terrae*, vol. 6, no. 1, pp. 30–41, 2009.

[40] L. Hu, D. Yue, and G. Zhao, "Reliability assessment of random uncertain multi-state systems," *Ieee Access*, vol. 7, pp. 22 781–22 789, 2019.

[41] J. C. for Guides in Metrology, "International vocabulary of metrology—basic and general concepts and associated terms (vim)," *VIM3 Int. Vocab. Metrol.*, vol. 3, p. 104, 2008.

[42] J. JCGM, "100 : 2008 (gum 1995 with minor corrections) evaluation of measurement data-guide to the expression of uncertainty in measurement," *Joint Committee for Guides in Metrology*, vol. 19, 2008.

[43] Z. Zeng, R. Kang, M. Wen, and E. Zio, "Uncertainty theory as a basis for belief reliability," *Information Sciences*, vol. 429, pp. 26–36, 2018.

[44] P. Kreiser and L. Marino, "Analyzing the historical development of the environmental uncertainty construct," *Management Decision*, 2002.

[45] D. Liu *et al.*, "Uncertainty theory," in *Uncertainty theory*. Springer, 2007, pp. 205–234.

[46] B. Liu, "Uncertainty theory : a branch of mathematics for modeling human uncertainty 2010 berlin springer 10.1007," *Google Scholar Google Scholar Cross Ref Cross Ref*.

[47] ——, "Uncertainty theory," in *Uncertainty theory*. Springer, 2010, pp. 1–79.

[48] A. Nair, D. Reckien, and M. F. van Maarseveen, "A generalised fuzzy cognitive mapping approach for modelling complex systems," *Applied Soft Computing*, vol. 84, p. 105754, 2019.

[49] M. Marinacci, "Model uncertainty," *Journal of the European Economic Association*, vol. 13, no. 6, pp. 1022–1100, 2015.

[50] L. Tsoukalas and A. Ikonomopoulos, "Uncertainty modeling in anticipatory systems," pp. 79–91, 1992.

[51] A. Grenyer, J. A. Erkoyuncu, Y. Zhao, and R. Roy, "A systematic review of multivariate uncertainty quantification for engineering systems," *CIRP Journal of Manufacturing Science and Technology*, vol. 33, pp. 188–208, 2021.

[52] C. F. Carobbi, S. Lalléchère, and L. R. Arnaut, "Review of uncertainty quantification of measurement and computational modeling in emc part i : measurement uncertainty," *IEEE Transactions on Electromagnetic Compatibility*, vol. 61, no. 6, pp. 1690–1698, 2019.

[53] L. Lin, H. Bao, and N. Dinh, "Uncertainty quantification and software risk analysis for digital twins in the nearly autonomous management and control systems : A review," *Annals of Nuclear Energy*, vol. 160, p. 108362, 2021.

[54] Y. Lin, M. Yang, C. Wan, J. Wang, and Y. Song, "A multi-model combination approach for probabilistic wind power forecasting," *IEEE Transactions on Sustainable Energy*, vol. 10, no. 1, pp. 226–237, 2018.

[55] C. Wang, Q. Duan, C. H. Tong, Z. Di, and W. Gong, "A gui platform for uncertainty quantification of complex dynamical models," *Environmental Modelling & Software*, vol. 76, pp. 1–12, 2016.

[56] Y. Atwa, E. El-Saadany, M. Salama, and R. Seethapathy, "Optimal renewable resources mix for distribution system energy loss minimization," *IEEE Transactions on Power Systems*, vol. 25, no. 1, pp. 360–370, 2009.

[57] A. Zakariazadeh, S. Jadid, and P. Siano, "Smart microgrid energy and reserve scheduling with demand response using stochastic optimization," *International Journal of Electrical Power & Energy Systems*, vol. 63, pp. 523–533, 2014.

[58] S. Talari, M. Yazdaninejad, and M.-R. Haghifam, "Stochastic-based scheduling of the microgrid operation including wind turbines, photovoltaic cells, energy storages and responsive loads," *IET Generation, Transmission & Distribution*, vol. 9, no. 12, pp. 1498–1509, 2015.

[59] M. Lydia, S. S. Kumar, A. I. Selvakumar, and G. E. P. Kumar, "A comprehensive review on wind turbine power curve modeling techniques," *Renewable and Sustainable Energy Reviews*, vol. 30, pp. 452–460, 2014.

[60] C. Justus and A. Mikhail, "Height variation of wind speed and wind distributions statistics," *Geophysical research letters*, vol. 3, no. 5, pp. 261–264, 1976.

[61] M. Albadi and E. El-Saadany, "Optimum turbine-site matching," *Energy*, vol. 35, no. 9, pp. 3593–3602, 2010.

[62] B. Belabes, A. Youcefi, O. Guerri, M. Djamai, and A. Kaabeche, "Evaluation of wind energy potential and estimation of cost using wind energy turbines for electricity generation in north of algeria," *Renewable and Sustainable Energy Reviews*, vol. 51, pp. 1245–1255, 2015.

[63] J. B. Copetti, E. Lorenzo, and F. Chenlo, "A general battery model for pv system simulation," *Progress in Photovoltaics Research and Applications*, vol. 1, no. 4, pp. 283–292, 1993.

[64] W. Zhou, H. Yang, and Z. Fang, "Battery behavior prediction and battery working states analysis of a hybrid solar–wind power generation system," *Renewable Energy*, vol. 33, no. 6, pp. 1413–1423, 2008. [Online]. Available : https://www.sciencedirect.com/science/article/pii/S0960148107002601

[65] Y. Li and E. Zio, "Uncertainty analysis of the adequacy assessment model of a distributed generation system," *Renewable Energy*, vol. 41, pp. 235–244, 2012.

[66] K. Liukko, "Model averaging with akaike weights," *Turku PET Centre Modelling report*, p. 1, 2007.

[67] F. E. Turkheimer, R. Hinz, and V. J. Cunningham, "On the undecidability among kinetic models : from model selection to model averaging," *Journal of Cerebral Blood Flow & Metabolism*, vol. 23, no. 4, pp. 490–498, 2003.

[68] S. Ge, M. J. Zuo, and Z. Tian, "Wind turbine power output estimation with probabilistic power curves," in *2020 Asia-Pacific International Symposium on Advanced Reliability and Maintenance Modeling (APARM)*. IEEE, 2020, pp. 1–6.

[69] M. Manhique, R. Kouta, D. Barchiesi, B. O'Regan, and F. Silva, "Energy transition x energy inclusion : A community energy concept for developing countries," in *2021 IEEE International Humanitarian Technology Conference (IHTC)*. IEEE, 2021, pp. 1–8.

[70] F. Silva, C. Soares, B. O'Regan, K. Mould, M. Manhique, and P. Lyons, "Social innovation for community energy in developing countries–new models and a mozambican case study," *Energy Proceedings*, pp. 1–6, 2022.

[71] WeatherSpark. (2022) Clima e condições meteorológicas médias em maputo no ano todo. [Online]. Available : https://pt.weatherspark.com/y/97168/Clima-caracter%C3%ADstico-em-Maputo-Mo%C3%A7ambique-durante-o-ano#Figures-Summary

[72] C. Carrero, J. Amador, and S. Arnaltes, "A single procedure for helping pv designers to select silicon pv modules and evaluate the loss resistances," *Renewable Energy*, vol. 32, no. 15, pp. 2579–2589, 2007.

[73] T. Adefarati and R. Bansal, "Integration of renewable distributed generators into the distribution system : a review," *IET Renewable Power Generation*, vol. 10, no. 7, pp. 873–884, 2016.

[74] H. Rauschenbach and S. C. A. D. Handbook, "Chapter 2," 1980.

[75] M. Villalva, J. Gazoli, and E. Filho, "Modeling and circuit-based simulation of photovoltaic arrays," vol. 14, 11 2009, pp. 1244 – 1254.

[76] A. Ortiz-Conde, F. J. G. Sanchez, and J. Muci, "Exact analytical solutions of the forward non-ideal diode equation with series and shunt parasitic resistances," *Solid-State Electronics*, vol. 44, no. 10, pp. 1861–1864, 2000.

[77] D. Qin, J. Li, T. Wang, and D. Zhang, "Modeling and simulating a battery for an electric vehicle based on modelica," *Automotive Innovation*, vol. 2, no. 3, pp. 169–177, 2019.

[78] D. Barchiesi and M. Lamy de la Chapelle, *Physique de la Matière et Interaction Rayonnement-Matière*, 1st ed., ser. Technosup. Paris : Ellipses, 2007.

[79] I. Reda and A. Andreas, "Solar position algorithm for solar radiation applications," *Solar Energy*, vol. 76, no. 5, pp. 577–589, 2004. [Online]. Available : https://www.sciencedirect.com/science/article/pii/S0038092X0300450X

[80] C. Seshan, "Cell efficiency dependence on solar incidence angle," in *2010 35th IEEE Photovoltaic Specialists Conference*, 2010, pp. 002 102–002 105.

[81] A. Azizi, P.-O. Logerais, A. Omeiri, A. Amiar, A. Charki, O. Riou, F. Delaleux, and J.-F. Durastanti, "Impact of the aging of a photovoltaic module on the performance of a grid-connected system," *Solar Energy*, vol. 174, pp. 445–454, 2018.

[82] P.-O. Logerais, O. Riou, M. A. Camara, and J.-F. Durastanti, "Study of photovoltaic energy storage by supercapacitors through both experimental and modelling approaches," *Journal of Solar Energy*, vol. 2013, p. 9, 2013.

[83] A. Ennemri, P. Logerais, M. Balistrou, J. Durastanti, I. Belaidi *et al.*, "Cracks in silicon photovoltaic modules : a review," *J. Optoelectron. Adv. Mater*, vol. 21, no. 1-2, pp. 74–92, 2019.

[84] Z. Pei, X. Zhao, H. Yuan, Z. Peng, , and L. Wu, "An equivalent circuit model for lithium battery of electric vehicle considering self-healing characteristic," *Journal of Control Science and Engineering*, vol. 2018, pp. ID 5 179 758, 11 pages, 2018.

[85] H. L. Wiegman and A. J. A. Vandenput, "Battery state control techniques for charge sustaining applications," *SAE Transactions*, vol. 107, pp. 1747–1758, 1998.

[86] R. L. Fares and M. E. Webber, "Combining a dynamic battery model with high-resolution smart grid data to assess microgrid islanding lifetime," *Applied Energy*, vol. 137, pp. 482–489, 2015. [Online]. Available : https://www.sciencedirect.com/science/article/pii/S0306261914004024

[87] S. Boumechta and A. Kaabeche, "Optimisation du dimensionnement d'un systéme hybride eolien/diesel," *Revue des énergies renouvelables*, vol. 18, no. 3, pp. 439–456, 2015. [Online]. Available : https://www.asjp.cerist.dz/en/article/121284

[88] F. Sanders, "On subjective probability forecasting," *Journal of Applied Meteorology and Climatology*, vol. 2, no. 2, pp. 191–201, 1963.

[89] M. A. Stephens, *Goodness-of-fit techniques*. Routledge, 2017.

Index

Thesis summary

Summary in English

General context of the thesis

The global energy generation sector continues to be identified as being the main responsible for the emission of greenhouse gases into the atmosphere due to the use of fossil fuel sources such as coal, oil and gas for energy generation. Greenhouse gases are a problem for planet earth, as they cause global warming and other environmental problems capable of making life on earth unfeasible. Thus, the global community (Government authorities and international organizations) is mobilized to reverse the situation (of the emission of greenhouse gases into the atmosphere, global warming, environmental damage and other consequences) proposing a global energy transition from fossil fuel sources to renewable energy sources. Although the generation of energy through the use of renewable energy sources is identified as an environmentally friendly process, it presents the challenge of the variable availability of renewable resources that causes fluctuations and interruptions in the generation of power, being therefore a process better approached in probabilistic terms, including the uncertainty that characterizes the process.

Basis of the research problem

The availability of renewable energies obeys to natural factors of the climatic system without human intervention. Renewable energies have an instantaneously variable availability

and such variations are often difficult to predict, leading to the field of probability and uncertainty. In power generation systems based on renewable energy sources, uncertainty propagates through the hybrid microgrid and influences the output power of the constituent subsystems, namely, wind turbine generators and photovoltaic generators, including battery energy storage systems. Uncertainty can arise not only as a result of the variable nature of the source of renewable resources, but also, it can arise from the model parameters of the power generating subsystems integrated in the hybrid microgrid. Power generation is affected by instantaneous weather changes throughout the day, thus, we evaluated the influence of uncertainty in the power produced of the subsystems, and in the parameters of the models of the subsystems in function of the hourly changes of the state of the weather throughout the 24 hours of the day. The objective is to produce a risk analysis and provide quantified uncertainty information by modeling the uncertainty of parameters as a function of hourly changes in weather conditions throughout the 24 hours of the day.

Short description of the microgrid diagram (Fig. 3.1, page 38)

The microgrid of interest is configured as isolated (or off-grid), it is not connected to a conventional power grid, there is no external energy supplement, depends solely and exclusively on local generation through wind turbine generators and photovoltaic solar panels. The constituent parts of the microgrid are as follows :

(i) **Environment**
The microgrid is totally dependent on renewable resources namely, wind power used as wind speed v, solar power used as solar radiation G and ambient/air temperature t_a.

Wind speed, solar radiation and ambient temperature are the connecting elements between the environment and the physical part of the system.

To simplify the model, other environmental variables such as air density and humidity are not considered.

(ii) **Wind Turbine Generator**
It is a generation subsystem that uses wind speed as an input variable, performs a series of electromechanical operations converting wind speed into electrical power as an output variable of the wind turbine generator.

(iii) **Photovoltaic solar panels**
It is a generation subsystem that uses solar radiation and ambient temperature as input variables, performs a series of photoelectric operations converting such solar radiation and ambient temperature into electrical power as output variables of photovoltaic solar panels.

(iv) **Battery Energy Storage System**
The microgrid has an integrated battery-based energy storage system, which stores excess energy after satisfying demand needs, and makes the stored energy available in case of a production deficit unable to satisfy demand needs, including mitigating the effects of instantaneous output power fluctuations, system overload and consumption peaks.

(v) **Demand load (Power consumers)**
All the power produced by the isolated hybrid microgrid through wind turbine generators and photovoltaic solar panels, including that stored in batteries, is intended to supply and fully satisfy the energy needs of consumers as required.

Description of input variables, page 40

(i) **Wind speed**
Wind speed is an environmental variable that characterizes the available wind power. From the point of view of the wind turbine generator, the wind speed is an input variable that, through its intensity, rotates the wind turbine's propellers, generating power as an output variable. The variable nature of wind speed is illustrated by the hourly variation profile over the 24 hours of the day in figure 3.2 page 42.

(ii) **Solar radiation**
Solar radiation is an environmental variable that characterizes the available solar power. From the point of view of the photovoltaic solar panel, solar radiation is an input variable that falls on the photocells, generating power as an output variable of the photovoltaic solar panel. The variable nature of solar radiation is illustrated through the hourly variation profile over the 24 hours of the day in figure 3.3, page 43.

(iii) **Ambient temperature**
The ambient temperature is an environment variable that influences the parameters of the photovoltaic cell such as the cell temperature, the photovoltaic current and the voltage

at the cell terminals, therefore, similar to solar radiation, the ambient temperature is also an input variable of the photovoltaic solar panel that influences the power generation as an output variable of the photovoltaic solar panel. The ambient temperature also has a variable nature, the hourly variation profile over the 24 hours of the day is illustrated in figure 3.4 page 44.

Mathematical models for power generation and storage

Wind-to-power conversion model

Modeling the output power of a wind turbine generator followed the following steps :

(i) **Selection of wind turbine generator features**
We selected the wind turbine generator by comparing manufacturers' catalogs, to find parameter values that best fit the wind speed data available for the simulation. We evaluated the distribution curves of the prevailing minimums, averages and maximums. From this procedure, we have selected the following wind turbine generator : **ENERCOM E-53, 800 kW**. Manufacturer's test data and technical specifications are illustrated in table 3.1 on page 46. The objective of this procedure is to make the most of the available wind potential, in order to maximize the generation of output power.

(ii) **Obtaining the mathematical model by the interpolation method**
Using the manufacturer's test data illustrated in table 3.1a on page 46, we applied the cubic spline interpolation method described in equation 2.11 on page 22 and obtained the piecewises functions illustrated in figure 3.6 on page 48. Piecewise functions is a set of sub-functions defined and delimited by domain ranges.

(iii) **Joining piecewise functions**
In this step we perform the sum of all the piecewise functions (or sub-functions) to obtain a generic function that allows us to obtain the estimated values of the output power of the wind turbine generator through interpolation. The power performance curve obtained by the piecewise cubic spline method as a mathematical model of converting wind speed into wind turbine generator output power is illustrated in figure 3.7 on page 49.

The curve of the average values of the hourly distribution of the output power of the wind turbine generator is illustrated in figure 3.8, page 50.

Irradiance-to-power conversion models

The conversion of solar radiation to power follows the steps of calculating the parameters in the following order :

(i) **Selected photovoltaic solar panel**
RECOM - Black Panther Mono crystalline module RCM-380-6MA.
The characteristics of this photovoltaic solar panel are presented in detail in table 3.3, page 57.

(ii) **Calculation of the output power of the photovoltaic panel**
The conversion of solar radiation and ambient temperature into output power of the photovoltaic solar panel follows a sequence of equations for calculating parameters whose details are discussed in section 2.9.2 on page 23 and are briefly presented below :

$$
\begin{aligned}
P_{pvg} &= N_i \cdot FF_i \cdot V_{yi} \cdot I_{yi} \\
FF_i &= \frac{V_{MPP_i} \cdot I_{MPP_i}}{V_{OC_i} \cdot I_{SC_i}} \\
V_{y_i} &= V_{OC_i} - K_{v_i} \cdot T_{C_i} \\
I_{y_i} &= s_i \cdot \left[I_{SC_i} + K_{C_i} \cdot (T_{C_i} - 25) \right] \\
T_{C_i} &= T_a + \frac{S_i}{800} \cdot (T_{NOCT} - 20)
\end{aligned}
$$

The powers obtained above are deterministic but do not take uncertainties into account. For uncertainties to be considered, a probabilistic modeling step, uncertainty propagation, risk analysis and production of quantified uncertainty information must be carried out.

Energy storage

Batteries are the considered devices for electrical energy storage. The battery efficiency depends on both the temperature and on the state of charge. Moreover, the internal resistances of charge and discharge, as well as the capacitance efficiency have been included in the model 3.19, page 104.

The optimization of the models of microgrid

The angle of incidence of sun light on the photovoltaic panel is calculated from the realistic sun trajectory at the considered latitude and longitude. Therefore, the best position of fixed photovoltaic panels is determined. Moreover, the incidence angle is used to modify the sun irradiance considering both the polarization of light (and the transmittance of the cover blade of photovoltaic panel) and the shading effect of the gridlines of the photovoltaic panel.

The optimization of microgrid

The models of wind turbine, photovoltaic panel and battery are used to describe the microgrid behavior. The goal is to calculate the required numbers of each of these devices to serve the consumer demand. This optimum includes the typical cost of the microgrid.

Overview of the approach and outlook

The choice of modeling of the three devices of the microgrid is based on the following motives. First, the cost of modeling is low : from other manufacturer data, the efficiency of the microgrid can be evaluated, the propagation uncertainties of these data on the produced power can be evaluated and the availability of demand serving is deduced from realistic inputs. Therefore, the cost of the best microgrids is evaluated and can help to address the decision making. The advantage of our approach is to be simple and flexible.

Finally, we proposed the method and gave an example of models, while giving a first optimization. Future work should consist of improving models, making comparisons with commercial software and developing decision-making criteria.

Résumé en Français

Contexte général de la thèse

Le secteur mondial de la production d'énergie continue d'être identifié comme étant le principal responsable de l'émission de gaz à effet de serre dans l'atmosphère en raison de l'utilisation de sources de combustibles fossiles telles que le charbon, le pétrole et le gaz pour la production d'énergie. Les gaz à effet de serre sont un problème pour la planète Terre, car ils provoquent le réchauffement climatique et d'autres problèmes environnementaux capables de rendre la vie sur terre impossible. Ainsi, la communauté mondiale (autorités gouvernementales et organisations internationales) est mobilisée pour renverser la situation (de l'émission de gaz à effet de serre dans l'atmosphère, du réchauffement climatique, des dommages environnementaux et autres conséquences) proposer une transition énergétique globale des énergies fossiles vers les énergies renouvelables. Bien que la production d'énergie par l'utilisation de sources d'énergie renouvelables soit identifiée comme un processus respectueux de l'environnement, présente le défi de la disponibilité variable des ressources renouvelables qui provoque des fluctuations et des interruptions dans la production d'électricité, étant donc un processus mieux abordé en termes probabilistes, y compris l'incertitude qui caractérise le processus.

Base du problème de recherche

La disponibilité des énergies renouvelables obéit aux facteurs naturels du système climatique sans intervention humaine. Les énergies renouvelables ont une disponibilité instantanément variable et ces variations sont souvent difficiles à prévoir, ce qui conduit au domaine de la probabilité et de l'incertitude.

Dans les systèmes de production d'électricité basés sur des sources d'énergie renouvelables, l'incertitude se propage à travers le micro-réseau hybride et influence la puissance de sortie des sous-systèmes constitutifs, à savoir les éoliennes et les générateurs photovoltaïques, y compris les systèmes de stockage d'énergie par batterie. L'incertitude peut résulter non seulement de la nature variable de la source de ressources renouvelables, mais également des paramètres du modèle des sous-systèmes de production d'électricité intégrés dans le micro-réseau hybride. La production d'électricité est affectée par les changements climatiques instantanés tout au long de la journée, ainsi, nous avons évalué l'influence de l'incertitude sur la puissance produite des sous-systèmes, et sur les paramètres des modèles des sous-systèmes en fonction des changements horaires de l'état du temps tout au long des 24 heures de la journée.
L'objectif est de produire une analyse de risque et de fournir des informations quantifiées sur l'incertitude en modélisant l'incertitude des paramètres en fonction des changements horaires des conditions météorologiques tout au long des 24 heures de la journée.

Brève description du diagramme du microréseau (Fig. 3.1, page 38)

Le micro-réseau d'intérêt est configuré comme isolé (ou hors réseau), il n'est pas connecté à un réseau électrique conventionnel, il n'y a pas d'apport d'énergie externe. Il la seule source d'énergie électrique produite par des éoliennes et des panneaux solaires photovoltaïques, éventuellement stockée dans des batteries. Les éléments constitutifs du micro-réseau sont les suivants :

(i) **Environnement**

Le micro-réseau dépend totalement des ressources renouvelables, à savoir

la vitesse du vent v, l'énergie solaire G et la température ambiante/de l'air t_a.

La vitesse du vent, le rayonnement solaire et la température ambiante sont les éléments de liaison entre l'environnement et la partie physique du système.

Pour simplifier le modèle, d'autres variables environnementales telles que la densité de l'air et l'humidité ne sont pas prises en compte. Par contre, la latitude et la longitude sont considérées dans une phase préliminaire d'optimisation de l'orientation des panneaux solaires (supposés fixes).

(ii) **Éolienne**
Il s'agit d'un sous-système de génération d'électricité qui utilise la vitesse du vent comme variable d'entrée, effectue une série d'opérations électromécaniques convertissant la vitesse du vent en énergie électrique (variable de sortie).

(iii) **Panneaux solaires photovoltaïques**
Le rayonnement solaire et la température ambiante sont leurs variables d'entrée. Il effectue une série d'opérations photoélectriques convertissant ce rayonnement solaire et cette température ambiante en énergie électrique comme variables de sortie des panneaux solaires photovoltaïques.

(iv) **Système de stockage d'énergie de type batterie**
Le micro-réseau dispose d'un système intégré de stockage d'énergie basé sur des batteries, qui stockent l'énergie excédentaire après avoir satisfait les besoins de la demande, et rend l'énergie stockée disponible en cas de déficit de production, si elle incapable de satisfaire la demande. Ce sous-système atténue les effets des fluctuations instantanées de la puissance

produite par les éoliennes et les panneaux photovoltaïques, de la surcharge du système et des pics de consommation.

(v) **La demande (par les consommateurs d'énergie électrique)**
Toute l'électricité produite par le micro-réseau hybride isolé, via des éoliennes et des panneaux solaires photovoltaïques, y compris celle stockée dans des batteries, est destinée à alimenter et à satisfaire pleinement les besoins énergétiques des consommateurs.

Description des variables d'entrée, Page 40

(i) **Vitesse du vent**
La vitesse du vent est une variable environnementale qui caractérise la puissance éolienne disponible. Du point de vue de l'éolienne, la vitesse du vent est une variable d'entrée qui, par son intensité, fait tourner les hélices de l'éolienne, générant de l'énergie comme variable de sortie. Le caractère variable de la vitesse du vent est illustré par le profil de variation horaire sur les 24 heures de la journée sur la figure 3.2 page 42. Nos données proviennent de mesures effectuées à Maputo. La vitesse du vent, mesurée au sol diffère de celle à la hauteur de la génératrice de l'éolienne. Nous avons donc corrigé les mesures à partir de la formule 2.12, page 22.

(ii) **Radiation solaire**
Le rayonnement solaire est une variable environnementale qui caractérise la puissance solaire disponible. Du point de vue du panneau solaire photovoltaïque, le rayonnement solaire est une variable d'entrée qui tombe sur les photocellules, générant de l'énergie en tant que variable de sortie du panneau solaire photovoltaïque. Le caractère variable du rayonnement solaire est illustré à travers le profil de variation horaire sur les 24 heures

de la journée sur la figure 3.3 page 43. L'irradiance G (en $\mathrm{W\,m^{-2}}$) est une variable d'entrée du modèle de panneaux photovolotaïques. Elle dépend de la latitude et de la longitude. Nos données proviennent de mesures effectuées à Maputo.

(iii) **Température ambiante**
La température ambiante est une variable d'environnement qui influence les paramètres de la cellule photovoltaïque tels que la température de la cellule, le courant photovoltaïque et la tension aux bornes de la cellule, par conséquent, à l'instar du rayonnement solaire, la température ambiante est également une variable d'entrée du panneau solaire photovoltaïque qui influence la production d'énergie en tant que variable de sortie du panneau solaire photovoltaïque. La température ambiante a également un caractère variable, le profil de variation horaire sur les 24 heures de la journée est illustré sur la figure 3.4 page 44. Nos données proviennent de mesures effectuées à Maputo.

Modèles mathématiques pour la production et de stockage d'électricité

Modèle de conversion de la vitesse du vent en puissance électrique

La modélisation de la puissance de sortie d'un générateur d'éolienne a suivi les étapes suivantes

(i) **Sélection des caractéristiques des éoliennes**
Nous avons sélectionné l'éolienne en comparant les catalogues des constructeurs, pour trouver les valeurs des paramètres qui correspondent le mieux aux données de vitesse du vent disponibles pour la simulation. Nous avons évalué les courbes de distribution des minimums, moyennes et

maximums en vigueur. A partir de cette procédure, nous avons sélectionné l'éolienne suivante : **ENERCOM E-53, 800 kW**. Les données de test et les spécifications techniques du fabricant sont illustrées dans le tableau 3.1 à la page 46. L'objectif de cette procédure est de tirer le meilleur parti du potentiel éolien disponible, afin de maximiser la production de puissance de sortie.

(ii) **Obtention du modèle mathématique par la méthode d'interpolation**
En utilisant les données de test du fabricant illustrées dans le tableau 3.1a à la page 46, nous avons appliqué la méthode d'interpolation de type spline cubique décrite dans l'équation 2.11 à la page 22 et obtenu les fonctions par morceaux illustrées à la figure 3.6 à la page 48. Les fonctions par morceaux sont un ensemble de sous-fonctions définies et délimitées par des plages de domaines.

(iii) **Joindre des fonctions par morceaux**
Dans cette étape, nous effectuons la somme de toutes les fonctions (ou sous-fonctions) par morceaux pour obtenir une fonction générique qui nous permet d'obtenir les valeurs estimées de la puissance de sortie de l'éolienne par interpolation. La courbe de performance de puissance obtenue par la méthode des splines cubiques par morceaux en tant que modèle mathématique de conversion de la vitesse du vent en puissance de sortie de l'éolienne est illustrée à la figure 3.7 à la page 49.

La courbe des valeurs moyennes de la répartition horaire de la puissance de sortie de l'éolienne est illustrée figure 3.8, page 50. Nous n'avons pas trouvé de modèle ou d'étude du vieillissement des éoliennes et de son influence sur la production d'énergie. Tout autre modèle d'éolienne pourrait être utilisé dans

notre approche, à condition d'être stable sur le domaine d'étude des entrées et sorties.

Modèle de conversion de l'irradiance en puissance

La conversion du rayonnement solaire en puissance suit les étapes de calcul des paramètres dans l'ordre suivant :

(i) **Panneau solaire photovoltaïque sélectionné**
RECOM - Black Panther Mono crystalline module RCM-380-6MA.
Les caractéristiques de ce panneau solaire photovoltaïque sont présentées en détail dans le tableau 3.3, page 57.

(ii) **Calcul de la puissance de sortie du panneau photovoltaïque**
La conversion du rayonnement solaire et de la température ambiante en puissance de sortie du panneau solaire photovoltaïque suit une séquence d'équations pour le calcul des paramètres dont les détails sont discutés dans la section 2.9.2 à la page 23 et sont brièvement présentés ci-dessous :

$$
\begin{aligned}
P_{pvg} &= N_i \cdot FF_i \cdot V_{yi} \cdot I_{yi} \\
FF_i &= \frac{V_{MPP_i} \cdot I_{MPP_i}}{V_{OC_i} \cdot I_{SC_i}} \\
V_{y_i} &= V_{OC_i} - K_{v_i} \cdot T_{C_i} \\
I_{y_i} &= s_i \cdot [I_{SC_i} + K_{C_i} \cdot (T_{C_i} - 25)] \\
T_{C_i} &= T_a + \frac{S_i}{800} \cdot (T_{NOCT} - 20)
\end{aligned}
$$

Les puissances obtenues par l'équation matricielle illustrée ci-dessus sont des puissances déterministes qui ne tiennent pas compte des incertitudes, notamment des données constructeur. Pour que les incertitudes soient

prises en compte, une étape de modélisation probabiliste, de leur propagation à travers les modèles mathématiques, d'analyse des risques et de production d'informations quantifiées aidant à la prise de décision doivent être réalisée.

De plus, l'angle d'incidence des rayons du soleil sur le panneau photvoltaïque varie au cours de la journée. Afin d'avoir un modèle le plus réaliste possible, nous avons utilisé l'algorithme décrit dans la référence [79] (section 3.13, page 94) afin de calculer l'angle d'incidence des rayons sur le panneau photovoltaïque. Ceci nous a permis de déterminer la meilleure orientation du panneau afin de produire le maximum d'énergie électrique (section 3.13.4, page 97). L'angle d'incidence est fonction de l'heure de la journée et du jour de l'année. Il permet également de calculer :

— la transmittance par la plaque transparente située au-dessus des cellules (section 3.14, page 97) ;
— l'effet d'ombrage, lié à la géométrie des panneaux photovoltaïques : les bords des motifs des cellules et du panneau induisent une ombre pour des angles d'incidence élevés (section 3.15, page 99).

Ces deux effets, réduisent l'efficacité du panneau photovoltaïque. Nous avons ainsi corrigé les mesures de l'irradiance reçue par le panneau photovoltaïque.

Nous proposons également d'introduire un modèle de vieillissement des panneaux, connu pour en diminuer l'efficacité au cours du temps. Même si nous n'avons pas utilisé ce modèle puisque le vieillissement est négligeable sur les deux années d'étude, il est nécessaire d'en tenir compte dans les choix de microgrids. Tout autre modèle de panneau solaire pourrait être utilisé dans notre approche, à condition d'être stable sur le domaine d'étude des entrées et

sorties.

Stockage de l'énergie électrique

Nous considérons les batteries comme dispositifs de stockage d'énergie électrique. L'efficacité de la batterie dépend à la fois de la température et de l'état de charge. En outre, les résistances internes de charge et de décharge, ainsi que l'efficacité déduite des effets capacitifs ont été inclus dans le modèle 3.19, page 104.
La section de modélisation de la batterie a effectué une tâche fastidieuse consistant à déduire des équations basées sur la combinaison d'approches et d'abstractions des méthodes les plus variées disponibles dans la littérature telles que les équations différentielles, les méthodes itératives, les équations déterministes, entre autres. Un exemple de la diversité des approches dans la modélisation des batteries est la capacité et l'état de charge de la batterie qui sont présentés dans la littérature sous différentes perspectives. En général, les modèles disponibles dans la littérature sont très complexes, ce qui nécessite dans de nombreux cas des efforts de calcul et du temps, ainsi, dans cette thèse, nous utilisons une modélisation déterministe avec des simplifications basées sur des approximations. Nous utilisons le principe de fonctionnement de la batterie flottante, qui consiste à charger et décharger simultanément en mode d'utilisation continue, visant à simplifier le comportement de la batterie dans le temps.
En général, nous discutons de la modélisation mathématique de la batterie basée sur la Réf. [4, 5, 63], nous utilisons leurs résultats numériques pour valider notre code en nous concentrant sur les équations des paramètres suivants (voir 3.19, page 104) :

— Capacité C en fonction de l'intensité du courant de la batterie I_{bat}
— État de charge EDC en fonction de la capacité C de la batterie
— Tension de décharge V_d en fonction du courant de décharge I_d de la batterie
— Résistance de décharge R_d en fonction de l'état de charge EDC
— Tension de décharge V_d en fonction du temps $t(h)$
— Tension de charge V_c en fonction du courant de charge I_c
— Tension de charge V_c en fonction du temps $t(h)$

Après une modélisation mathématique basée sur des approximations pour obtenir les codes, nous utilisons les résultats numériques de Ref. [63, 4] pour comparer et valider les modèles. Lors de la validation des modèles de paramètres, nous avons comparé les courbes de paramètres obtenues par nos codes et les courbes de paramètres similaires à l'aide de modèles de Réf. [63, 4]. Voir la comparaison des courbes de paramètres tout au long de la section 3.19, à partir de la page 104.

L'étape suivante consistait essentiellement à appliquer les données d'entrée aux modèles de paramètres de batterie validés à l'étape précédente, rappelant que dans cette thèse nous avons utilisé comme variables d'entrée, la vitesse du vent, le rayonnement solaire et la température ambiante, qui sont appliqués sur les modèles paramétriques validés pour modéliser le comportement de ces paramètres avec l'évolution horaire de l'état météorologique au cours des heures de la journée. Dans la section 3.30 de la page 119. Ensuite, la modélisation des paramètres de la batterie en fonction de l'évolution horaire de l'état météorologique au cours des heures de la journée est présentée. Les paramètres modélisés sont les suivants :

— Courant de charge I_c et courant de décharge I_d

— Capacité de la batterie C
— État de charge EDC
— Tension de charge V_c et tension de décharge V_d
— Force électromotrice de charge E_c et force électromotrice de décharge E_d
— Puissance de charge P_c et puissance de décharge P_d

Un aspect important à garder à l'esprit lors de la modélisation des paramètres listés ci-dessus, est qu'ils sont tous présentés sous forme de cartographie par échelle de couleurs pour évaluer le comportement (ou la réponse) de chaque paramètre en fonction de l'évolution horaire de la état météorologique compte tenu des données d'entrée sur deux ans (2019-2020). La cartographie par échelle de couleurs est insérée dans une matrice jours (731 jours) X heures (24 heures).

Les paramètres de fonctionnement de la batterie montrent une variation horaire du comportement au cours des heures de la journée, ce fait peut être vérifié analytiquement à travers les équations mathématiques qui contiennent la dépendance à la température, c'est-à-dire que la variable de température affecte le fonctionnement de la batterie. De plus, l'effet des heures diurnes et nocturnes détermine le comportement des courants de charge et de décharge, qui affectent évidemment d'autres paramètres tels que la capacité de la batterie, l'état de charge, la puissance de charge et la puissance de décharge.

Le modèle de batterie comportant des variables reliées entre elles (notamment à l'état de charge) par des équations phénoménologiques, comportant des dénominateurs pouvant s'annuler. Le code permettant de calculer la puissance accumulée et fournie par la batterie comporte donc des tests de validité (les résistances de charge et de décharge doivent avoir des valeurs raisonnables, la tension d'entrée et de sortie doivent appartenir à des intervalles physiques). Ceci est d'autant plus important lorsque l'objectif est de propager des incerti-

tudes sur les données constructeur : la stabilité du modèle doit être garantie dans les intervalles de variations des paramètres. De même, le comportement du modèle de batterie doit être stable pour toutes les entrées (puissance électrique produite par les éoliennes et les panneaux photovoltaïques) et les sorties (puissance consommée) pour chacune des 24 heures et chacun des 731 jours étudiés. Tout autre modèle de batterie pourrait être utilisé dans notre approche, à condition de vérifier cette condition de stabilité. Les effets de température, voire d'ébullition dans les cellules à acide sont intégrés. Un refroidissement des batteries pourrait améliorer leur durabilité et leur capacité, mais demanderait de l'énergie.

Optimisation des modèles de microgrids

Connaître le comportement des paramètres des sous-systèmes est fondamental pour évaluer les performances du système hybride dans son ensemble. Cependant, le micro-réseau dans sa configuration isolée, doit être en mesure de répondre aux besoins de la demande mais à des coûts faibles, en étant durables et contrôlables. La capacité de production dépend entièrement de la disponibilité et de l'intensité des ressources renouvelables, à savoir la vitesse du vent et le rayonnement solaire.
L'angle d'incidence de la lumière sur le panneau photovoltaïque est calculé à partir de la trajectoire réaliste du soleil à la latitude et à la longitude considérées. Par conséquent, la meilleure position des panneaux photovoltaïques fixes est déterminée. De plus, l'angle d'incidence est utilisé pour modifier l'irradiance du soleil en tenant compte de la polarisation de la lumière (et la transmittivité par la lame transparente de couverture du panneau photovoltaïque) et l'effet d'ombrage des bandes conductrices de chaque cellule du panneau

photovoltaïque.
Pour soutenir le processus de prise de décision sur la faisabilité technique et financière du micro-réseau, une analyse comparative est présentée entre deux localités, à savoir la province de Maputo et le district de Mecula, en comparant des données telles que :

— Rayonnement solaire brut
— Rayonnement solaire utile
— Vitesse du vent
— Énergie produite par des panneaux solaires photovoltaïques
— Énergie produite par les éoliennes
— Demande (ou consommation) de puissance

Les modèles d'éoliennes, de panneaux photovoltaïques et de batteries sont utilisés pour décrire le comportement du microgrid. Le but est de calculer le nombre requis de chacun de ces appareils pour répondre à la demande des consommateurs. Cet optimum inclut le coût typique du microgrid. Les résultats ont présentés sous la forme d'options de coût optimisé tout en assurant la capacité à satisfaire la demande, en intégrant éventuellement un taux identifié de défaut tolérable de service. Ainsi, la méthode très simple proposée permet de choisir une option financièrement viable, en intégrant les différents sous-systèmes du micro-réseau, à savoir WTG, PVG et BESS. Bien sûr, le modèle de batterie peut être changé à volonté. Encore, une fois, nous proposons une méthode simple, basée sur des modèles dont le calcul est rapide, afin de permettre à la fois des calculs déterministes sur de nombreuses données, des calculs de propagation d'incertitude de type Monte Carlo et statistiques.

Aperçu de l'approche et perspectives

Le choix de la modélisation des trois dispositifs du microgrid est basé sur les motifs suivants. Le coût de la modélisation est faible : à partir d'autres données du fabricant, l'efficacité du microgrid peut être évaluée, les incertitudes de propagation de ces données sur la puissance produite peuvent être évaluées et la réponse à la demande est déduite d'intrants réalistes. L'avantage de notre approche est d'être simple et flexible, le prix des différents composants pouvant être également ajusté.

Enfin, nous avons proposé la méthode et donné un exemple de modèles, tout en donnant une première optimisation. Les travaux futurs devraient consister à améliorer les modèles, à établir des comparaisons avec les logiciels commerciaux et à élaborer des critères de prise de décision.

Prévision probabiliste de P_{wtg} and P_{pvg}

La puissance de sortie de l'éolienne P_{wtg} (figure 3.8, page 50) et celle du générateur photovoltaïque P_{pvg} (figure 3.9, page 52) sont des puissances de sortie estimées déterministes. Les systèmes de production d'électricité basés sur des sources d'énergie renouvelables sont caractérisés par des incertitudes sur la disponibilité et l'intensité du potentiel renouvelable (potentiel éolien et potentiel solaire) rendant difficile la prévision précise de la puissance pouvant être produite à un moment donné.

De nombreux modèles de prédiction probabiliste sont composés de modèles uniques (ou de modèles individuels). Les modèles probabilistes simples peuvent rarement être parfaits pour la tâche de prévision, une solution statistique pour améliorer la précision des prévisions consiste à utiliser le principe de combi-

naison multi-modèle probabiliste. Le principe MMC est appliqué séparément à chaque puissance de sortie P_{wtg} et P_{pvg} comme suit :

(i) Pour chaque jeu de données horaire h_j de la puissance déterministe P_{wtg} et P_{pvg}, un test de normalité est effectué.
Le test de normalité vise uniquement à comprendre le comportement statistique des données d'entrée. Le résultat obtenu indiquant si les données suivent une distribution normale ou non normale n'est pas considéré comme une fin mais comme un moyen d'évaluer le comportement statistique de chacun de P_{wtg} et P_{pvg}.

(ii) Considérons deux ensembles m_1 et m_2, chaque ensemble composé de modèles uniques (modèles individuels) $f(x)$ et $g(y)$ tels que :

$$m_1 = \{f_1(x), f_2(x), \cdots, f_n(x)\}$$
$$m_2 = \{g_1(y), g_2(y), \cdots, g_n(y)\}$$

Chaque modèle unique appartenant à m_1 ou m_2 est appelé modèle candidat

(iii) Tester les modèles sur les données de puissance de sortie
— L'ensemble des modèles candidats m_1 est testé sur le jeu de données P_{wtg}
— L'ensemble des modèles candidats m_2 est testé sur le jeu de données P_{pvg}.
Cette étape vise à déterminer la qualité de l'ajustement de chaque modèle candidat lorsqu'il est appliqué à l'ensemble de données de puissance de sortie horaire.
Lorsqu'un ensemble donné de modèles candidats m_1 ou m_2 est appliqué

aux données de puissance de sortie P_{wtg} ou P_{pvg}, la qualité de l'ajustement des modèles de cet ensemble est déterminée par la méthode Akaike Information Criteria (AIC), en calculant la valeur AIC, puis comparez les valeurs AIC de chaque modèle unique appartenant à un ensemble, positionnez-les par ordre croissant. Le modèle avec la valeur AIC la plus basse a la meilleure qualité d'ajustement, le modèle avec la valeur AIC la plus élevée a la pire qualité d'ajustement, plus la valeur de l'AIC est élevée, plus la qualité du modèle est faible par rapport aux autres modèles candidats appartenant au même ensemble testé par rapport à un ensemble de données statistiques.

(iv) Détermination des poids du modèle
Sachant que l'objectif est de construire un modèle probabiliste avec une approche multi-modèle, les modèles déjà triés par ordre croissant en fonction de la qualité de l'ajustement doivent avoir un poids avec lequel chaque modèle individuel participe à la combinaison.
Le poids avec lequel chaque modèle participe à la combinaison est déterminé par les poids d'Akaike, calculés en fonction de la valeur AIC de chaque modèle. Ainsi, l'ampleur de chaque poids et le positionnement dans l'ordre décroissant des poids des modèles coïncident avec le positionnement de la qualité d'ajustement de chacun des modèles de l'ensemble (exemple : si le modèle a la troisième meilleure qualité d'ajustement, le poids aura également la troisième position dans l'ordre décroissant des poids).

(v) Composition du modèle de combinaison multi-modèles
Dans le classement décroissant des poids, la position de chaque poids du modèle calculé en fonction de la valeur de l'AIC coïncide avec le clas-

sement du modèle en fonction de la qualité d'ajustemen, ainsi, pour la composition du modèle de combinaison multi-modèle, on multiplie la fonction (modèle candidat) par le poids correspondant en utilisant le principe de combinaison linéaire exprimé par :

$$p\left(data|f_1(x), f_2(x), \cdots, f_n(x)\right) = \sum_{i=1}^{n} \omega_i \cdot p_i(data|f_n(x))$$

Par conséquent, le modèle de combinaison multimodèle pour prédire la puissance de sortie de l'éolienne P_{wtg} et la puissance de sortie du générateur photovoltaïque P_{pvg} sera exprimé comme :

$$\begin{aligned} Pour \quad WTG: \quad & f(x) = \omega_1 \cdot f_1(x) + \omega_2 \cdot f_2(x) + \cdots + \omega_n \cdot f_n(x) \\ Pour \quad PVG: \quad & g(y) = \lambda_1 \cdot g_1(y) + \lambda_2 \cdot g_2(y) + \cdots + \lambda_n \cdot g_n(y) \end{aligned}$$

Supposons que $x = P_{wtg}$, $y = P_{pvg}$, $f(x)$ x est un modèle MMC pour prévoir et estimer la puissance de sortie du WTG, $g(x)$ est un modèle MMC pour prévoir et estimer la puissance de sortie du PVG, ω et λ représentent les poids avec lesquels chaque modèle membre participe au combinaison pour former le modèle combiné. $(\omega, \lambda) \in [0, 1]$.
L'objectif de cette procédure est de construire un modèle probabiliste basé sur le principe de combinaison multi-modèles applicable aux systèmes hybrides de production d'électricité composés de WTG et PVG, visant à améliorer la précision de la prévision de puissance horaire et la capacité de production horaire du système.

Milagre Alfredo MANHIQUE

Doctorat : Optimisation et Sûreté des Systèmes

Année 2022

Optimisation multi-objectif et aide à la décision dans le contexte de systèmes/processus complexes et multi-physiques

Les systèmes de production d'énergie hybride batterie-solaire-éolienne sont très instables en raison de la fluctuation de la puissance de sortie causée par les variations instantanées de la disponibilité de l'énergie solaire et éolienne, faisant de la puissance de sortie une variable incertaine. Cette thèse se propose d'évaluer l'influence de l'incertitude et de produire une analyse de risque de chaque sous-système constitutif, à savoir l'Eolienne et le Générateur Photovoltaïque, afin de fournir des informations quantifiées sur l'incertitude pour faciliter le processus de prise de décision dans la conception d'une configuration optimale d'un système de production d'énergie hybride batterie-solaire-éolienne. La puissance de sortie de l'éolienne et du générateur photovoltaïque en tant que variables incertaines ont été modélisées en termes probabilistes en utilisant le principe du modèle de combinaison multimodèle probabiliste afin d'améliorer la précision de l'estimation de la puissance de sortie. En bref, cette thèse tente d'optimiser les paramètres d'équipement et la modélisation probabiliste de la puissance de sortie d'un système de production d'énergie hybride batterie-solaire-éolienne pour évaluer l'influence de l'incertitude et de l'analyse des risques menant au processus de prise de décision.

Mots clés : énergies renouvelables – éoliennes – générateurs photovoltaïques – énergie, stockage – incertitude.

Multi-objective Optimization and Decision-making in the Context of Complex and Multi-physical Systems/Processes

Hybrid Battery-Solar-Wind Power Generation Systems are highly unstable due to the fluctuation of the output power caused by instantaneous variations in the availability of solar and wind energy, making the output power an uncertain variable. This thesis intends to evaluate the influence of uncertainty and produce a risk analysis of each constituent subsystem, namely the Wind Turbine Generator and the Photovoltaic Generator, to provide quantified uncertainty information to aid in the decision-making process in designing an optimal configuration of an Hybrid Battery-Solar-Wind Power Generation System. The output power of the Wind Turbine Generator and Photovoltaic Generator as uncertain variables were modeled in probabilistic terms using the principle of Probabilistic Multi-Model Combination Model in order to improve the accuracy of the output power estimation. Briefly, this thesis makes an attempt to optimize equipment parameters and probabilistic modeling of the output power of an Hybrid Battery-Solar-Wind Power Generation Systems to assess the influence of uncertainty and risk analysis leading to the decision-making process.

Keywords: renewable energy sources – wind turbines – photovoltaic cells – energy storage – uncertainty.

Thèse réalisée en partenariat entre :

AFD AGENCE FRANÇAISE DE DÉVELOPPEMENT

utt UNIVERSITÉ DE TECHNOLOGIE TROYES

Ecole Doctorale "Sciences pour l'Ingénieur"